Fall 2013

Use of ultra-high performance concrete to mitigate impact and explosive threats

Julie Anne Willey

Department:

USE OF ULTRA-HIGH PERFORMANCE CONCRETE TO MITIGATE IMPACT AND EXPLOSIVE THREATS

by

JULIE ANNE WILLEY

A THESIS

Presented to the Faculty of the Graduate School of the

MISSOURI UNIVERSITY OF SCIENCE AND TECHNOLOGY

In Partial Fulfillment of the Requirements for the Degree

MASTER OF SCIENCE IN CIVIL ENGINEERING

2013

Approved by

Dr. John J. Myers, Advisor
Dr. Jason Baird
Dr. Lesley Sneed

ABSTRACT

This study is a continuation of research conducted by Natalia Carey, Anthony Wulfers, and Dr. John Myers under the DHS ALERT Center. Carey investigated the use of polyurea coating systems to mitigate close range blast threats on wall panels. Wulfers continued this by using both polyurea coatings as well as a sacrificial wood fiber fly ash (WF-FA) layer to try to get increased performance.

This research was aimed at the study of ultra-high performance concrete (UHPC) for the use in impact and blast mitigation. There is little information on the performance of UHPC under close range blast loading; therefore it was the goal of this project to determine the performance of UHPC when undergoing a close range blast threat, as well as to determine if an ultimately thinner wall section could outperform systems previously tested by Carey (2012) and Wulfers (2012). Three panel systems were examined with differing levels of fiber content; no fiber, 2% fiber by weight, and 6% fiber by weight. One aspect of interest in this study was to determine the impact of fiber content on the effectiveness of the panel under blast loading. The panels used in this research were tested at the Missouri S&T Experimental Mine, and the damage was reported both visually as well as quantitatively. Visual inspection was used to compare the overall level of damage. Quantitative results, such as mass loss and residual deflections, were used to determine the effectiveness of the wall system in mitigating the blast event. After examining the results, it is shown that UHPC without fiber does not perform well under this type of loading, but that increasing fiber content did increase performance of the wall panel in equivalent blast events. It is also shown that this material undergoes minimal spalling and fragmentation which is favorable for structures that are at risk to blast events. There is also little information on the performance of UHPC under impact loading. As such, this work also included testing to determine the impact capabilities of this material and compare the performance of UHPC panels to other types of high performance concrete systems that have undergone impact testing at Missouri S&T by Gliha (2011).

ACKNOWLEDGMENTS

I would like to thank my advisor, Dr. John Myers, for his guidance and support during this project and my program coursework. Without his encouragement and advice, I would not have been able to take full advantage of my continued education and ultimately obtain my Master's Degree. I would also like to thank my committee members, Dr. Jason Baird and Dr. Lesley Sneed for their time and involvement in this project. Their knowledge and encouragement was instrumental in my learning and overall experience at Missouri S&T.

In addition to my committee, I would like to thank the ALERT program for providing the funding for this study, and the many material donations from companies including Bekeart Corporation, BASF, The Chemical Company, LeHigh Cement, and LaFarge.

I would also like to thank the lab technicians at Missouri S&T including John Bullock, Gary Abbott, Scott Parker, and Brian Swift and the Experimental Mine Staff including Dewayne Phelps, and Jimmie Taylor. Their help with testing setups, specimen fabrication, and laboratory equipment was vital to completing my work. Additionally I would like to give a big thank you to my fellow graduate students, Dane Shaw, Renee Earley, Mahdi Valipour, Caleb Baumgart, Kevin Phelps, Phillip Mulligan, Clay Reichle, Tom West, Ben Gliha, Nathan Muncy, and Wei Wang, for their endless help and support. Another person who was instrumental to my learning and was always ready to lend some helpful advice is Mike Lusher. Without these wonderful colleagues this study would not have been possible, and I cherish all the friendships that have grown from my time with each of them, so once again, thank you!

Finally I would like to thank my family. To my parents, Stephen and Janice Willey, my brother, David Willey, and extended family who have supported all my life decisions and encouraged my dreams, thank you from the bottom of my heart! You're all the best!

TABLE OF CONTENTS

LIST OF ILLUSTRATIONS

Page

LIST OF TABLES

Page

1. INTRODUCTION

1.1. BACKGROUND

As anyone who pays attention to history and current events knows, buildings are often targets of explosive threats and terrorist attacks. Most notably are the Oklahoma City Bombing of April 19, 1995, and the World Trade Center attacks of September 11, 2001. While barriers placed outside these buildings are effective ways of increasing the standoff distance for manmade threats such as a car bomb, they are not effective at increasing the standoff distance of a device such as a backpack explosive. For these types of threats, the most common way to mitigate a blast is by conventional reinforced concrete wall systems. Unfortunately, conventional reinforced concrete has a tendency to spall which results in high velocity debris. When trying to protect building occupants from a blast, not only does the protective system have to mitigate the blast from outside, but the spalling behavior must be controlled or else it can turn into projectile fragmentation and still potentially harm the building occupants in the at-risk structure. The purpose of this study is to research an alternate material to effectively mitigate a blast event, specifically ultra-high performance concrete (UHPC). This study investigates the effectiveness of this material under blast and impact loading, as well as if a smaller system could be used to create the same level of protection as a larger conventional concrete wall panel.

1.2. OBJECTIVES

The main goal of this research was to study the blast mitigation characteristics of UHPC as a thin protective wall panel. There are multiple types of UHPC on the market today that were considered for this project, however due to the nature of proprietary products, and the fact that their exact contents could not be fully disclosed, the research team decided to investigate an in-house mix design in order to better understand the material, as well as to be able to disclose exact ingredients in this work. Based on previous research done at Missouri University of Science and Technology led by Dr. John Myers, the team also wanted to explore the performance of this relatively new material under impact loading as well as its creep and shrinkage properties due to its

unique curing requirements. During testing, it became apparent that there were differences between using current blast mitigation software to predict UHPC material performance under blast loading and the actual tested specimens. Because of the trends being seen, this topic is also addressed.

1.3. ORGANIZATION OF REPORT

This report is organized in 7 sections. The first two chapters give an introduction to the study and objectives of the research. The third chapter discusses the scope of the work that was done. The fourth section describes the mix design process to finalize the concrete mix design to be used in the remainder of the project. The fifth section discusses the experimental program and testing methods, while the sixth and seventh chapters give the results and conclusions of testing performed, followed by recommendations for future investigation. Each section is laid out by topics in the same order. The order of discussion in each chapter is creep and shrinkage performance, impact performance, and lastly blast performance.

2. LITERATURE REVIEW

2.1. ULTRA-HIGH PERFORMANCE CONCRETE

2.1.1. Definition. Currently, there are many types of ultra-high performance concretes being researched and used around the world. This material classification also has many different names such as ultra-high performance fiber-reinforced concrete (UHPFRC), reactive powder concrete (RPC), and very-high strength concrete (VHSC), just to name a few. As a result of the wide range of types, many different proprietary versions of this material are being produced on the market such as Ductal by LaFarge, Densit, and Hi-Con. The American Concrete Institute (ACI) does not currently have a definition of UHPC. Regardless, there is a general consensus of what types of concretes fall under this designation of UHPC. Most literature agrees that ultra-high performance concretes have the following criteria (Toutlemonde and Resplendino, 2011):

- Compressive strength greater than 21.7 ksi (150 MPa).
- Fiber reinforcement (typically steel) to achieve non-brittle behavior and possibly overcome the use of passive reinforcement.
- High binder content that reduces capillary porosity.
- Tensile matrix strength greater than 1.0 ksi (7 MPa).
- Low water content.

2.1.2. Typical UHPC Composition. For this study, the compressive strength was the target during mix design trials. The in-house mix design was similar in nature to other commercially available products such as Ductal®, a product manufactured by LaFarge. This product has been used in the United States mainly in bridges built by the Federal Highway Administration (FHWA). This product has no large or coarse aggregate so it falls in the RPC category of UHPC. The FHWA publication HRT-06-103 titled "Material Property Characterization of Ultra-High Performance Concrete" lists the typical UHPC composition shown in Table 2.1 (Graybeal, 2006). The composition shown was the basis for the material mix designs conducted for this study.

Table 2.1. Typical UHPC composition

Material	Amount (kg/m^3 (lb/yd^3))	Percent by Weight
Portland Cement	712 (1,200)	28.5
Fine Sand	1020 (1,720)	40.8
Silica Fume	231 (390)	9.3
Ground Quartz	211 (355)	8.4
Superplasticizer	30.7 (51.8)	1.2
Accelerator	30.0 (50.5)	1.2
Steel Fibers	156 (263)	6.2
Water	109 (184)	4.4

2.1.3. Mechanical Properties. As mentioned above, there are multiple proprietary blends of UHPC on the market, as well as a range of types and definitions. In this study, the goal of the mix design process was to create a mix that achieved roughly the same properties as the proprietary product Ductal produced by LaFarge. Table 2.2 displays the mechanical properties of Ductal as they appear on VSL International's website ("Ductal® Characteristics", 2011).

Table 2.2. Mechanical properties of Ductal ("Ductal® Characteristics", 2011)

	Steam Treated			
	SI Units		English Units	
Density	1,450 - 2,550	kg/m^3	153 - 159	lb/ft^3
Compressive Strength	170-230	MPa	24.6 - 33.4	ksi
Flexural Strength	40-50	MPa	5.8 - 7.3	ksi
Young's Modulus	50-60	GPa	7252 - 8702	ksi
Poisson's Coefficient	0.2			
Shrinkage*	<10 microstrain			
Creep Coefficient	0.2-0.5			

* Post-Cure Shrinkage

2.1.4. Curing Methods. The curing process used with UHPC greatly effects the properties of the final concrete product. LaFarge recommends that their product Ductal be steam cured for 48 hours at a temperature of 194 °F (90 °C) and 95% relative humidity before de-molding occurs. Multiple research studies have been done to investigate other curing techniques and the effect they have on the material properties of UHPC. The other typical curing methods that have been investigated are ambient air curing, delayed steam curing, and "tempered" steam curing. Ambient air curing is simply allowing the specimens to cure in an open air laboratory environment. The delayed steam cure consists of the same curing method as recommended by LaFarge except the curing is delayed until 15 days after casting. The tempered steam cure is a steam curing process that occurs at a lower temperature of 140 °F (60 °C) at 95% relative humidity for 48 hours (Graybeal and Hartmann, 2003).

2.2. CREEP AND SHRINKAGE

2.2.1. Definitions. Concrete shrinkage is the strain measured on a load-free concrete specimen as a result of a change in length. Values of shrinkage are usually reported in dimensionless units of microstrain ($1x10^{-6}$) which represents the change in length as a percentage. Shrinkage is broken down into many types, but the main ones for this research are autogeneous shrinkage and drying shrinkage. Drying shrinkage, as it sounds, occurs when a specimen is exposed to the environment and is allowed to dry. Typically for normal strength concretes, it is assumed that all shrinkage is drying shrinkage. (ACI 209.1R-05, 2005) Autogeneous shrinkage is "shrinkage that occurs in the absence of moisture exchange due to the hydration reactions taking place inside the cement matrix (ACI 209.1R-05, 2005)". This is relevant in the case of UHPC because of the cement hydration process which will be discussed in section 2.2.2.

Concrete creep is defined as "the time-dependent increase in strain under a sustained constant load taking place after the initial strain at loading" and is obtained by subtracting the initial strain due to loading from the total load-induced strain (ACI 209.1R-05, 2005). Creep strain is divided between basic creep and drying creep. Basic creep is the creep strain induced by loading a specimen that is sealed and therefore prevents moisture losses or gains. Drying creep is additional creep that occurs in

specimens that are exposed to their environment and allowed to dry. (ACI 209.1R-05, 2005)

2.2.2. Creep and Shrinkage of UHPC. Creep and shrinkage behavior of UHPC differs from normal strength concrete. The three main factors that affect this behavioral difference are the lack of coarse aggregate in UHPC, low water-cementitious material (w/cm) ratio, and curing of the material.

A study done by Loukili et al. found that due to the low w/cm ratio, the cement hydration of RPC does not increase with time because the water necessary for this is unavailable. Because of this lack of hydration, there is a high amount of unhydrated cement which allows for a high potential of "auto-healing" of the material. They also found that the curing treatment improves durability and mechanical properties because the high temperature accelerated the hydration reactions. This improves the material properties because all the free water is consumed during curing, and since there is no additional free water, the post-curing shrinkage cannot occur. This curing method dries out the core which also leads to a reduction in creep strains versus a typical curing procedure. (Loukili, Richard, and Lamirault, 1998)

2.3. IMPACT TESTING

There are many types of test set-ups for impact testing of fiber-reinforced concrete (FRC) such as drop weight tests, swinging pendulum tests, and projectile ballistics tests just to list a few testing methods. As described in a paper by Banthia in 2006, the wide range in testing methods is one reason that our understanding of impact response of concrete is still not fully understood. Banthia's paper makes comment of the wide ranges of results of similar types of materials that have been obtained using different test methods (Banthia, 2006). The research study presented in this report focuses on the use of the drop weight method for impact, and therefore the remainder of information presented will be based on similar testing.

No matter the scatter of data, some facts remain consistent when analyzing impact response of FRC. All agree that the presence of fibers increases the impact performance of the material. This is because the pull-out of the fibers from the concrete matrix during the impact absorbs more energy. The aspect ratio (length/diameter) of the fiber and the

fiber content are also factors that affect the performance of the specimen being tested. In a drop weight study done by Elavenil and Knight they show that the aspect ratio of the fibers used has a great impact on the performance of the specimens. Their results show that with an increase in fiber aspect ratio, the amount of energy required to initiate cracking and failure increases. They also show the same behavior for an increase in fiber content. (Elavenil and Knight, 2012)

A study was recently conducted by Gliha (2011) which investigated the performance of carbon fiber reinforced concrete under impact loading. This test was conducted using the drop weight method, and was conducted in the Missouri University of Science and Technology (Missouri S&T) Structural Engineering Research Laboratory (SERL) in the Civil Engineering Building. In this study, panels which were 48 in x 48 in x 2 in (1.2 m x 1.2 m x 0.05 m) thick were tested by simply supporting them on all sides on a steel frame. A 50 lb (22.7 kg) weight was dropped at increasing heights being guided to the center of the panels by use of a Polyvinyl chloride (PVC) guide pipe that was only slightly larger in diameter than the weight. Information such as drop height which caused the first crack, drop height which caused failure, impact load, and deflection were collected for each of the six specimens. Two plain unreinforced concrete panels, two concrete panels containing welded wire reinforcing (WWR), and two panels made of long carbon fiber reinforced concrete (LCFRC) were tested and compared. Results of this study showed that the plain concrete panels cracked and failed at very low impact events (15-20-in (0.4-0.5 m)), the WWR and LCFRC panels cracked at roughly the same height (24-in (0.6 m)), but the WWR panels failed at a higher drop height than the LCFRC panels (120-130-in (3.0-3.3 m), and 78-in (1.9 m) respectively). While the WWR specimens did experience failure at a height after the LCFRC panels, they also showed that in the case of an impact event, the LCFRC panels would actually be a more protective barrier. This was due to the fact that the LCFRC panels displayed much less spalling and fragmentation which would be potentially harmful to building occupants. (Gliha, 2011)

In order to compare results, the test method used in this study is the same as that used by Gliha. The testing method is documented in section 5.4 of this report.

2.4. BLAST TESTING

Limited blast testing has been documented using UHPC, however two studies were found using Ductal for blast and ballistic impact applications. One study was performed in Woomera, Australia in 2004 that examined full scale extreme explosion applications. A total of 7 specimens were tested at standoff distances of 30 m (98.4 ft), 40 m (131.2 ft), and 50 m (164.0 ft) from the explosive, and a charge of 5 tonnes of Hexolite: RDX/TNT (60:40). The panels varied in makeup and were mounted at their standoff locations in large reinforced concrete frames as shown in Figure 2.1. Some were reinforced with high strength strands, typical of Ductal, and others were left unreinforced. The panels also varied in thickness from 50 mm (1.9 in) to 100 mm (3.9 in) with the majority being 100 mm (3.9 in) thick. The results showed the panels had "extremely high ductility" reaching deflections of up to span/28 without fracture. The Ductal panels also displayed no fragmentation, even at fracture, which is highly desirable for protective blast panels because it increases the safety of the target the panel is protecting. (Rebentrost, 2006)

Figure 2.1. "Large-scale blast testing of Ductal protective panels at Woomera in 2004" (Rebentrost, 2006)

The second study was performed in England and Australia in 2005. This study used Ductal panels that were tested with close range charges. Two panels were tested in England using C4 explosive, and in Australia, one Ductal panel, and one conventional reinforced concrete panel were tested using Composition B. The test matrix is shown in Table 2.3. Panels 1 and 2 were tested in England, and panels 3 and 4 were tested in Australia.

Table 2.3. Panel details for close charge tests (Cavill, Rebentrost, and Perry, 2006)

Panel	Dimensions (m)	Material	Reinforcement	Explosive	Stand-off
1	1.0 x 1.0 x 0.1	Ductal®	High Strength Steel Strands	3 kg C-4	1.0 m
2	1.0 x 1.0 x 0.15	Ductal®	High Strength Steel Strands	5 kg C-4	0.5 m
3	1.3 x 1.0 x 0.1	Ductal®	High Strength Steel Strands	0.5 kg Comp B	0.1 m
4	1.3 x 1.0 x 0.1	Concrete (50 MPa)	N20 at 75 mm back face N20 at 150 mm front face	0.5 kg Comp B	0.1 m

Conversions: 1 m = 3.28 ft

1 kg = 2.2 lb

1 mm = 0.04-in

The results of this testing were again very favorable for the Ductal panels. Figure 2.2 was copied from the documented report, and shows the results of panels 3 and 4. This figure displays that again, the UHPC panel had sustained only minor cracking and light scabbing on the tension surface, which was classified as "structurally undamaged". Panels 1 and 2 were reported to have sustained only minor hairline cracking on the tension face as well. (Cavill, Rebentrost, and Perry, 2006)

Panel 3 (Ductal®) front surface after explosion - No cracks.

Panel 4 (conventional reinforced concrete) front surface after explosion – Slight cracks.

Panel 3 rear surface after explosion
- Very slight scabbing at surface of the panel
-Minor cracks through panel.
-Structurally undamaged.

Panel 4 rear surface after explosion
- Heavy scabbing, reinforcing bars exposed.
-Cavity approximately 480 mm x 300 mm (18.9-in x 11.8-in), with a maximum depth of 50 mm (1.9-in) (1/2 section depth).

Figure 2.2. "Test panels 3 and 4 after close charge explosion" (Cavill, Rebentrost, and Perry, 2006)

A study was recently conducted at Missouri S&T by Wulfers in 2012. This study investigated the use of high volume fly ash-wood fiber (FA-WF) and polyurea layers for blast mitigation. The idea behind this study was a combination of previous research conducted at the university by Tinsley (2007) and Carey (2012). Tinsley's research investigated the use of a FA-WF material for blast panels due to its low cost (Tinsley, 2007). Carey's research investigated the use of polyurea coating systems on concrete panels to help improve blast mitigation properties such as containing spalling and

increasing ductility (Carey, 2012). Both of these endeavors proved successful which lead to Wulfer's research in 2012.

Wulfer's research study combined recommendations from its predecessors and explored the performance of such panels as it pertained to close charge blast events. The testing was performed in the Experimental Mine on the campus of Missouri S&T and the testing was limited to two blast events. The first was equivalent to the testing done by Carey in 2012, and was a 3 lb (1.4 kg) charge of C-4 explosive, at a standoff distance of 12-in (304.8 mm). Due to the increased performance of the panels from the previous research, the second event was used at a closer standoff distance. This event was again a 3 lb (1.4 kg) charge of C-4, but instead at a standoff distance of 6-in (152.4 mm). In each case, the panels were the same depth and width, 46.5-in x 46.5-in (3.9 ft x 3.9 ft), but had varying thicknesses of SRFC and sacrificial FA-WF layers. The panels were always supported along 2 edges by wide flange steel beams that provided roughly 2.5-in (63.5 mm) of bearing on each side. (Wulfers, 2012)

The findings showed that using the FA-WF as a sacrificial layer was effective in improving performance over an equivalent panel with no sacrificial layer, and also that the polyurea coatings proved successful in improving performance by adding stiffness and reducing fragmentation of the panels. (Wulfers, 2012)

In order to compare results and performance, the blast test set-up used in this study was the same as that used by both Carey (2012) and Wulfers (2012). The specifics of the tests are presented in section 5.5 of this report.

2.4.1. Blast Prediction Software. There are many software packages available to help predict the magnitude of a blast event as well as the damage the event will impart on a system. Two that were used in this study are Conventional Weapons Effects (ConWep) and Component Explosive Damage Assessment Workbook (CEDAW) which are both available to cleared users from the United States Army Corps of Engineers Protective Design Center.

ConWep is a "collection of conventional weapons effects calculations from the equations and curves of TM 5-855-1, 'Design and Analysis of Hardened Structures to Conventional Weapons Effects'. (ConWep, 2007)" The features of ConWep used in this study include calculations of airblast effects (peak pressure and average impulse), breach,

and cratering. ConWep's results are based on a database of empirical results collected from various material testing. Due to the limited blast test data for UHPC materials, this software was not designed specifically to predict blast damage on the specimens presented in this study. The information that ConWep uses to run its airblast predictions are based on variables such as specimen geometry, support conditions, and threat information (geometry, location, charge weight, etc.) but do not account for specimen strength or reinforcement. Input information for breaching and cratering included factors such as specimen compressive strength, and threat information (location, charge weight, etc.) but do not account for specimen geometry.

CEDAW is an "Excel© based tool for the assessment of structural components subjected to airblast loads from explosives using pressure-impulse (P-i) methodology. (CEDAW, 2013)" CEDAW was designed to produce graphic curves to show the expected level of protection a structural element would provide in the event of a given threat. (CEDAW, 2013) This study utilized P-i curves generated by CEDAW to determine a number of blast tests as discussed in sections 5.5 and 6.3 of this report. CEDAW used inputs such as threat information (geometry, location, charge weight, etc.), specimen support conditions, specimen geometry, and specimen material properties such as section modulus, moment of inertia, density, and compressive strength.

3. SCOPE OF WORK

3.1. BLAST TESTING AND CONCRETE SELECTION

This research is a continuation of research conducted at Missouri S&T by Carey and Wulfers. In the previous studies, blast panels made of conventional concrete, and hybrid panels made of conventional concrete, polyurea, and fly-ash wood fiber (FA-WF) concrete were investigated. This study was aimed at determining if one could achieve similar or improved performance using either an equivalent UHPC panel, or possibly a thinner UHPC panel. In the process of exploring the effectiveness of a UHPC panel system, two other systems were investigated including a plain UHPC panel with no fibers, as well as a reduced fiber content UHPC panel to evaluate the effect the fibers play on the performance of the system. If effective, these alternate types of UHPC panels would be a cost savings over the typical UHPC composition with a 6% fiber content. The panel designation is broken down as shown in Figure 3.1 and Table 3.1 shows the testing matrix.

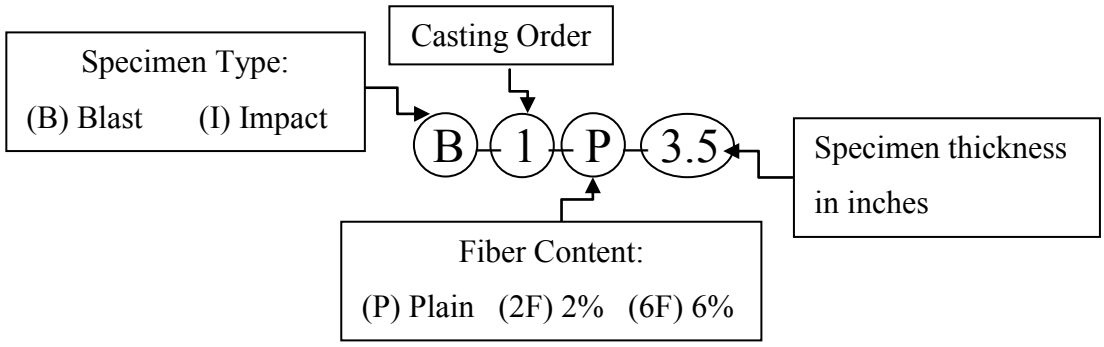

Figure 3.1. Blast and impact specimen designation

For example, the designation shown above as B-1-P-3.5 represents the first blast panel, which was a plain UHPC, 3.5-in thick panel. As shown in the blast results in

section 6.3, only one replicate of each specimen test was performed. While more replicates would have provided an improved statistical dataset, it was cost prohibitive for this study.

Rather than using a proprietary product, the research team decided to create an in-house UHPC mix design similar in nature to other commercially available products such as Ductal® by LaFarge that utilize steel fibers, cement, and fines as well as chemical and mineral admixtures. Proprietary versions of UHPC do not have the luxury of publishing the exact nature of their product. Because of this, an in-house mix design was important to the research team in order to fully describe the material that was used in this study. This mix design process is discussed further in Chapter 4 of this report.

3.2. IMPACT TESTING

The impact investigation was undertaken to compare performance of UHPC specimens to those produced in the studies conducted by Gliha (2011) at Missouri S&T. As summarized in section 2.3, Gliha's study was examining the performance of carbon fibers in impact specimens. In the current study, impact specimens of the same size were produced and tested in the same manner so that a direct comparison could be made. The testing matrix for the impact testing is also shown in Table 3.1, and the panel designations follow the same convention as the blast testing specimens explained in section 3.1. As shown in the test matrix below, one replicate of each specimen was tested for impact performance. Multiple replicates were cost prohibitive for this project.

Table 3.1. Blast and impact testing matrix

		% Fiber by Wt.	Thickness (in)	Panel Designation
Blast	Plain UHPC	0	3.5	B-1-P-3.5
	UHPC with Fibers	2	3.5	B-2-2F-3.5
	UHPC with Fibers	6	3.5	B-3-6F-3.5
	Plain UHPC	0	2	B-5-P-2
	UHPC with Fibers	2	2	B-4-2F-2
	UHPC with Fibers	6	2	B-6-6P-2
Impact	Plain UHPC	0	2	I-1-P-2
	UHPC with Fibers	6	2	I-2-6F-2

Conversion: 1-in = 25.4 mm

3.3. CREEP AND SHRINKAGE

UHPC has various curing regimes that can be used in its fabrication. Typically, the curing methods are standard ambient air curing, steam or thermal curing, and tempered curing which were described in section 2.1.4. Since Missouri S&T does not have the facilities for steam curing, a unique heat curing method was produced in which the specimens were submerged in heated water to the same temperature, and for the same duration, as the steam curing method. The goal of the creep and shrinkage monitoring was to evaluate the impact of the heat curing method on the creep and shrinkage performance of the material, as well as to investigate the impact of the addition of fibers versus the plain non-fiber UHPC mix. In addition to evaluating the curing process, this test will also be used to compare the in-house mix design with the current proprietary versions of UHPC. Figure 3.2 shows the way the creep and shrinkage specimens were named within the identification process in this study. For example, the designation shown below represents the first plain concrete specimen that was ambient air cured. The creep and shrinkage replicates are shown in the test matrix for this study in Table 3.2.

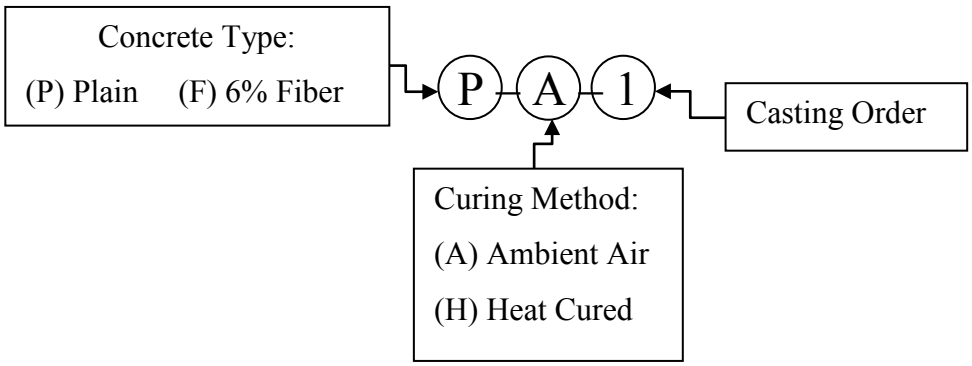

Figure 3.2. Creep and shrinkage specimen designation

Table 3.2. Creep and shrinkage test matrix

Concrete Type	Curing Method	Specimen Type	Compressive Stress Applied (lb)*	Compressive Stress Applied (psi)*	Designation
Plain	Ambient Air	Shrinkage	-	-	P-A-1
	Ambient Air	Shrinkage	-	-	P-A-2
	Ambient Air	Creep	13030	1840	P-A-3
	Heat Cured	Creep	21420	3030	P-H-1
	Heat Cured	Shrinkage	-	-	P-H-2
	Heat Cured	Shrinkage	-	-	P-H-3
6% Fiber	Ambient Air	Creep	15030	2130	F-A-1
	Ambient Air	Shrinkage	-	-	F-A-2
	Ambient Air	Shrinkage	-	-	F-A-3
	Heat Cured	Shrinkage	-	-	F-H-1
	Heat Cured	Shrinkage	-	-	F-H-2
	Heat Cured	Creep	27300	3860	F-H-3
* Creep specimens loaded to 20% of their respective compressive strengths at the day of loading					

Conversions: 1 lb = 0.45 kg

1 psi = 0.006895 MPa

4. MIX DEVELOPMENT

4.1. MATERIALS

The materials chosen for this research project were based on a 2006 publication sponsored by the U.S. Department of Transportation Federal Highway Administration entitled "Material Property Characterization of Ultra-High Performance Concrete". Chapter 2 of this report lists the typical constituent materials in UHPC as Portland Cement, Fine Sand, Silica Fume, Ground Quartz, Superplasticizer, Accelerator, Steel Fibers, and Water (Graybeal, 2006). The typical material composition is also shown in Table 2.1 found in section 2.1.2 of this report. The following discussion will address each of these materials as they pertain to this study.

4.1.1. Portland Cement. Four different types of Portland cement were tried during the course of this project and are shown in Figure 4.1. These cements were used during the mix design process discussed in section 4.2. Once a mix design was chosen, only the cement type of that mix design was used for the duration of the research project.

Type III cement was originally chosen for this study due to its small particle size and high early strength characteristics. The initial thought was that these attributes would help attain the high strength that the research team was targeting. When this approach was not achieving the desired results, a new type of cement was evaluated.

While waiting for a Type I cement with slag replacement, and a Type V cement, the trials were continued with more locally available cements. The next cement used was a Type I/II blended cement (not pictured). This choice helped the strength gain, but still fell short of the target strength. At this point, a Type I cement was used and was able to attain the target strength of 20,000 psi (137.9 MPa). Unfortunately, with the Type I/II blend, as well as the Type I cement, the flow values of the mix were low as shown in Table 4.16. This outcome lead the research trials to continue with the other cement options upon their arrival.

The first to arrive was the Type I cement with slag replacement from LaFarge. This material was chosen as an option because it is more readily available than Type V in the Midwest, and has similar characteristics due to the slag content. This cement

dramatically improved the flow characteristics of the mix over the typical Type I cement; however, the mix designs using this cement did not reach the target strength.

The next option was a Type V cement mainly due to its particle size and low C_3A content. The particle size is important because of the particle packing theory that is behind the heart of this type of concrete. Once this cement was introduced and a few small changes were made, the desired strengths were achieved and this cement was chosen for the large scale mix designs.

Figure 4.1. Cements

4.1.2. Sand. The sand used in this study was a natural Missouri River Sand shown in Figure 4.2. This material was selected as it is a local material. In order to facilitate ease of mixing, the sand (fine aggregate) was not sieved to the size shown in literature (Graybeal, 2006) however, for the small scale mixing of the trials; large chunks that would clog the mixer were removed. This approach was successful, but if the trials would not have resulted in a positive outcome, the sand would have been sieved to the size cited in the report mentioned.

Figure 4.2. Sand (i.e. Fine aggregate)

4.1.3. Silica Fume. The silica fume used in this project was a densified silica fume from Elkem Materials shown in Figure 4.3. The silica fume used in the mix is mostly used as filler that is necessary due to the particle packing nature of UHPC.

Figure 4.3. Silica fume

4.1.4. Ground Quartz. The ground quartz used for this research was "MIN-U-SIL 10, Fine Ground Silica" from Reade Advanced Materials, shown in Figure 4.4. The finely graded quartz also serves as a filler material, like the silica fume, due to the particle packing nature of UHPC. This product was chosen for its particle size which meets the literature recommendation (Graybeal, 2006).

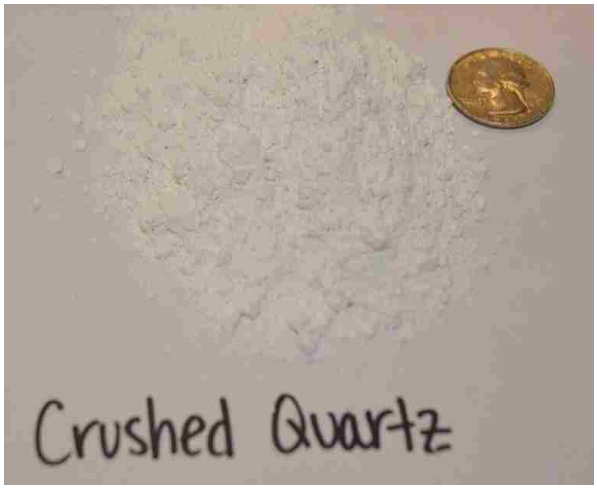

Figure 4.4. Crushed quartz

4.1.5. Admixtures. The high range water reducer (HRWR) or superplasticizer used in this study was Glenium 3030 from BASF, The Chemical Company. This was chosen based on information from the literature review. The mix design was based on a mix used by the Federal Highway Association (FHWA), which called for Glenium 3000. Upon contacting BASF, The Chemical Company, it was discovered that this product was no longer in production. The closest products were Glenium 3030 and Glenium 7500. Due to the dosing proportion and advice from the professionals at BASF, The Chemical Company, the Glenium 3030 was chosen.

The accelerator used at the beginning of the mix trials was Rheocrete CNI from BASF, The Chemical Company. After the first trial, a second trial batch was made to test a batch without the use of the accelerator to see if it was necessary. After conducting a batch without the use of accelerator, there were no observed issues with set time, and the slightly increased time to work with the material was preferred, therefore the use of the accelerator was abandoned in all subsequent mix trials.

4.1.6. Steel Fibers. Two types of steel fibers were used throughout the course of this research project. During the trial mix design phase, SF Type I fibers (low-carbon wires) made by Nycon were used, and during the full-scale specimen casting, Bekeart Corporation's Dramix OL 13/.20 fibers (high-carbon wires) were used. The goal was to use Bekeart Corporation fibers for the entire program, but due to difficulties in timing and acquiring of materials, the Nycon fibers were used so that the project could progress.

The Nycon fibers were chosen because they were the same size as the steel fibers that were trying to be replicated in these trials, and the Bekeart Corporation fibers were chosen based on information found in the literature review (Graybeal, 2006). The two types of fibers are shown in Figure 4.5 and Figure 4.6, and the properties of the fibers are shown below in Table 4.1.

Figure 4.5. Nycon fibers used in small scale trials

Figure 4.6. Bekeart fibers used in large scale specimens

Table 4.1. Fiber properties

	NYCON NEEDLES	**BEKAERT NEEDLES**
Filament Diameter	0.008 in (0.2 mm)	0.008 in (0.2 mm)
Fiber Length	0.5 in (13 mm)	0.5 in (13 mm)
Specific Gravity	7.8	7.85
Tensile Strength	285 ksi (1,900 MPa)	313 ksi (2,160 MPa)
Coating	Copper	Brass

4.2. MIX DESIGN TRIALS

A series of mix design trials were conducted to determine a mix design and curing method appropriate for this study. The goal of the research team was to achieve a mix with a compressive strength of above 20,000 psi (137.9 MPa).

4.2.1. Trial Specimens. The mix design trials were conducted using 2-in x 2-in x 2-in (50 mm x 50 mm x 50 mm) cubes. These specimens were chosen to minimize materials used, as well as for testing purposes. These specimens minimized the loads on the testing equipment, as well as are cast with already plane and smooth surfaces for testing. The molds for the trials were brass cube molds made by Forney shown in Figure 4.7, and the average compressive strength of three cube specimens was reported for each test age. It is important to note that the typical definition of 28 day concrete cylinder strength is not being used for the remainder of this report, and the ultimate compressive strengths noted from this study are based on the cube specimen strength.

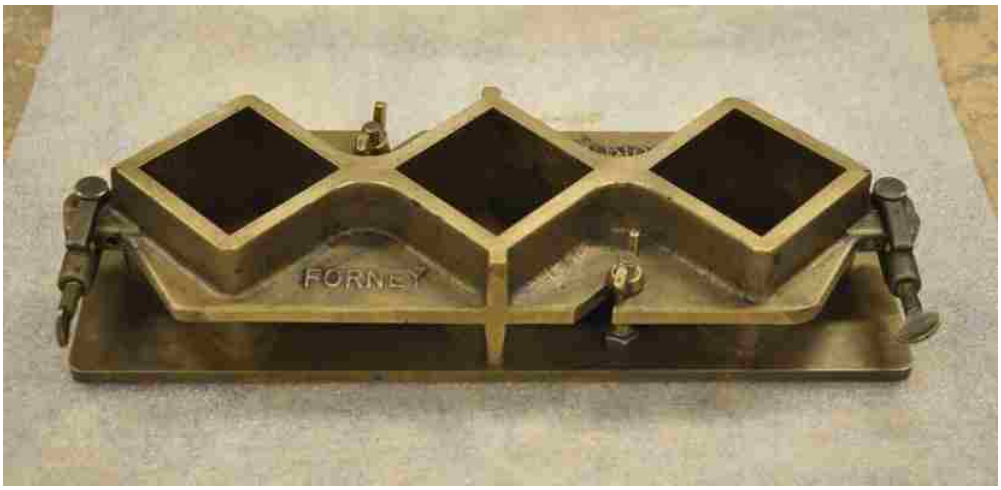

Figure 4.7. 2-in x 2-in x 2-in (50 mm x 50 mm x 50 mm) brass cube mold

4.2.2. Mix Designs. A total of 13 mix design trials were conducted until a mix design was chosen. The trials began by mimicking the typical composition shown in Table 2.1 and were slowly adjusted until the desired strength was reached. The mix combinations attempted are listed in Table 4.2 through Table 4.14 below.

The starting point for the mix design trials was to try mixing the typical UHPC mix design found in the literature review listed as Table 2.1, but without the steel fibers. The composition is shown in Table 4.2. During the first mixing process, 231 g (0.5 lb) of additional water were added in excess of what was required by the mix design to get a fluid mixture. Due to the excessive additional water, the steel fibers were not added as to not waste materials. The mixture was also not very flowable, so the cube specimens were cast while sitting atop a vibrating table to assist with consolidation. After the specimens were cast, wet rags were placed over the specimens, and they were allowed to set for 24 hours at which point they were de-molded. Once de-molded, they were allowed to continue curing in the moist cure room until testing.

Table 4.2 Trial #1 composition

Material	Amount (kg/m^3 (lb/yd^3))	Percent by Weight
Type III Cement	712 (1,200)	28.5
Fine Sand	1020 (1,720)	40.8
Silica Fume	231 (390)	9.3
Ground Quartz	211 (355)	8.4
Superplasticizer	30.7 (51.8)	1.2
Accelerator	30.0 (50.5)	1.2
Steel Fibers	N/A	0.0
Water	109 (184)	4.4

As the compressive strength gain curve shows in Figure 4.8. Compressive strength gain curve for trial #1, this mix only reached a 28 day strength of 14,600 psi (100.7 MPa), which was well below target. After meeting with a faculty member, it was

suggested to use a new type of cement (either a Type V cement, or a cement with slag replacement), as well as to immediately submerse the specimens after casting to allow them to fully hydrate. It was also suggested to attempt the mix without the use of the accelerator to allow for more time to work with the concrete before setting.

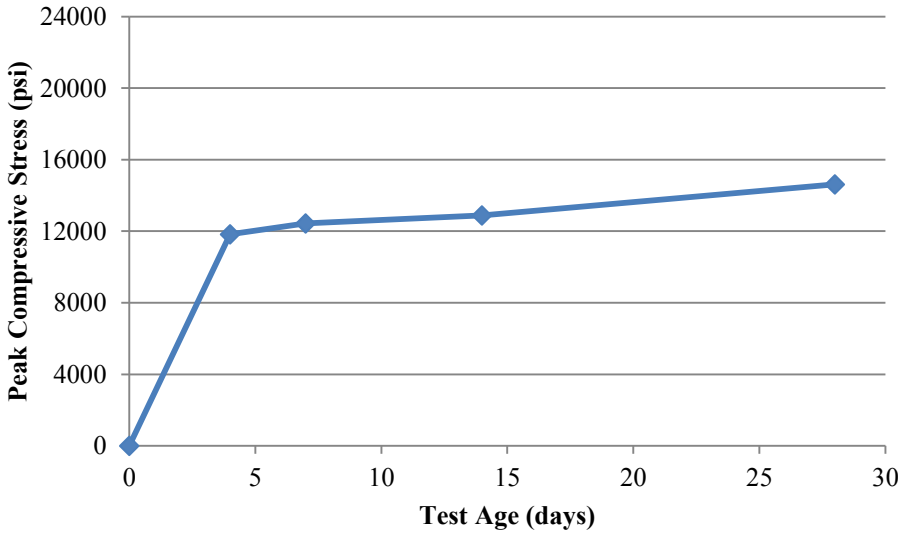

Conversion: 1 psi = 0.006895 MPa

Figure 4.8. Compressive strength gain curve for trial #1

In order to continue the trial process, the Type III cement was used until alternate cements could be obtained. The second trial composition is shown in Table 4.3. During this mixing process, 170 g (0.37 lb) of additional water were added in order to get a fluid mix. Due to the low flow of this mixture, these specimens were also cast atop the vibrating table to assist with consolidation. After specimens were cast, they were placed gently into a lime bath tank to set for 24 hours. After 24 hours, the specimens were de-molded, and submerged in a 194° Fahrenheit (90° Celsius) water tank for 72 hours to cure. As the compressive strength gain curve shows in Figure 4.9, this mix reached a 28

day strength of 16,800 psi (115.8 MPa) which was a slight improvement, but still below target.

Table 4.3. Trial #2 composition

Material	Amount (kg/m^3 (lb/yd^3))	Percent by Weight
Type III Cement	784 (1,321)	30.0
Fine Sand	1,122 (1,891)	42.9
Silica Fume	256 (431)	9.8
Ground Quartz	231 (389)	8.8
Superplasticizer	33 (56)	1.3
Accelerator	N/A	0.0
Steel Fibers	N/A	0.0
Water	190 (320)	7.3

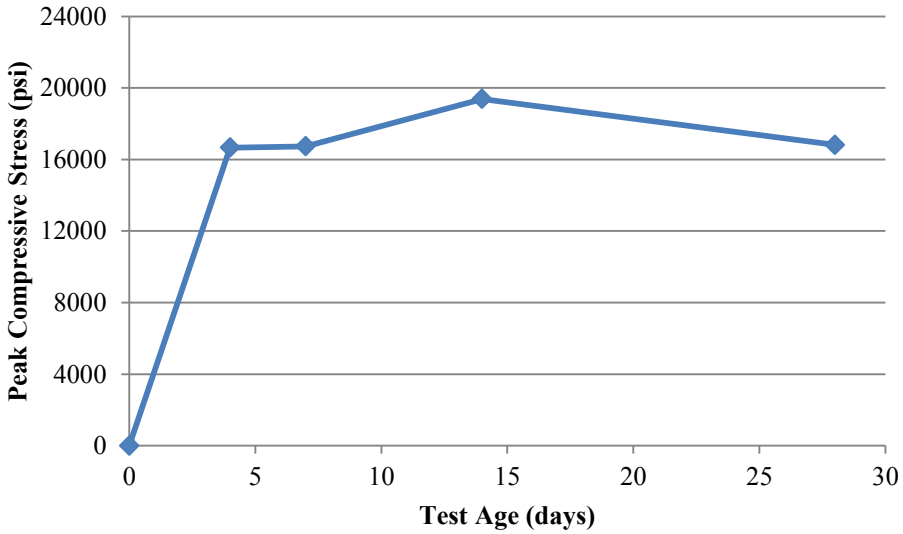

Conversion: 1 psi = 0.006895 MPa

Figure 4.9. Compressive strength gain curve for trial #2

Observing that the Type III cement was not helping obtain the targeted strength, in the third trial, a Type I/II blended Portland Cement was used. This trial's composition is shown in Table 4.4. During the mixing process, 107 g (0.24 lb) of additional water were added in order to achieve a fluid mixture. While the flow tests were more favorable, the specimens were still cast atop the vibrating table to assist with consolidation. After specimens were cast, they were placed gently into a lime bath tank to set for 24 hours. After 24 hours, the specimens were de-molded, and submerged in a 194° Fahrenheit (90° Celsius) water tank for 72 hours to cure. As the compressive strength gain curve shows in Figure 4.10, this mix reached a 28 day strength of 19,200 psi (132.4 MPa) which was another improvement, but still below target.

Table 4.4. Trial #3 composition

Material	**Amount (kg/m^3 (lb/yd^3))**	**Percent by Weight**
Type I/II Cement	784 (1,321)	30.0
Fine Sand	1,122 (1,891)	42.9
Silica Fume	256 (431)	9.8
Ground Quartz	231 (389)	8.8
Superplasticizer	33 (56)	1.3
Accelerator	N/A	0.0
Steel Fibers	N/A	0.0
Water	190 (320)	7.3

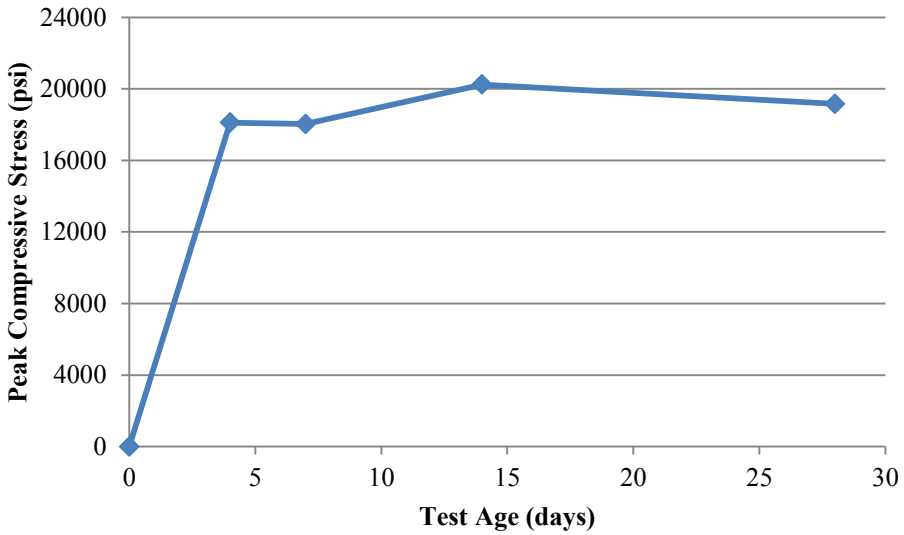

Conversion: 1 psi = 0.006895 MPa

Figure 4.10. Compressive strength gain curve for trial #3

The next cement used was a Type I Portland Cement, and the trial composition is displayed in Table 4.5. In order to achieve a fluid mixture, 104 g (0.23 lb) of additional water were added during the mixing process. This mix had lower flow values than the third trial, so again, the specimens were cast atop the vibrating table to assist with consolidation. After specimens were cast, they were placed gently into a lime bath tank to set for 24 hours. After 24 hours, the specimens were de-molded, and submerged in a 194° Fahrenheit (90° Celsius) water tank for 72 hours to cure. As the compressive strength gain curve shows in Figure 4.11, this mix reached a 28 day strength of 21,000 psi (144.8 MPa) which achieved the target strength narrowly.

Table 4.5. Trial #4 composition

Material	Amount (kg/m^3 (lb/yd^3))	Percent by Weight
Type I Cement	784 (1,321)	28.1
Fine Sand	1,122 (1,891)	40.3
Silica Fume	256 (431)	9.2
Ground Quartz	231 (389)	8.3
Superplasticizer	33 (56)	1.2
Accelerator	N/A	0.0
Steel Fibers	170 (287)	6.1
Water	190 (320)	6.8

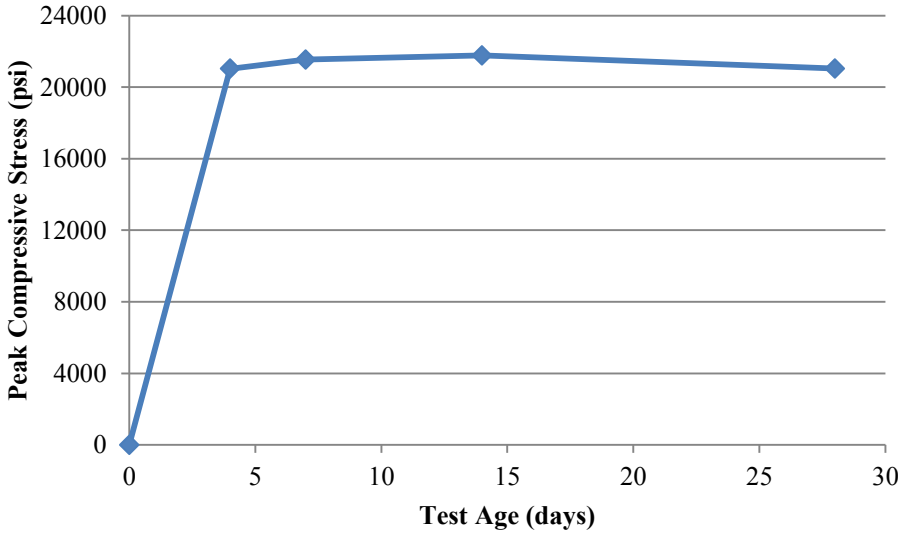

Conversion: 1 psi = 0.006895 MPa

Figure 4.11. Compressive strength gain curve for trial #4

In order to study the effect the heat curing had on the mix trial, the fifth trial had an identical mix design composition as seen in Table 4.6. In order to achieve a fluid mixture, 54 g (0.12 lb) of additional water were added during the mixing process. This mix had consistently low flow values with the previous mix, and the specimens were cast

atop the vibrating table to assist with consolidation. After specimens were cast, they were placed gently into a lime bath tank to set for 24 hours. After 24 hours, the specimens were de-molded, and placed in a moist cure room until the age of testing. As the compressive strength gain curve shows in Figure 4.12, this mix reached a 28 day strength of 15,000 psi (103.4 MPa) which was considerably below the fourth trial's strength. This demonstrated the importance of the heat curing method.

Table 4.6. Trial #5 composition

Material	Amount (kg/m^3 (lb/yd^3))	Percent by Weight
Type I Cement	784 (1,321)	30.0
Fine Sand	1,122 (1,891)	42.9
Silica Fume	256 (431)	9.8
Ground Quartz	231 (389)	8.8
Superplasticizer	33 (56)	1.3
Accelerator	N/A	0.0
Steel Fibers	N/A	0.0
Water	190 (320)	7.3

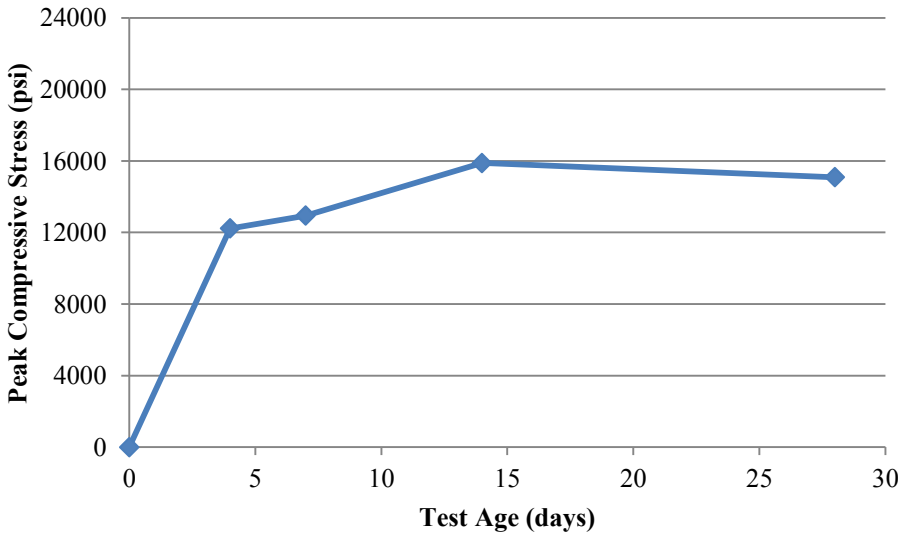

Conversion: 1 psi = 0.006895 MPa

Figure 4.12. Compressive strength gain curve for trial #5

At this point, a Type I cement with slag replacement had been obtained from Lafarge, and was therefore included in the sixth mix design trial. Since the fourth trial had been most successful to this point, the mix design was repeated using the new cement rather than the Type I cement. The mix design composition is shown in Table 4.7. During the mixing process, 100 mL (3.4 fl. oz.) of additional water were added in order to achieve a fluid mixture. This trial had much higher flow values, and therefore the use of the vibrating table deemed unnecessary. After specimens were cast, they were placed gently into a lime bath tank to set for 24 hours. After 24 hours, the specimens were de-molded, and submerged in a 194° Fahrenheit (90° Celsius) water tank for 72 hours to cure. As the compressive strength gain curve shows in Figure 4.13, this mix reached a 28 day strength of 15,100 psi (104.1 MPa) which was well below target.

Table 4.7. Trial #6 composition

Material	**Amount (kg/m^3 (lb/yd^3))**	**Percent by Weight**
LaFarge Cement	784 (1,321)	30.0
Fine Sand	1,122 (1,891)	42.9
Silica Fume	256 (431)	9.8
Ground Quartz	231 (389)	8.8
Superplasticizer	33 (56)	1.3
Accelerator	N/A	0.0
Steel Fibers	N/A	0.0
Water	190 (320)	7.3

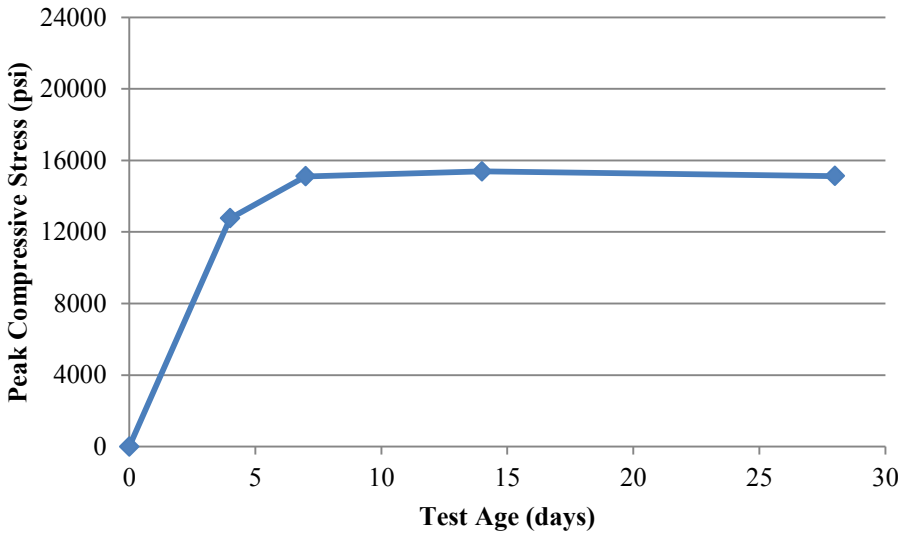

Conversion: 1 psi = 0.006895 MPa

Figure 4.13. Compressive strength gain curve for trial #6

The previous mix design was also tested with the addition of the steel fibers to determine the effect of the fibers on the compressive strength of the concrete. This seventh trial mix design is shown in Table 4.8. During the mixing process, 100 mL (3.4 fl. oz.) of additional water were added to achieve a fluid mixture. This batch had flow values that exceeded the flow table, and therefore the vibrating table was not used during casting. After specimens were cast, they were placed gently into a lime bath tank to set for 24 hours. After 24 hours, the specimens were de-molded, and submerged in a 194° Fahrenheit (90° Celsius) water tank for 72 hours to cure. As the compressive strength gain curve shows in Figure 4.14, this mix reached a 28 day strength of 19,400 psi (133.7 MPa) which was close to the target strength, but still under.

Table 4.8. Trial #7 composition

Material	Amount (kg/m^3 (lb/yd^3))	Percent by Weight
LaFarge Cement	799.7 (1,348)	27.6
Fine Sand	1,145.0 (1,930)	39.5
Silica Fume	261.0 (440)	9.0
Ground Quartz	235.5 (397)	8.1
Superplasticizer	33.8 (57)	1.2
Accelerator	N/A	0.0
Steel Fibers	173.8 (293)	6.0
Water	246.8 (416)	8.5

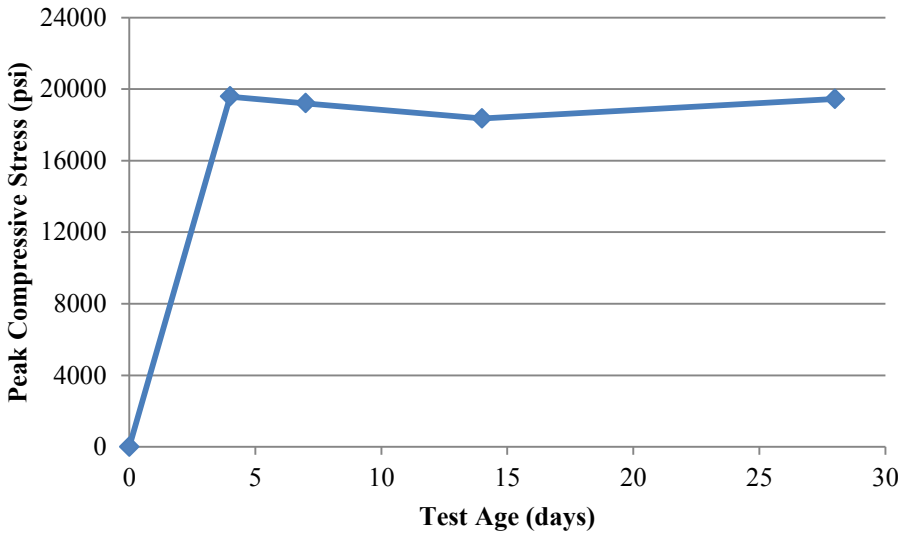

Conversion: 1 psi = 0.006895 MPa

Figure 4.14. Compressive strength gain curve for trial #7

The seventh trial was repeated to study if the mix design was getting consistent results. The mixing process and curing process were identical, and the composition has been displayed as Table 4.9. As the compressive strength gain curve shows in Figure 4.15, this mix reached a 28 day strength of 17,400 psi (119.9 MPa) which was well below target, and inconsistent with the strengths achieved with trial #7.

Table 4.9. Trial #8 composition

Material	Amount (kg/m^3 (lb/yd^3))	Percent by Weight
LaFarge Cement	799.7 (1,348)	27.6
Fine Sand	1,145.0 (1,930)	39.5
Silica Fume	261.0 (440)	9.0
Ground Quartz	235.5 (397)	8.1
Superplasticizer	33.8 (57)	1.2
Accelerator	N/A	0.0
Steel Fibers	173.8 (293)	6.0
Water	246.8 (416)	8.5

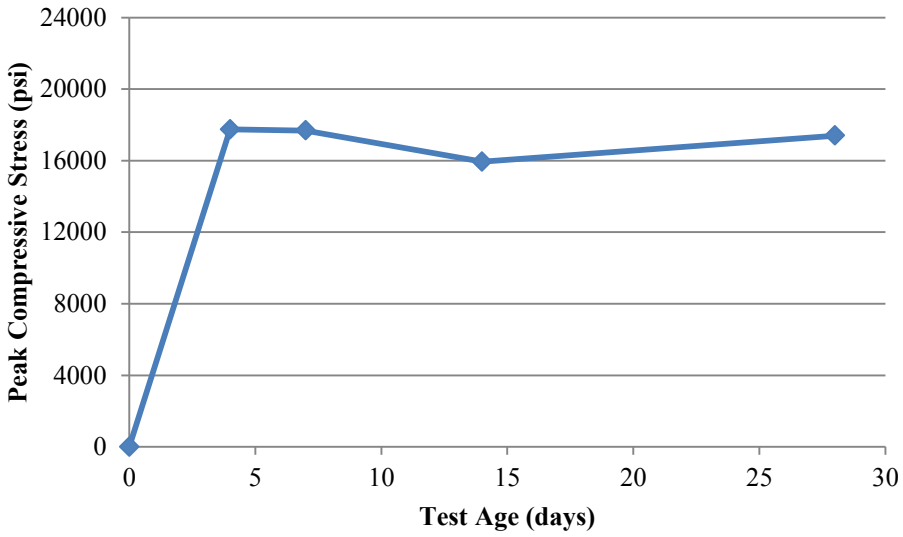

Conversion: 1 psi = 0.006895 MPa

Figure 4.15. Compressive strength gain curve for trial #8

At this point, Type V Portland cement had been obtained from Lehigh Cement, and was therefore included in the ninth mix design trial. Also since in all trials, excess water had to be added to achieve a fluid mix, and in trials #6 through trial #8, consistently 100 mL (3.4 fl. oz.) of excess water had to be added during the mixing process, this 100 mL (3.4 fl. oz.) amount was added into the mix design. The adjusted mix design is

shown in Table 4.10 below. As shown in the table, due to the new cement type and added water in the mix design, fibers were omitted from this trial to avoid potentially wasting fiber material. This trial batch turned out to be very soupy, and once again exceeded the flow table, so the vibrating table was not used during casting. After specimens were cast, they were placed gently into a lime bath tank to set for 24 hours. After 24 hours, the specimens were de-molded, and submerged in a 194° Fahrenheit (90° Celsius) water tank for 72 hours to cure. As the compressive strength gain curve shows in Figure 4.16, this mix only reached a 28 day strength of 10,000 psi (68.9 MPa) which was well below target.

Table 4.10. Trial #9 composition

Material	Amount (kg/m^3 (lb/yd^3))	Percent by Weight
Type V Cement	771.3 (1,300)	28.4
Fine Sand	1,104.1 (1,861)	40.6
Silica Fume	251.5 (424)	9.3
Ground Quartz	227.2 (383)	8.4
Superplasticizer	32.6 (55)	1.2
Accelerator	N/A	0.0
Steel Fibers	N/A	0.0
Water	332.2 (560)	12.2

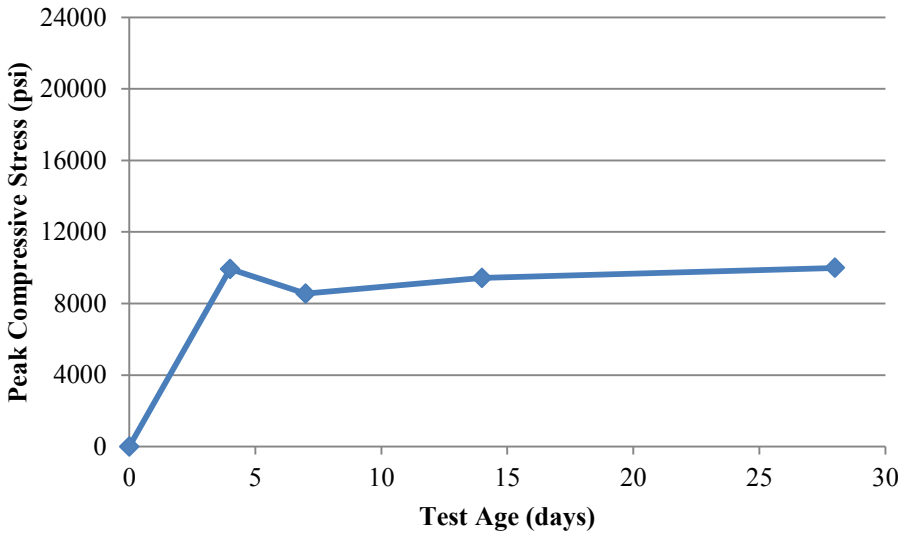

Conversion: 1 psi = 0.006895 MPa

Figure 4.16. Compressive strength gain curve for trial #9

For this trial, three 3-in x 6-in (76.2 mm x 152.4 mm) cylinders were also made to investigate the size effect between the cubes and a cylinder. The cylinders were hand ground using a Kobalt Rub Brick shown in Figure 4.17 to create a smooth surface for testing. When tested, their strengths were 6,650 psi (45.8 MPa), 8,430 psi (58.1 MPa), and 3,564 psi (24.6 MPa), which were highly inconsistent, and much lower than the tested cube strength. The research team attributed these values to the way the cylinders were ground before testing.

Figure 4.17. Kobalt Rub Brick

Due to the soupy nature of the previous trial, the tenth mix design was adjusted to take out the additional water that was added to the mix design. Again, Type V cement was used, and the composition is shown in Table 4.11. During the mixing process, 50 g (0.11 lb) of additional water had to be added to achieve a fluid mix. The mix had high flow values, so once again, the vibrating table was omitted from the casting process. Once the specimens were cast, they were placed gently into a lime bath tank to set for 24 hours. After 24 hours, the specimens were de-molded, and submerged in a 194° Fahrenheit (90° Celsius) water tank for 72 hours to cure. As the compressive strength gain curve shows in Figure 4.18, this mix reached a 28 day strength of 16,700 psi (115.1 MPa) which was below target, but an improvement from the ninth trial.

Table 4.11. Trial #10 composition

Material	Amount (kg/m^3 (lb/yd^3))	Percent by Weight
Type V Cement	730.9 (1,232)	29.8
Fine Sand	1,045.9 (1,763)	42.7
Silica Fume	238.5 (402)	9.7
Ground Quartz	215.4 (363)	8.8
Superplasticizer	30.8 (52)	1.3
Accelerator	N/A	0.0
Steel Fibers	N/A	0.0
Water	189.8 (320)	7.7

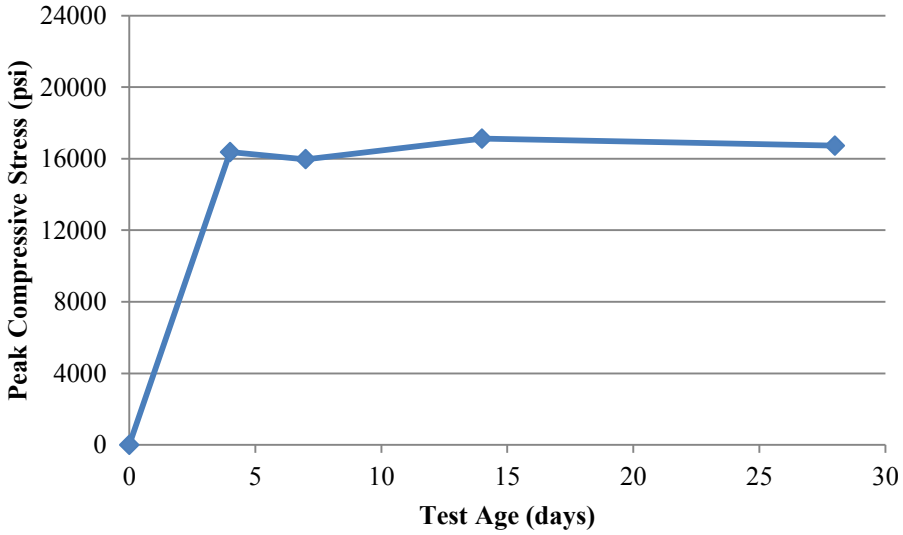

Conversion: 1 psi = 0.006895 MPa

Figure 4.18. Compressive strength gain curve for trial #10

For the eleventh trial, the 50 g (0.11 lb) of additional water added in the previous trial was added into the mix design, as well as the addition of steel fibers. Table 4.12 shows the adjusted design values. No additional water was added during the mixing process, and the material had high flow values as desired. Once the specimens were cast,

they were placed gently into a lime bath tank to set for 24 hours. After 24 hours, the specimens were de-molded, and submerged in a 194° Fahrenheit (90° Celsius) water tank for 72 hours to cure. As the compressive strength gain curve shows in Figure 4.19, this mix reached a 28 day strength of 22,400 psi (154.4 MPa) which met the trial target.

Table 4.12. Trial #11 composition

Material	Amount (kg/m^3 (lb/yd^3))	Percent by Weight
Type V Cement	785.5 (1,324)	27.8
Fine Sand	1,124.9 (1,896)	39.8
Silica Fume	256.3 (432)	9.1
Ground Quartz	231.4 (390)	8.2
Superplasticizer	33.2 (56)	1.2
Accelerator	N/A	0.0
Steel Fibers	170.9 (288)	6.0
Water	226.6 (382)	8.0

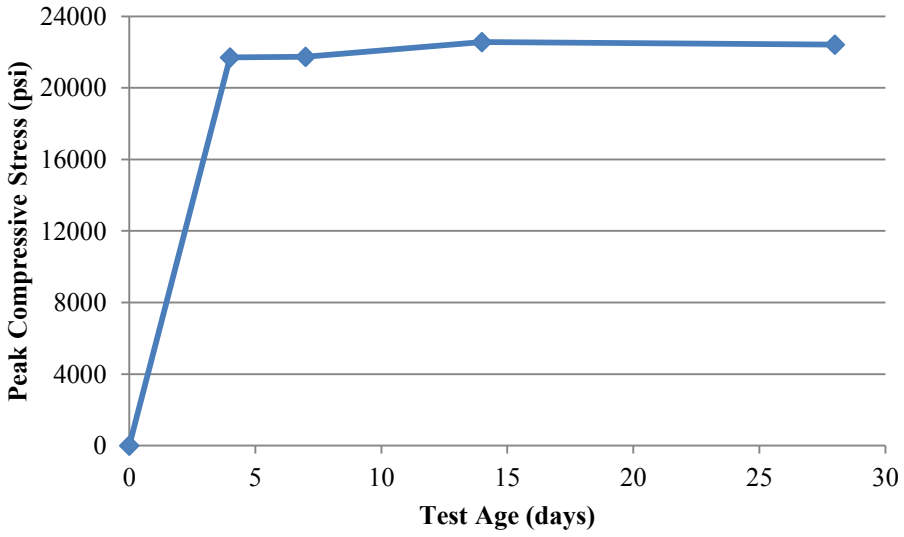

Conversion: 1 psi = 0.006895 MPa

Figure 4.19. Compressive strength gain curve for trial #11

For this trial, one 3-in x 6-in (76.2 mm x 152.4 mm) cylinder was also made to once again investigate the size effect between the cubes and a cylinder. This time, the cylinder was ground with the end grinder shown in Figure 4.20 rather than the hand grinder used in trial #9.

Figure 4.20. Cylinder end grinder

Using the end grinder, the cylinder performed equivalently to the cubes, which allowed the research team to continue use of the cube specimens to measure compressive strength in all subsequent testing. Due to the success of this mix design, it was selected for the full scale specimens.

For the next trial, the effect of heat curing was again explored using the same mix design as in trial #11. The composition is shown in Table 4.13. No additional water was added during the mixing process, and the material had the same flow values that were measured in trial #11, which demonstrated consistency. Once the specimens were cast, they were placed gently into a lime bath tank to set for 24 hours. After 24 hours, the

specimens were de-molded, and placed in the moist cure room until the age of testing. As the compressive strength gain curve shows in Figure 4.21, this mix only reached a 28 day strength of 16,000 psi (110.3 MPa) which was considerably below the eleventh trial's strength. This again demonstrated the importance of the heat curing method.

Table 4.13. Trial #12 composition

Material	Amount (kg/m^3 (lb/yd^3))	Percent by Weight
Type V Cement	785.5 (1,324)	27.8
Fine Sand	1,124.9 (1,896)	39.8
Silica Fume	256.3 (432)	9.1
Ground Quartz	231.4 (390)	8.2
Superplasticizer	33.2 (56)	1.2
Accelerator	N/A	0.0
Steel Fibers	170.9 (288)	6.0
Water	226.6 (382)	8.0

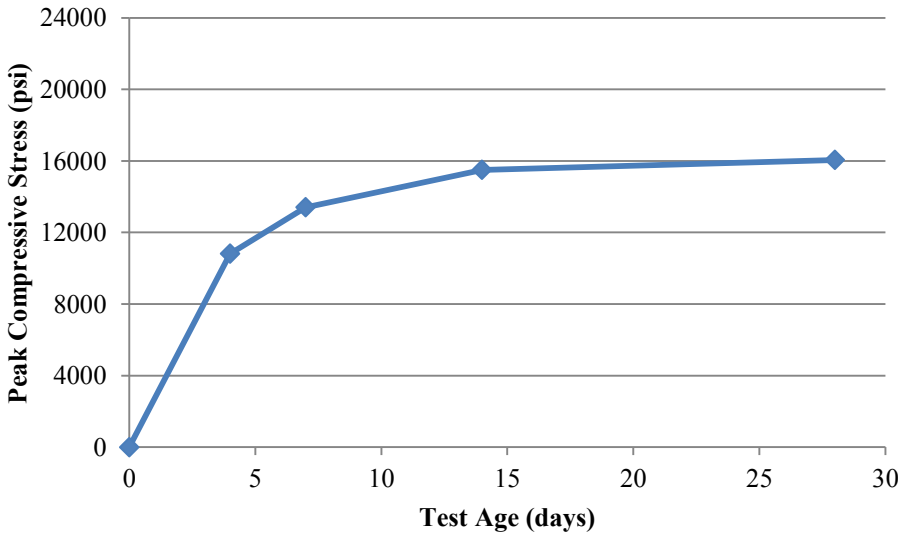

Conversion: 1 psi = 0.006895 MPa

Figure 4.21. Compressive strength gain curve for trial #12

After the first full scale test was made using a conventional concrete mixer, the research team decided to try a mortar mixer for the subsequent full scale specimens. Since mortar mixers typically have a reversed mixing order, beginning with the water and slowly adding in the cementitious materials, final trial batch was conducted to investigate the reverse mixing order as well as to prove that it would not have an impact on the material properties. As shown in Table 4.14, the mix composition and curing method for this trial is the same as trial #11 which was selected for full scale batching. The mixing process was successful, and not seen as a problem to apply to full scale mixing with a mortar mixer. This mix reached a 4 day strength of 22,200 psi (153.1 MPa) which met the trial target and was consistent with trial #11.

Table 4.14. Trial #13 composition

Material	Amount (kg/m^3 (lb/yd^3))	Percent by Weight
Type V Cement	785.5 (1,324)	27.8
Fine Sand	1,124.9 (1,896)	39.8
Silica Fume	256.3 (432)	9.1
Ground Quartz	231.4 (390)	8.2
Superplasticizer	33.2 (56)	1.2
Accelerator	N/A	0.0
Steel Fibers	170.9 (288)	6.0
Water	226.6 (382)	8.0

4.2.3. Mixing Process. For trials #1-#12, the same mixing procedure was used, and in all trials, a 20 quart (19 L) Hobart stand mixer, shown in Figure 4.22 was used for the mixing. To begin, all material quantities were batched into small pans and 75% of the superplasticizer was added to the water. Next, the dry materials were all poured into the mixing bowl, and the mixer was started to combine the materials until homogeneous. The water and superplasticizer combination was then added to the dry materials, and the mixer was allowed to mix for five (5) minutes at which time, the final 25% of the

superplasticizer was added. Once all the ingredients were included, the mixer was allowed to run until fluid. When the water was added, the material appeared to remain dry with a few small clumps. After roughly ten (10) minutes, the material started to ball into small beads.

Figure 4.22. Hobart 20 qt. (19 L) mixer

After five (5) more minutes, the mixture began to look like bread dough, and within another two to five (2-5) minutes, the material became a fluid cementitious material. Once the concrete was fluid, if the trial called for steel fibers, they were slowly metered in to prevent clumping (although most clumps dissipated voluntarily even when large amounts were added accidentally). Once the fibers were added, the mixer was allowed to mix for an additional five (5) minutes. The phases of mixing are shown in Figure 4.23

(a) Dry powder (Stage 1) (b) Small beads (Stage 2)

(c) Dough like (Stage 3) (d) Fluid (Stage 4)

Figure 4.23. Stages of mixing

For trial #13, a reverse mixing order was used to simulate the mixing process of a mortar mixer rather than a typical concrete mixer. The reason for this is discussed further in section 5.4.2 of this report. To begin, all the materials were batched into small pans, and then the dry materials were mixed together into a larger pan until homogenous. As before, 75% of the superplasticizer was combined with the water and this mixture was added to the mixing bowl. The mixer was turned on and the dry materials were slowly added to the mixer, making sure to keep a fluid mix. After roughly 2/3 of the dry mixture had been added, the remaining 25% of the superplasticizer was added. After all the

powders were fully integrated, the steel fibers were added in the same manner as mentioned in trials #1-#11.

4.2.4. De-molding and Curing. All cube specimens were de-molded after 24 hours. To de-mold the specimens, the top of the form was detached from the bottom by removing the vertical clamps and lifting off the bottom plate. Next, the end clamps that held the top together were loosened, and the two pieces were separated using a small metal spatula. After this point, the concrete cubes were slid out of the forms and set aside to cure.

Three curing regimes were tested in the mix trial process. The first curing method was to allow a wet rag to sit atop the freshly cast specimens for 24 hours at room temperature. After 24 hours, the specimens were de-molded and put into a moist cure room until testing.

The second curing method was to immediately submerge the freshly cast specimens into a room temperature lime water bath for the first 24 hours. After 24 hours, the specimens were de-molded, and placed in a moist cure room until testing.

The final curing method was to immediately submerge the freshly cast specimens into a room temperature lime water bath for 24 hours. After 24 hours, the specimens were de-molded, and submerged in a hot water bath heated to 194° Fahrenheit (90° Celsius) for 72 hours. The small scale hot water bath is shown in Figure 4.24. After the heat bath, the specimens were placed in a moist cure room until testing.

Figure 4.24. Heat curing tank used for small scale curing

The third curing method proved to be the most beneficial to the concrete strength being targeted, therefore a similar curing method was used for the full scale specimens.

4.2.5. Strength Testing. Trial mix design specimens were cast and tested in accordance with ASTM C109, "Standard Test Method for Compressive Strength of Hydraulic Cement Mortars (Using 2-in. or [50-mm] Cube Specimens)". They were tested at ages of 4 days, 7 days, 14 days, and 28 days to get a representative strength gain curve for each mix design attempted. Cubes were tested in Missouri S&T's 200,000 lb (90.7 ton) capacity Tinius-Olsen machine with PC station. The test set-up is shown below in Figure 4.25. The loading rate was 200 psi/second (1.38 MPa/second). A summary of trial specimen strengths is included in Table 4.15. Each compressive strength shown is an average of three cube specimens that were tested at each test age.

Figure 4.25. Mix trial compression test setup

Table 4.15. Summary of mix trial compressive strengths

	Compressive Strength (psi)			
	4 day	7 day	14 day	28 day
Trial #1	11,830	12,430	12,880	14,620
Trial #2	16,660	16,730	19,380	16,820
Trial #3	18,110	18,040	20,240	19,160
Trial #4	21,030	21,540	21,770	21,040
Trial #5	12,230	12,940	15,890	15,090
Trial #6	12,760	15,110	15,380	15,130
Trial #7	19,580	19,200	18,360	19,440
Trial #8	17,740	17,680	15,940	17,390
Trial #9	9,930	8,550	9,430	9,990
Trial #10	16,370	15,970	17,120	16,730
Trial #11	21,700	21,740	22,560	22,420
Trial #12	10,820	13,410	15,500	16,050

Conversion: 1 psi = 0.006895 MPa

4.2.6. Flow. Flow tests were conducted during the mix trial portion of this study in accordance with ASTM C1437, “Standard Test Method for Flow of Hydraulic Cement Mortar”. This test was run to ensure the trial mixes were getting adequate flow values to make sure the mix would work for full scale casting. The equipment used for this testing is shown in Figure 4.26 and the flow measurements taken during each mix trial are displayed in Table 4.16.

Figure 4.26. Flow testing equipment

Table 4.16. Trial mix flow values

	Caliper Reading				
	1	2	3	4	**Flow (%)**
Trial #1	17	14	16	14.5	**61.5**
Trial #2	15	15	14.5	15.5	**60**
Trial #3	27	28	29	26	**110**
Trial #4	19	19.5	20	20	**78.5**
Trial #5	19	21	21	20	**81**
Trial #6	32	33	33	35	**133**
Trial #7	Exceeded table				
Trial #8	25	26	25	27	**103**
Trial #9	Exceeded table				
Trial #10	31.5	31	31	32	**125.5**
Trial #11	30	31	30.5	31.5	**123**
Trial #12	31	32	30	30.5	**123.5**
Trial #13	32	30	29	31	**122**

5. EXPERIMENTAL PROGRAM

5.1. CURING METHOD

5.1.1. Curing Tank Construction. An original curing tank had to be constructed for this project that was large enough to heat cure the impact and blast panel specimens. The tank was built using plywood, 2-in x 6-in (38 mm x 140 mm) lumber, blue board rigid insulation, silicone, and a rubber roof liner. To begin, the plywood base was attached to the bottom row of 2-in x 6-in (38 mm x 140 mm) boards through the bottom using screws. Next, the second row of 2-in x 6-in (38 mm x 140 mm) boards were toe-nailed into the first row to create the shell of the box. Supporting 2-in x 4-in (38 mm x 89 mm) boards were then attached to the outside of the box, two per side. 1-in (25.4 mm) thick blue board rigid foam insulation was also attached to the inside of the box on both the bottom and sides using the adhesive product, Liquid Nails. Once placed, all seams and edges of the insulation were filled with silicone to create a water-tight seal. Because the water inside the tank needed to be heated, a rubber roof liner was laid inside the box to both add to the water-tight characteristics of the tank, and to resist the heat during curing. The box was also filled with water and heated in a trial curing process to check for potential leaking prior to use.

Once the box had been constructed and tested, it needed to be connected to the heat source and pump that would circulate the water. The heat source was a residential Whirlpool hot water heater. All the plumbing used for the connections was chlorinated polyvinyl chloride (CPVC) pipe. On the suction side of the line, 1-in (25.4 mm) CPVC was used, and on the inlet side, 0.75-in (19.1 mm) CPVC was used. In order to create good and even flow throughout the tank, on the inlet side, 4 tees and 1 elbow distributed the flow along the length of the box, and on the suction side, 2 elbows were used to bring water back to the pump. In order to increase the efficiency of the heating system, the pipes were also wrapped in foam insulation tubing.

In order to control the heat of the water, a thermocouple was installed into the inlet side of the plumbing line. It was monitored by a control box and a mechanical relay that read the temperature in the line, and using that information, controlled the heating

elements in the hot water heater. The pump and control box are pictured in Figure 5.1 and Figure 5.2 respectively.

Figure 5.1. Pump used to circulate water in full scale curing system

Figure 5.2. Temperature control box for full scale specimen curing system

Finally, in order to contain the heat and steam, a lid had to be fabricated for the box. The lid was constructed using plywood and blue board foam insulation. The foam was attached to the plywood using both Liquid Nails, as well as wood screws. Due to the large span of the tank, a 2-in x 4-in (38 mm x 89 mm) board had to be toenailed into the top of the plywood in order to keep the lid from sagging. In addition, since the smaller specimens would have to be placed in, and removed from the box once the panel was curing, the lid had a hinged smaller portion to allow for easy access. The hinged side had a rebar handle. The curing box was built and operated in the Missouri S&T Structural Engineering Research Laboratory (SERL) as shown in Figure 5.3.

Figure 5.3. Full scale curing system

5.1.2. Curing Tank Operation. The curing tank was turned on the morning of each panel specimen casting date in order to allow the water to reach a steady temperature of 194 °F (90° C) by the time of de-molding. Once the tank was heating, the lid was also in place to help insulate the tank and assist the heating process. Once a panel

was de-molded, the lid was removed (using gloves to protect from steam) and set aside to allow for the panel to be added to the hot water. Once the panel was in place atop 4 bricks to allow water to readily access the bottom side of the panel, the lid was placed back on top of the box. Next, the matching specimens for property testing were de-molded and placed into the water next to the panel via the hinged lid and a pair of tongs to lower the specimens into the water. The specimens remained in the water for a total of 72 hours (3 days) to be consistent with the curing method used in the mix design process, and at that time, the tank was turned off, and the lid was opened to allow for the water to begin cooling. Once the water cooled to room temperature, the specimens were removed from the water and stored nearby in the Missouri S&T SERL until they were ready to be moved to the Missouri S&T Experimental Mine for testing. When the tank was in operation or during the cooling process, caution tape was placed around the tank to keep other workers in the lab safe from the potential of escaping steam.

5.2. MECHANICAL PROPERTIES

For consistency among tests, the same testing machine was used for all properties specimens. The machine used was the 200,000 pound (90.7 ton) Tinius-Olsen machine (shown in Figure 4.25) located in the Load Frame Laboratory in Butler-Carlton Hall at Missouri S&T. All specimens were covered with a wet burlap cloth after casting for the first 24 hours. After 24 hours, the specimens were de-molded and cured in the same manner as their respective panel specimens.

5.2.1. Compressive Strength. Compression specimens were cast and tested in accordance with ASTM C109, “Standard Test Method for Compressive Strength of Hydraulic Cement Mortars (Using 2-in. or [50-mm] Cube Specimens)”. They were tested at ages of 4 days, 28 days, and the day of the corresponding panel testing.

2-in x 2-in x 2-in (50 mm x 50 mm x 50 mm) cubes were chosen due to the capacity of the testing equipment, as well as the practicality of the specimen in relation to testing the material. Using a standard 4-in x 8-in (101.6 mm x 203.2 mm) cylinder would have demanded too high of a load from the testing equipment. In addition, due to the strength of the material, capping methods could not be used. This fact would have forced the ends of cylinder specimens to be ground plane for testing. In order to lessen the

demand on the grinding machine and the testing equipment, the cubes were chosen. When cast, these specimens already have plane edges that do not need to be ground, and they could be tested safely within the range of the machine. The following Figure 5.4 shows the various types of cube molds that were used during this project.

Figure 5.4. Cube molds

The brass molds were used when possible, however on a few occasions, more specimens were being made in a day than there were brass molds. In the event that this happened, either the steel molds, or plastic molds were used to supplement the brass molds.

Compression specimens were tested in the Tinius Olsen in the Load Frame Room at Missouri S&T. The testing configuration was as shown in Figure 5.5, and the loading rate was 200 lb/second (90.7 kg/s). The compressive strengths for the corresponding panel specimens are listed in Table 5.1.

Figure 5.5. Compression test set-up

Table 5.1. Summary of specimen compressive strengths at test age

	Specimen	% Fiber by Wt.	Thickness (in)	Compressive Strength at Test Age (psi)
Blast	B-1-6F-3.5	6	3.5	22,660
	B-2-P-3.5	0	3.5	N/A
	B-3-2F-3.5	2	3.5	19,700
	B-4-2F-2	2	2	21,450
	B-5-P-2	0	2	18,150
	B-6-6F-2	6	2	20,900
Impact	I-1-P-2	0	2	16,120
	I-2-6F-2	6	2	23,640

Conversion: 1 psi = 0.006895 MPa

1 in = 25.4 mm

5.2.2. Splitting Tensile Strength. Splitting tensile specimens used for this study were cast and tested in accordance with ASTM C496, “Standard Test Method for Splitting Tensile Strength of Cylindrical Concrete Specimens” with the exception that

they were 3-in x 6-in (76.2 mm x 152.4 mm) cylinders rather than 4-in x 8-in (101.6 mm x 203.2 mm). These smaller specimens were chosen due to the loading capabilities of the testing equipment. They were tested at 28 days, and the day of the corresponding panel testing. The 3-in x 6-in cylinder mold is shown in Figure 5.6.

Figure 5.6. Splitting tensile specimen mold

Splitting tensile specimens were tested in the Tinius Olsen in the Load Frame Room at Missouri S&T. The testing configuration was as shown in Figure 5.7, and the loading rate was 60 lb/second (27.2 kg/s). The tensile properties for the corresponding panel specimens are listed in Table 5.2.

Figure 5.7. Splitting tensile test setup

Table 5.2. Splitting tensile strength of specimens at test age

	Specimen	% Fiber by Wt.	Thickness (in)	Splitting Tensile Strength at Test Age (psi)
Blast	B-1-6F-3.5	6	3.5	2,840
	B-2-P-3.5	0	3.5	N/A
	B-3-2F-3.5	2	3.5	2,080
	B-4-2F-2	2	2	2,270
	B-5-P-2	0	2	1,190
	B-6-6F-2	6	2	2,330
Impact	I-1-P-2	0	2	860
	I-2-6F-2	6	2	2,710

Conversion: 1 psi = 0.006895 MPa

1 in = 25.4 mm

5.2.3. Modulus of Elasticity. Modulus of elasticity specimens used for this study were cast and tested in accordance with ASTM C469, "Standard Test Method for Static Modulus of Elasticity and Poisson's Ratio of Concrete in Compression", and the cylinder mold is shown in Figure 5.8.

Figure 5.8. Modulus of elasticity specimen mold

Modulus of elasticity specimens were tested in the Tinius Olsen in the Load Frame Room at Missouri S&T. Due to the fact that capping compounds do not meet the strength required for this test, the ends of the cylinders were ground smooth and plane using an end grinder. The testing configuration was as shown in Figure 5.9, and the loading rate was 500 lb/second (227 kg/s). The modulus properties for the corresponding panel specimens are listed in Table 5.3.

Figure 5.9. Modulus of elasticity test setup

Table 5.3. Material properties summary of specimens at test age

		Test Age Properties		
	Specimen	Compressive Strength (psi)	Tensile Strength (psi)	Modulus of Elasticity (psi)
Blast	B-1-6F-3.5	22,660	2,840	5,975,000
	B-2-P-3.5	N/A	N/A	N/A
	B-3-2F-3.5	19,700	2,080	5,766,670
	B-4-2F-2	21,450	2,270	5,850,000
	B-5-P-2	18,150	1,190	5,466,670
	B-6-6F-2	20,900	2,330	5,450,000
Impact	I-1-P-2	16,120	860	5,200,000
	I-2-6F-2	23,640	2,710	5,716,670

Conversion: 1 psi = 0.006895 MPa

5.3. CREEP AND SHRINKAGE SPECIMEN FABRICATION AND TESTING PROCEDURE

Creep and shrinkage behavior were determined by following modified versions of ASTM C512, "Standard Test Method for Creep of Concrete in Compression" and ASTM C157, "Standard Test Method for Length Change of Hardened Hydraulic-Cement Mortar and Concrete" respectively. The specimen fabrication, preparation, and data acquisition methods are described in the sub-sections that follow.

5.3.1. Creep and Shrinkage Molds. The creep and shrinkage specimens used in this study were made using 4-in (101.6 mm) diameter PVC pipe attached to a plywood base using silicon. The PVC was cut to 18-in (0.46 m) lengths, and notched on opposite sides to aid in the de-molding process. The notch was cut just shy of the wall thickness of the pipe.

5.3.2. Creep and Shrinkage Casting. Creep and shrinkage specimens were cast using a modified version of ASTM C31, “Standard Practice for Making and Curing Concrete Test Specimens in the Field”. The mold was filled with three lifts, rather than two. Each lift was rodded 25 times, and tapped to allow air to escape. Once filled, the specimens were left slightly over-filled. This allowed for slight settlement and also ensured that the grinding process would not decrease the overall height of the specimen. The specimens were allowed to cure under wet burlap until de-molding.

5.3.3. Creep and Shrinkage De-Molding and Preparation. The creep and shrinkage specimens were de-molded 24 hours after casting. First, the specimen was removed from the plywood base. A dremmel was then used to cut through the remainder of the notch and a screwdriver was used to wedge the pipe apart. Once the specimens were de-molded, the ends were ground to a smooth and plane condition using the cylinder end grinder shown in Figure 4.20.

Before readings could be taken, or curing began, the specimens needed to be instrumented with DEMEC points to facilitate strain readings. First, the specimens were outfitted with DEMEC points using a high strength, rapid setting adhesive manufactured by LOCTITE. The points on the specimens that were marked for the heated bath curing, were then further protected using epoxy to ensure they would not detach during the curing process. Each specimen was equipped with 3 columns of DEMEC points, each

column 120 degrees apart, and each column consisted of 5 points, for a total of 15 DEMEC points per specimen.

5.3.4. Specimen Curing. This study was also to focus on the effects of heat curing on the creep and shrinkage behavior of this material. To do this, one specimen of each concrete type was placed in the basement of the high-bay, and the other two (2) specimens of each concrete type were placed in the hot water bath to cure. Cubes and cylinders for testing material properties were match cured with their respective creep and shrinkage specimens until the age of testing.

5.3.5. Creep Specimen Loading. The creep specimens were loaded at an age of four (4) days. This was chosen because UHPC that is cured in the recommended method (a steam or heat bath) has reached its target strength by this age which means that in a field application, the concrete could be loaded by this time. Due to the high strength of the concrete when heat cured, the creep frames at Missouri S&T were not capable of loading the specimens to the specified 40% of the compressive strength at age of loading. Therefore, the specimens were loaded to only 20% of the compressive strength. In order to evaluate the effects of curing, as well as fiber addition, all specimens were loaded at the same age (4 days), and to 20% of their respective concrete strengths at the time of loading. Pictures of the loading process are shown in Figure 5.10.

Figure 5.10. Loading of creep specimen

5.3.6. Data Acquisition. A digital DEMEC gauge was used to record strain readings that were taken daily for one week, weekly for one month, and then at monthly intervals. As described in section 5.3.3, each specimen had a total of 15 DEMEC points, applied in three columns of five points per column. This configuration resulted in nine readings per specimen, per day. The average of these readings was used to create the figures that display the creep and shrinkage results in section 6.1. Strain readings were taken daily on all specimens until four (4) days, at which time the creep specimens were loaded into the testing apparatus. The specimens were loaded at 4 days because all testing showed that at this time the concrete had reached full strength. Research undertaken by other institutions discussed in section 2.2 also suggested that due to the early age behavior of this material, loading the specimens at 4 days was appropriate. When the creep specimens were loaded, a reading was recorded immediately before and after loading, as well as both 2 and 6 hours after the load had been applied. The specimens that were curing in the submerged heat bath were removed on a daily basis long enough to obtain these readings, after which time they were placed back in the hot water bath to complete their curing process. A sample strain reading is shown in Figure 5.11, and the

raw strain data is provided in Appendix B. It should be noted that the creep and shrinkage specimens were not stored in a constant humidity or temperature controlled environment, therefore these variables were also recorded daily. Current capabilities at Missouri S&T do not allow for a controlled creep and shrinkage space/environment.

Figure 5.11. Sample strain gage reading

5.4. IMPACT SPECIMEN FABRICATION AND TESTING PROCEDURE

5.4.1. Panel Mold. The impact specimens for this study were fabricated in a similar fashion to those used by Gliha (2011) in order to compare results from varying specialized concrete mixture formulations. The panel forms were made by outlining the bottom of a plywood base with 2-in x 4-in (38 mm x 89 mm) boards, and then attaching additional 2-in x 4-in (38 mm x 89 mm) boards to the sides of the form to create a 4-ft x 4 ft x 2-in (1.2 m x 1.2 m x 50.8 mm) thick mold. Before casting, the formwork was sealed with a bead of silicone along all edges. Once the silicone had set, the form was coated with form bar and chain oil to aid in the de-molding process.

5.4.2. Material Mixing. The first impact panel (I-1-P-2) was mixed using a 6 cubic foot (0.03 cubic meter) concrete mixer in the Missouri S&T Construction Materials Laboratory pictured in Figure 5.12.

Figure 5.12. Concrete mixer

First, all the materials were batched in accordance to the specific mix design for the panel shown in Table 5.4. The mixer was turned on and all the dry materials were combined in the mixer. The dry materials were allowed to mix until a homogenous mix was achieved (about 10 minutes). Once a homogenous mixture was achieved, 75% of the water and superplasticizer were added and allowed to mix for about 20 minutes, after which the remainder of the water and superplasticizer were added. This was allowed to mix for an additional 40 minutes. During this time, only the material in the front half of the mixer had reached stage 1 (the ball phase of mixing) in spite of periodically slowing the mixer and pulling the dry material to the front using a garden hoe and shovel. It became clear that the mix was still too dry and that more water and superplasticizer would have to be added to make the material combine. At this point, the mixer was stopped and the dry fines were pulled to the front. When the mixer was re-started, 3 lbs

(1.36 kg) of water and 0.25 lbs (0.11 kg) of superplasticizer were added. After 10 minutes, 60 mL (2.0 o.z.) of superplasticizer was added. After an additional 5 minutes, another 1 lb (0.45 kg) of water was added. After 8 minutes, the mixer was stopped, the fines were pulled to the front once again, and the mixer was restarted while adding 2 lbs (0.91 kg) of water and 0.2 lbs (0.09 kg) of superplasticizer. The concrete began to reach stage 2 (bread dough phase) and was allowed to mix another 10 minutes before adding 1.5 lbs (0.68 kg) water and 0.5 lbs (0.23 kg) superplasticizer. After 2 more minutes, 1.5 lbs (0.68 kg) of water were added, and after an additional 3 minutes of mixing, 1.5 lbs (0.68 kg) of water and 0.25 lbs (0.11 kg) of superplasticizer were added. The concrete mixed for 10 more minutes and then it was ready to place. The wet concrete was ejected from the drum directly into the formwork which sat atop a pallet jack for easy maneuvering. After this experience, it was clear that this volume of material could not be mixed in this mixer because it was too full to allow the barrel to lean forward enough for proper mixing of the concrete.

The second impact panel (I-2-F-2) was mixed using an 8 cubic foot mortar mixer rented from United Rental in Rolla, identical to the mixer pictured in Figure 5.13. The panel was mixed on the loading dock of the Missouri S&T Concrete Materials Laboratory to minimize dust in the campus lab.

Table 5.4. Impact panel #1 batch weights

UHPC Composition			
Material	Amount (lb/yd^3)	Percent by Weight (%)	Batch Weight** (lb)
Type V Portland Cement	1324	29.6	191.3
Fine Sand	1896	42.3	273.8
Silica Fume	432	9.6	62.4
Ground Quartz	390	8.7	56.4
Glenium 3030NS Superplasticizer	56	1.2	8.1
Rheocrete CNI Accelerator	N/A	N/A	N/A
Steel Fibers	N/A	N/A	N/A
Water*	382	8.5	50.8

*Water adjusted on mix date to account for sand moisture content

**Batch Volume = 3.9 ft^3

Conversions: 1 lb/yd^3 = 0.59 kg/m^3

1 lb = 0.45 kg

Figure 5.13. 8 Cubic foot (0.23 cubic meter) mortar mixer

First, all the materials were batched in accordance to the mix design for the panel shown in Table 5.5. All the dry powder materials were combined using a garden hoe in a metal trough in the Materials lab and were mixed until a homogeneous mixture was achieved. Once achieved, the mixture was shoveled back into buckets in preparation for mixing. The mixing process began by adding 50% of the water and superplasticizer into the mixer. Next, the dry powder, sand, and remaining water were metered into the mixing basin. The addition of powder and sand were alternated, and when the mix began to get thick, small amounts of water were added to keep the mixture fluid and not seize the mixer. This process continued until all the materials had been added. Next, the steel fibers were added slowly to minimize clumping of fibers. The mixing process lasted roughly 45 minutes.

Table 5.5. Impact panel #2 batch weights

UHPC Composition			
Material	Amount (lb/yd^3)	Percent by Weight (%)	Batch Weight (lb)
Type V Portland Cement	1324	27.8	224.0
Fine Sand	1896	39.8	320.7
Silica Fume	432	9.1	73.1
Ground Quartz	390	8.2	66.0
Glenium 3030NS Superplasticizer	56	1.2	9.4
Rheocrete CNI Accelerator	N/A	N/A	N/A
Steel Fibers	288	6.0	48.7
Water*	382	8.0	64.7

*Water adjusted on mix date to account for sand moisture content

**Batch Volume = 4.6 ft^3

Conversion: 1 lb/yd^3 = 0.59 kg/m^3

1 lb = 0.45 kg

5.4.3. Panel Casting. The impact panels were cast by ejecting the "wet" concrete directly into the formwork from the respective mixer. To do this, the forms were placed centered on a pallet, and then a pallet jack was used to move the formwork into place for filling. As the "wet" concrete was being ejected, a garden hoe was used to distribute the mixture evenly into the forms. This process is pictured in Figure 5.14.

Figure 5.14. Panel specimen casting

As the form was being filled, rubber mallets were used to tap the outsides of the mold to help air escape. Once the mold was filled, the panel was maneuvered over a sheet of plastic, and a metal screed was used to initially level and finish the concrete. Finally, hand trowels were used to give the panels a smooth finish as shown in Figure 5.15. After roughly 1 hour, wet burlap was placed over the form, followed by a sheet of plastic, to help keep the concrete from drying out during the initial setting.

Figure 5.15. Trowel finished panel specimen

5.4.4. De-molding and Curing. After 24 hours, the panels were moved into the Missouri S&T SERL and were removed from their forms. The sides were unscrewed from the base, and then a rubber mallet was used to knock the sides free from the form base. A crowbar was used to elevate the panel off the base enough to slide a strap underneath. Once a strap was in-place on two edges, a crane was used to maneuver the panel into the heat bath. This process is pictured in Figure 5.16 and Figure 5.17 below. In order to allow for removal of the straps, as well as good flow through the curing bath, the panel was set onto bricks to keep it off the floor of the curing bath.

Figure 5.16. Panel de-molding process

Figure 5.17. Panel being added to heated curing bath

5.4.5. Test Setup. The impact panel test setup simulates flying debris striking a building panel in the event of a tornado, and is shown below in Figure 5.18. It is the same setup that was used by Gliha his testing in 2011. The panel was placed atop a steel frame which provided 2-in of bearing on each edge of the panel and allowed for a linear potentiometer to be placed below the panel to record deflections during testing. The linear potentiometer setup is shown in Figure 5.19. The potentiometer had a 3-in (76.2 mm) stroke and was depressed 1.5-in (38.1 mm) at the beginning to allow for both upward and downward deflection to be measured. Masonry sand was also placed on the bearing locations to ensure an even bearing surface on each edge. Thin metal shims were also used when necessary to make the panel level on the steel support. The center of each panel was marked using a chalk line and a thin neoprene pad and load cell were placed on this mark. The neoprene pad was used to dampen vibrations as well as to protect the bottom face of the load cell during impacts.

Figure 5.18. Impact test setup

A steel rod was used to impact the load cell and panel for each test. The steel rod weighed 50 lb (22.7 kg), and measured 2.75-in (70 mm) in diameter. It had an eye bolt attached at the top to allow for a rope to be attached in order to position it for each drop height. The steel weight was placed inside a 3-in (76.2 mm) diameter PVC guide pipe and the rope was pulled through the top of the pipe. Using pipe clamps, this guide pipe was attached at 4 locations to the side of a scaffolding to keep it steady and in position during testing. The guide pipe had a small hole at each drop height along its height that allowed for a screwdriver to hold the steel weight in position until testing was ready to commence. In order to reduce vibrations and damage to the load cell, a 0.5-in (12.7 mm) piece of high durometer neoprene the same diameter as the steel weight was fixed to the bottom of the weight.

Figure 5.19. Linear potentiometer setup

Once the panel was in place atop the frame, the scaffolding was moved in position until the guide pipe and steel weight were centered over the load cell. When all data acquisition devices were ready, the rope was used to lift the weight just enough to remove

the screwdriver at the specified drop height. Once the screwdriver was removed, the technician let go of the rope allowing the weight to fall and impact the load cell and panel specimen.

The drop heights were the same as the study done by Gliha (2011). The first drop was from 3-in (76.2 mm) and each drop increased by 3-in (76.2 mm) up to a height of 24-in (0.6 m). After the 24-in (0.6 m) mark, the drop heights increased by 6-in (152.4 mm) up to the maximum height of the scaffolding and guide pipe which was 186-in (4.7 m). A Synergy Data Acquisition system shown in Figure 5.20 was used to collect the deflection and load data at each drop test height.

Figure 5.20. Synergy data acquisition system

5.5. BLAST SPECIMEN FABRICATION AND TESTING PROCEDURE

5.5.1. Panel Mold. The blast specimens for this study were made in a similar fashion to those used by Carey (2012), and Wulfers (2012) in order to compare results. The panel forms were made by framing the bottom of a plywood base with 2-in x 4-in

(38 mm x 89 mm) lumber, and then attaching additional 2-in x 4-in (38 mm x 89 mm) boards to the sides of the form to create either a 46.5-in x 46.5-in x 2-in (1.18 m x 1.18 m x 50 mm) thick mold, or a 46.5-in x 46.5-in x 3.5-in (1.18 m x 1.18 m x 89 mm) thick mold depending on the panel required. Before casting, the formwork was sealed with a bead of silicone along all edges. Once the silicone had set, the form was coated with bar and chain oil to aid in the de-molding process.

5.5.2. Panel Fabrication. The blast panel specimens were fabricated in the same fashion as the second impact panel (I-2-6F-2). Pictures of this process are shown in section 5.4 of this report. The blast panels were mixed using an 8 cubic foot (0.23 cubic meter) mortar mixer rented from United Rental in Rolla, pictured in Figure 5.13. The panel was mixed on the loading dock of the Missouri S&T Concrete Materials Laboratory to minimize dust in the campus lab. First, all the materials were batched in accordance to the mix design for the panel. These batch weights are shown in Table A.3 through Table A.8 in Appendix A. All the dry powder materials were combined using a garden hoe in a metal trough in the Concrete Materials lab and were mixed until a homogeneous mixture was achieved. Once achieved, the mixture was shoveled back into buckets in preparation for mixing. The mixing process began by adding 50% of the water and superplasticizer into the mixer. Next, the dry powder, sand, and remaining water were metered into the mixing basin. The addition of powder and sand were alternated, and when the mix began to get thick, small amounts of the remaining water were added to keep the mixture fluid and not seize the mixer. This process continued until all the materials had been added. Finally, if the panel contained fibers, they were added slowly to minimize clumping of fibers. The mixing process lasted roughly 45 minutes.

The blast panels were cast by ejecting the “wet” concrete directly into the formwork from the mortar mixer. To do this, the forms were placed centered on a pallet, and then a pallet jack was used to move the formwork into place for filling. As the “wet” concrete was being ejected, a garden hoe was used to distribute the mixture evenly into the forms. As the form was being filled, rubber mallets were used to tap the outsides of the mold to help air escape. Once the mold was filled, the panel was maneuvered over a sheet of plastic, and a metal screed was used to initially level and finish the concrete. Finally, hand trowels were used to give the panels a smooth finish. After roughly 1 hour,

wet burlap was placed over the form, followed by a sheet of plastic, to help keep the concrete from drying out during the initial setting.

After 24 hours, the panels were moved into the Missouri S&T SERL and were removed from their forms. The sides were unscrewed from the base, and then a rubber mallet was used to knock the sides free from the form base. A crowbar was used to elevate the panel off the base enough to slide a strap underneath. Once a strap was in-place on two edges, a crane was used to maneuver the panel into the heat bath. In order to allow for removal of the straps, as well as good flow through the curing bath, the panel was set onto bricks to keep it off the bottom of the curing bath.

5.5.1. Full Panel Test Setup. Two wide flange steel members were used to support the full panel specimens for testing. The steel members were placed roughly panel width apart in the center of the testing bay of the Wombat, an underground blast chamber at the Missouri S&T Experimental Mine. The panels were brought into the mine by a Bobcat and the supports were adjusted so that when the panels were placed, the edge of the panel was supported directly over the web of each of the steel members. This placement provided roughly 2.5 inches (63.5 mm) of bearing surface on each panel edge. Once the panel was in place, the specified charge weight was hung from the ceiling of the mine and positioned over the center of the panel. Using a measuring tape, the standoff distance was measured and the charge placement was set. The C-4 was prepared for testing, and the team safely detonated the explosive from outside the Wombat entrance. A picture of this test set-up is shown in Figure 5.21, and the full panel blast testing matrix is shown in Table 5.6.

Figure 5.21. Full panel blast test setup

Table 5.6. Full specimen blast testing matrix

Specimen	Detonation	Charge Weight (lb)	Standoff Distance (in)
B-1-6F-3.5	1	3	36
	2	3	18
B-2-2F-3.5	N/A	Broken Pre-Testing	
B-3-2F-3.5	1	3	36
	2	3	36
B-4-2F-2	1	3	12
B-5-P-2	1	0.25	72
	2	1	72
B-6-6F-2	1	3	48

Conversions: 1 lb = 0.45 kg

1-in = 25.4 mm

5.5.2. Half Panel Fabrication and Test Setup. After testing of the 3.5-in (89 mm) thick panels occurred, the specimens were re-used for further testing. The goal of the continued testing was to target the spalling behavior of UHPC since minimal to no spalling was observed in the full panel testing.

5.5.2.1 Fabrication. The 3.5-in (89 mm) thick square panels failed with a flexural crack down the center during testing which lead the team to decide to cut the panels in half along the failure for further testing. The panels were cut using a portable saw with a concrete blade. A line was drawn on the top of the panel along the line of the failure, and this line was followed by the technician's saw. The panels were supported in the center and at each end by railroad ties and stacked lumber. The saw used, and this process are depicted in Figure 5.22 below.

Figure 5.22. Half panel fabrication process

5.5.2.2 Test setup. A portion of the frame used in Carey's (2012) impact study was used for the blast setup of the half blast panels. Two red angle frames were used to support the back and bottom of the panels, and a steel I-beam that was bolted to the angled supports was used at the top of each end to brace the panel from falling forward after the blast event. In order to make sure the I-beam provided even clamping force, a spacer bar was placed above the panel between the two pieces of steel providing an even surface at the point of bolting. It also provided rigidity to the frame during the blast events. The panels were loaded into the frame such that they were supported over the web of each of the vertical beams to simulate the same support conditions as the horizontally tested panels. A picture of this test setup is shown in Figure 5.23.

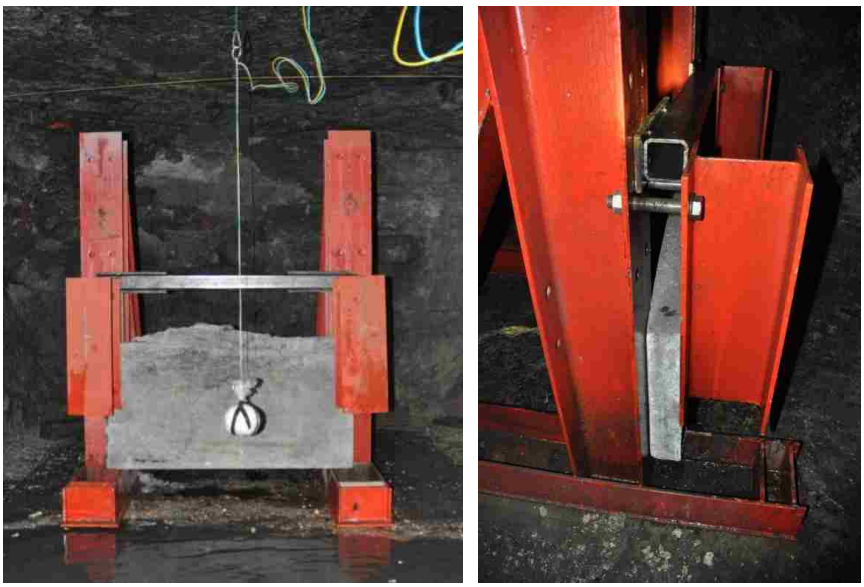

Figure 5.23. Half panel blast test setup

To begin the spalling investigation, the research team used ConWep to estimate a blast event that would achieve a targeted level of spalling. The program estimated that a 3 lb (1.36 kg) charge at a 36-in (0.9 m) standoff distance would produce roughly 10%

spalling and 20% breaching of the thickness of the 2% fiber panel. Using this as a baseline, one half panel of each fiber content was setup to experience this blast event so that a relationship between fiber content and spalling could be made.

The results of this testing led to little or no spalling after each blast event. In order to try to force spalling behavior, the 6% fiber panel from the first half panel setup was re-tested to experiment with a charge weight and standoff distance that would induce spalling. The blast event that was tested was a 0.5 lb (0.23 kg) charge at a distance of 1-in (25.4 mm) from the edge of the panel to the edge of the C-4 spherical charge (roughly 2.25-in (57.2 mm) from the center). As it is shown in the results section that follows, this blast event was successful in inducing spalling and cratering behavior. Due to the success, this blast event was used on the final 3 half panel tests. This test setup is shown below in Figure 5.24. The frame setup was the same as the previous vertical panel tests.

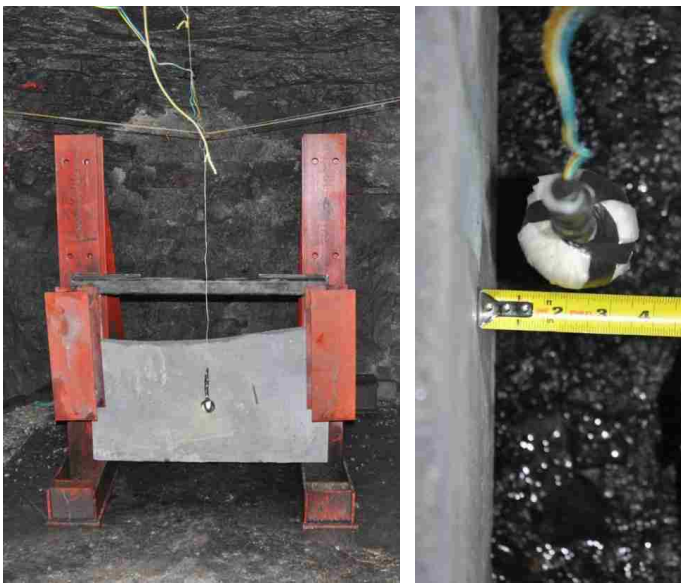

Figure 5.24. Half panel spalling test setup

6. RESULTS AND DISCUSSION

6.1. CREEP AND SHRINKAGE

The results of the creep and shrinkage testing are shown in the following figures. The first set of plots that follow represent the creep and shrinkage behavior of specimens of the same concrete type that were in the same curing regime. For example, all of the plain UHPC specimens that were ambient air cured would be in Figure 6.1.

Figure 6.1 shows the creep and shrinkage behavior of plain UHPC specimens that were cured in the ambient air method. As the figure shows, the shrinkage strain exceeded the creep strain, but the shape of the curves show that they follow the same trend. As expected, these specimens show a trend more like that of typical normal strength concrete in that the strain increases in a logarithmic fashion as the specimens age.

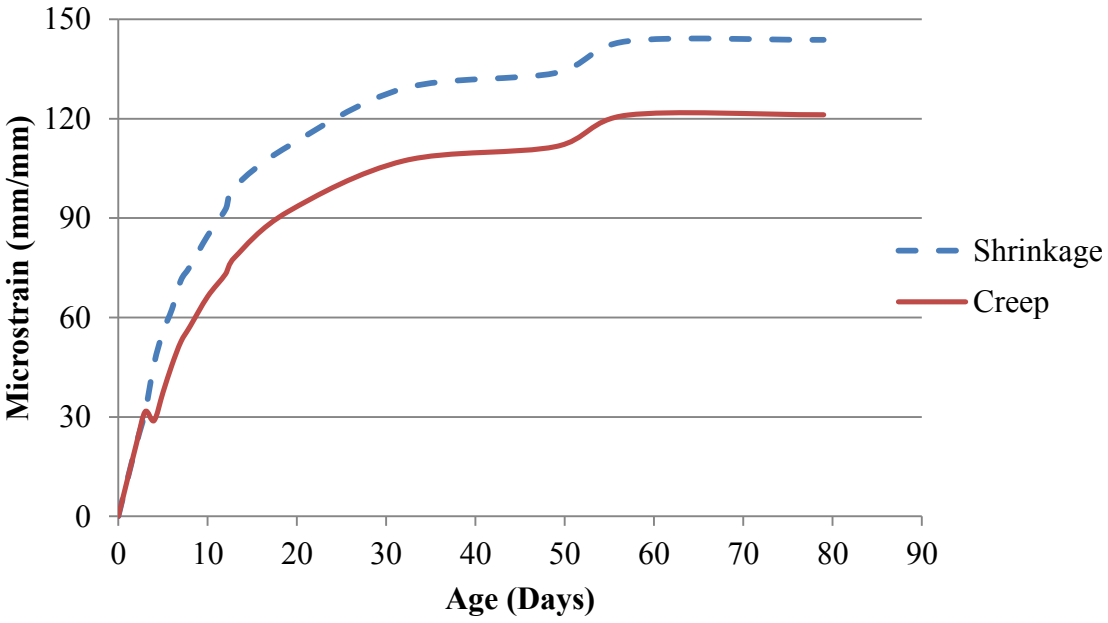

Figure 6.1. Creep and shrinkage of plain, ambient air cured UHPC

Figure 6.2 shows the creep and shrinkage behavior of the plain UHPC specimens that were cured in the hot water bath. As the figure shows, the creep strain exceeded the shrinkage strain, but the shape of the curves show that they again follow the same trend. The curves also show that there was little additional creep or shrinkage strain after the heat treatment was applied (roughly 10 microstrain). This behavior is consistent with the properties presented in 2.1.3 and previous research presented in section 2.2, even though this concrete had no fiber in the paste. This plain UHPC material behaved in the same general way as the UHPC with fibers, which shows that as expected, it is the heat curing and not the fiber content that controls the behavior.

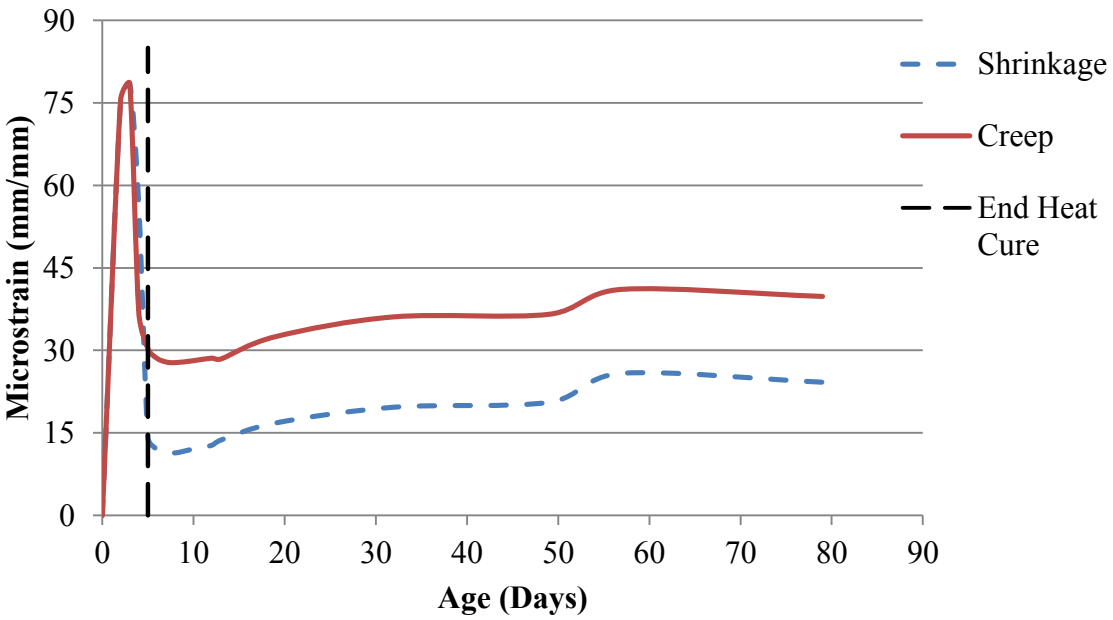

Figure 6.2. Creep and shrinkage of plain, heat cured UHPC

Figure 6.3 shows the creep and shrinkage behavior of the 6% fiber content UHPC specimens that were cured in the ambient air method. As the figure shows, the shrinkage strain exceeded the creep strain, but the shape of the curves show that they follow the

same trend. As expected, these specimens show a trend more like that of typical normal strength concrete in that the strain increases in a logarithmic fashion as the specimens age.

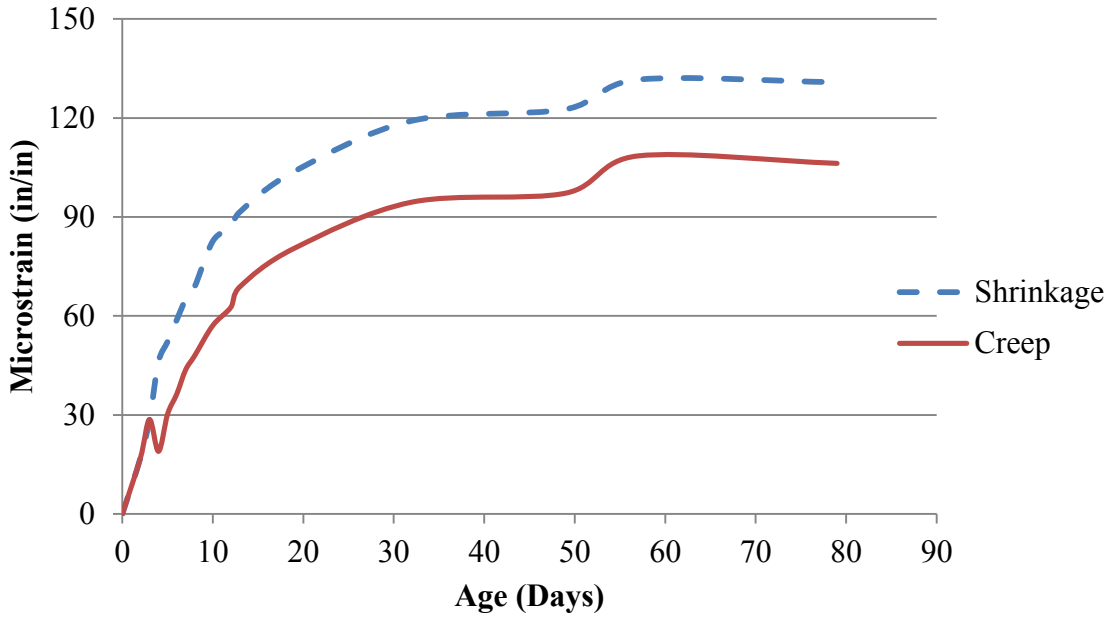

Figure 6.3. Creep and shrinkage of 6% fiber, ambient air cured UHPC

Figure 6.4 shows the creep and shrinkage behavior of the 6% fiber content UHPC specimens that were cured in the hot water bath. As the figure shows, the creep strain exceeded the shrinkage strain, but the shape of the curves show that they follow the same trend. As expected, these specimens show little additional creep and shrinkage strain after heat treatment (roughly 15 microstrain), which is consistent with the properties shown in Table 2.2.

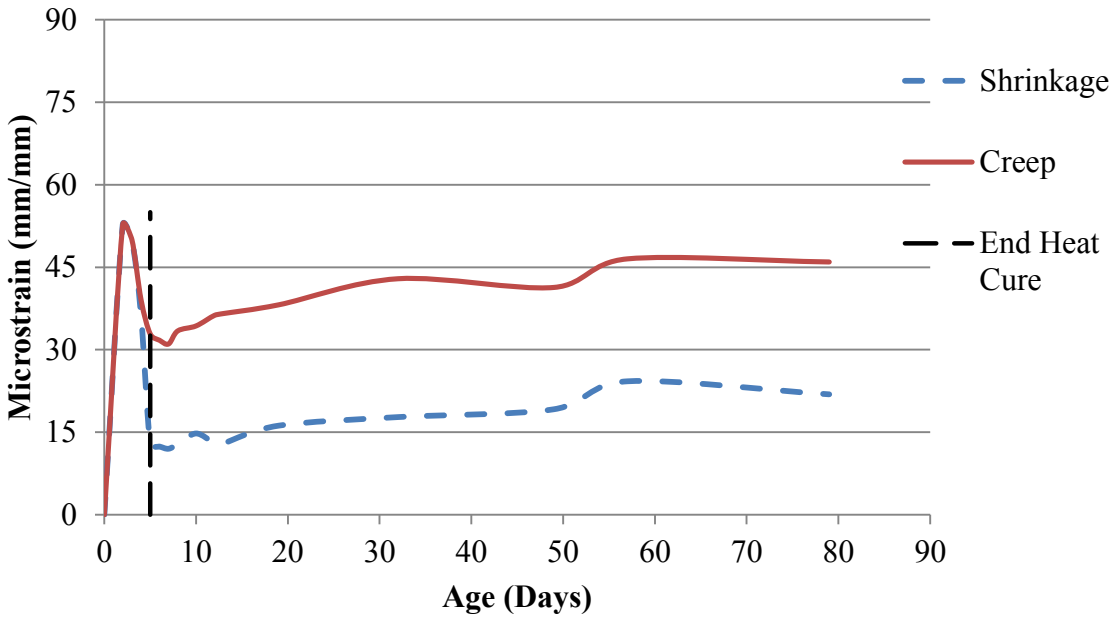

Figure 6.4. Creep and shrinkage of 6% fiber, heat cured UHPC

One trend seen in all specimens is a small jump in strain between the ages of 50 to 60 days. This increase is due to a change in relative humidity in the experimental environment. As shown in Table 6.1, the relative humidity before and after this set of readings is higher than the humidity at the day of the strain spike. This day of dry air between dates of more moist air allowed for an increase in shrinkage and creep and is reflected in the data. Another trend seen across all the heat cured specimens is the large spike in strain that peaks during the curing process and drops off at the end of curing. This phenomena appears due to the fact that these results are not accounting for the length change that occurs as a result of the thermal gradient these specimens undergo during curing.

Another point this data illustrates is that both the creep and shrinkage strains seen in the UHPC specimens were much lower than conventional concrete, which is consistent with information seen in the literature review. The average shrinkage strain for conventional concrete is roughly 780 microstrain (Tarr and Farny, 2008). As shown in Figure 6.1 and Figure 6.3 the results of this study show that the UHPC cured in the

ambient air conditions reached a strain of between 120 to 150 microstrain which is significantly less than the traditional average of 780 microstrain in conventional concrete. In addition, Figure 6.2 and Figure 6.4 show that the heat cured UHPC specimens exhibited even less shrinkage strain, coming our below 30 microstrain. While these values are lower than other studies presented in the literature review, the data still shows that the shrinkage properties of UHPC are still much better than those of conventional concrete.

Table 6.1. Summary of creep and shrinkage environment data

Age (Days)	1	2	3	4	5	6	7	8	10	12	13	19	32	49	57	79
Temperature (°F)	71	69	69	69	69	71	71	71	70	68	68	68	66	70	69	73
Relative Humidity (%)	30	30	31	33	31	31	31	31	41	32	35	35	42	58	41	55

Conversion: 32°F = 0°C

The data obtained in this study also show favorable creep behavior from UHPC. Typical creep coefficients for traditional concrete range from 2.0 to 6.0 (Idiart, 2009). Table B.1 through Table B.4 show the creep coefficients obtained from this study. The results show that for plain UHPC specimens which were ambient air cured, the creep coefficient was an average of 0.55, and with heat curing, the creep coefficient was an average of 0.65. For the UHPC with 6% fiber, the specimens cured in ambient air had an average creep coefficient of 0.85, and the heat cured specimens had an average of 0.25. These results show a significant reduction in creep strain from conventional concrete.

The next set of plots group the specimens by concrete type. Figure 6.5 shows the plain UHPC concrete specimens, and Figure 6.6 shows the UHPC specimens with 6% fiber. These plots are important to explore the effect of curing on the concrete. As the

figures clearly show, the heat curing specimens have greatly reduced creep and shrinkage strains relative to their ambient air cured counterparts. The figures also show that no matter the curing process, the specimens have the same behavioral trends, except the heat cured specimens experience the behavior at a lower strain.

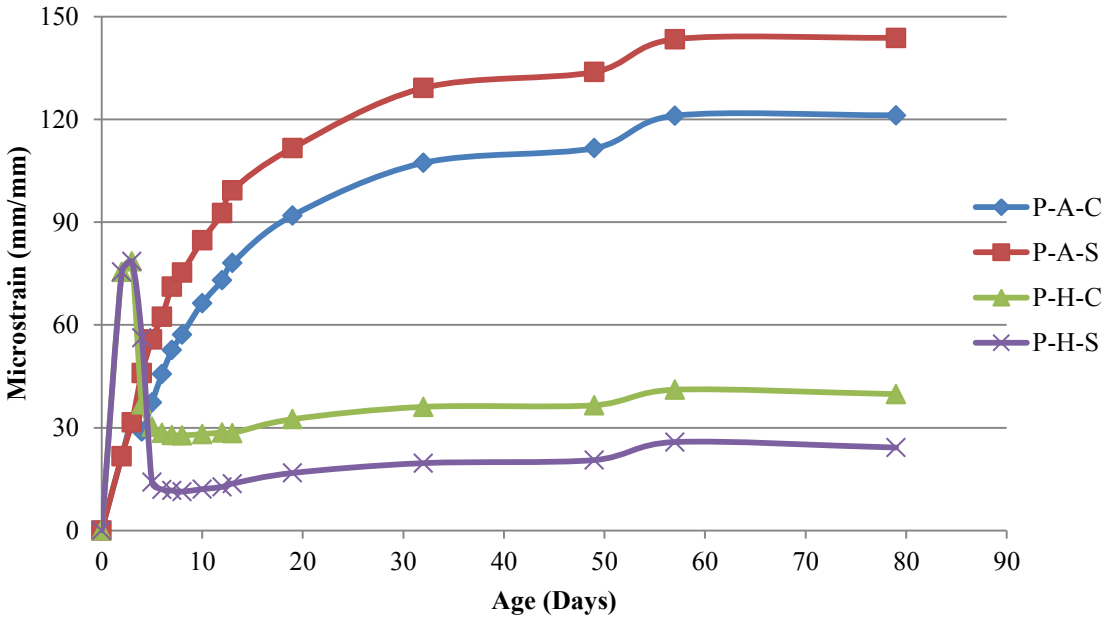

Figure 6.5. Creep and shrinkage of plain UHPC specimens

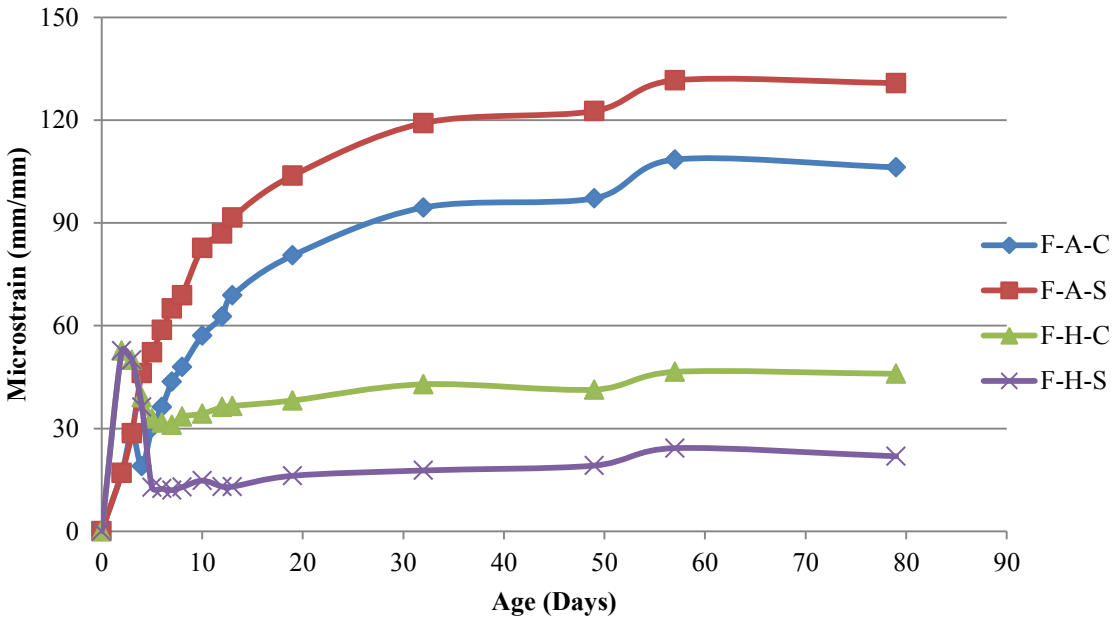

Figure 6.6. Creep and shrinkage of UHPC specimens with 6% fiber

Table 6.2 through Table 6.5 are summaries of the strains recorded (shown in microstrain) for each set of specimens. Also included are the creep coefficients for each type of UHPC studied. The creep coefficients for heat cured UHPC in this study are considerably higher than what research suggests is typical. The complete table of creep and shrinkage readings is available in Appendix B.

Table 6.2. Strain summary for plain, ambient air cured, UHPC

Mix	Curing Condition	Load	Strain (microstrain)	Age at Reading (days)					
				4	7	19	28*	32	79
Plain UHPC (P)	Air Cured (A)	$0.2f_c$	Total	-28.90	-52.66	-91.95	-102.58	-107.30	-121.19
			Shrinkage	-45.96	-71.19	-111.65	-123.77	-129.16	-143.80
			Elastic	-23.14	-23.14	-23.14	-23.14	-23.14	-23.14
			Creep	17.06	18.52	19.70	21.19	21.86	22.61
			Creep Coefficient	0.74	0.80	0.85	0.92	0.94	0.98

*Values at 28 days were interpolated

Table 6.3. Strain summary for plain, heat cured, UHPC

Mix	Curing Condition	Load	Strain (microstrain)	Age at Reading (days)					
				4	7	19	28*	32	79
Plain UHPC (P)	Heat Cured (H)	$0.2f_c$	Total	-36.84	-27.89	-32.50	-34.99	-36.09	-39.81
			Shrinkage	-21.28	-11.66	-16.80	-18.79	-19.67	-24.21
			Elastic	-36.56	-36.56	-36.56	-36.56	-36.56	-36.56
			Creep	-15.55	-16.23	-15.70	-16.20	-16.42	-15.59
			Creep Coefficient	0.43	0.44	0.43	0.44	0.45	0.43

*Values at 28 days were interpolated

Table 6.4. Strain summary for 6% fiber, ambient air cured, UHPC

Mix	Curing Condition	Load	Strain (microstrain)	Age at Reading (days)					
				4	7	19	28*	32	79
6% Fiber (F)	Air Cured (A)	$0.2f_c$	Total	-18.97	-43.69	-80.49	-90.18	-94.49	-106.23
			Shrinkage	-46.21	-65.01	-103.78	-114.41	-119.14	-130.82
			Elastic	-17.38	-17.38	-17.38	-17.38	-17.38	-17.38
			Creep	27.24	21.32	23.29	24.23	24.65	24.59
			Creep Coefficient	1.57	1.23	1.34	1.39	1.42	1.41

*Values at 28 days were interpolated

Table 6.5. Strain summary for 6% fiber, heat cured, UHPC

Mix	Curing Condition	Load	Strain (microstrain)	Age at Reading (days)					
				4	7	19	28*	32	79
6% Fiber (F)	Heat Cured (H)	$0.2f_c$	Total	-39.07	-31.05	-38.17	-41.45	-42.91	-45.96
			Shrinkage	-20.60	-12.00	-16.20	-17.28	-17.76	-21.89
			Elastic	-36.25	-36.25	-36.25	-36.25	-36.25	-36.25
			Creep	-18.47	-19.06	-21.97	-24.17	-25.15	-24.07
			Creep Coefficient	0.51	0.53	0.61	0.67	0.69	0.66

*Values at 28 days were interpolated

6.2. IMPACT TESTING

The results of the impact testing are displayed in Table 6.6. As expected, the performance of the specimen with 6% fiber far exceeded the plain UHPC specimen. It is useful to note, that the failure height of the plain UHPC panel is the same as the failure height of the plain concrete panels observed by Gliha (2011), but both the cracking height, and the failure height exceeded the carbon-fiber reinforced specimens tested in that study. It should also be noted that the failure height listed for the panel with 6% fiber is the height at which the test stopped, rather than the failure height. The specimen experienced 10 impacts from the highest drop height of 186-in (4.7 m), and did not show imminent signs of failure, so the test was stopped. The cracking and failure data are also displayed graphically in Figure 6.7 and Figure 6.8 respectively.

Table 6.6. Impact specimen results

Specimen	Cracking Height (in)	Failure Height (in)
I-1-P-2	12	15
I-2-6F-2	102	186*
*Maximum drop height. Panel did not exhibit failure.		

Conversion: 1-in = 25.4 mm

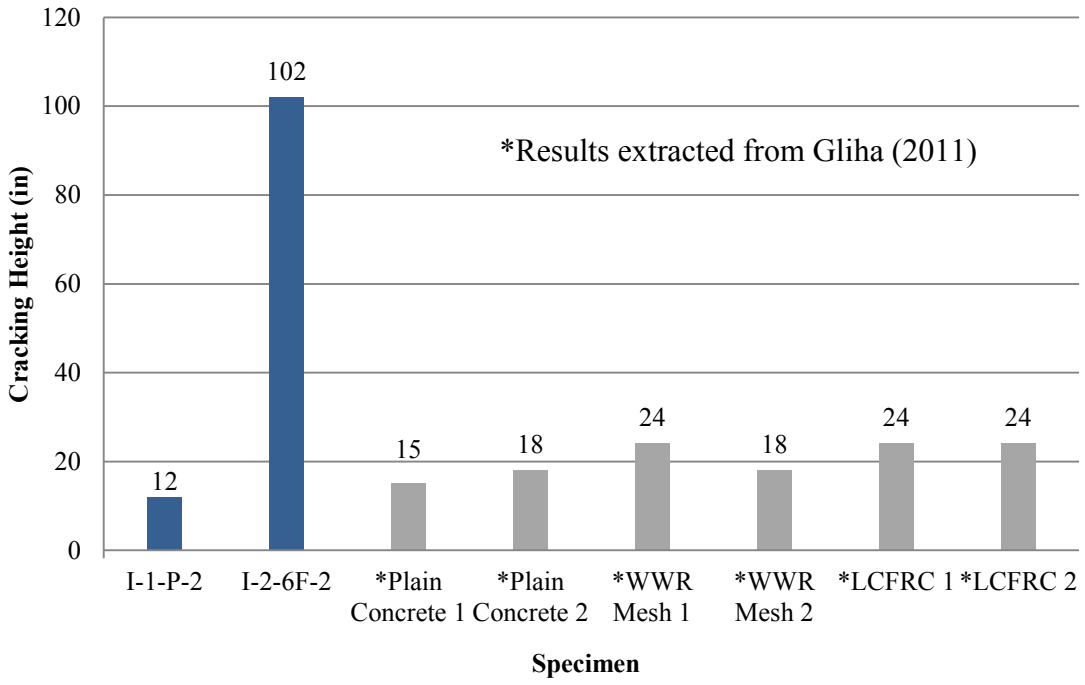

Conversion: 1-in = 25.4 mm

Figure 6.7. Impact specimen cracking heights

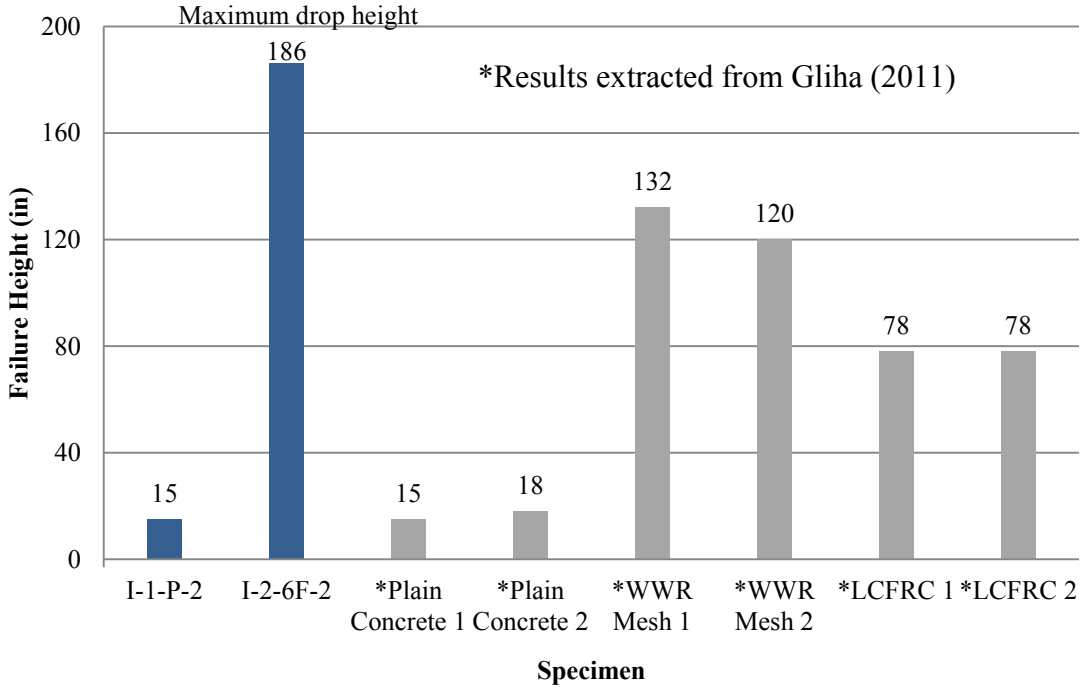

Conversion: 1-in = 25.4 mm

Figure 6.8. Impact specimen failure heights

It is also important to examine the panel's physical performance. Figure 6.9 through Figure 6.11 show the two panels after they had completed impact testing. The failure pattern of the plain UHPC concrete panel shown in Figure 6.9 consisted of 4 cracks radiating from the center of the panel to the middle of each edge. This failure is consistent with findings from Gliha (2011) for a plain concrete panel. Typically one would expect a failure pattern forming an x-pattern rather than a cross. One possible explanation is that the initial crack formed along the entire length at the center of the panel. When the next impact occurred, it caused the failure to complete the original crack, and the support along the other two edges caused the other half of the cross cracking pattern to form. More studies should be conducted to investigate this failure pattern.

Figure 6.9. Failure of I-1-P-2

The specimen that contained 6% fiber, had a much different reaction to the testing. As shown in Figure 6.11, this panel exhibited much more of a spider-web

cracking pattern on the bottom (tension face), and almost no cracking on the edges or top face of the panel. It is also shown that the panel had no spalling behavior which is favorable in an impact or blast scenario because it does not create fragments that could potentially harm building occupants in an at-risk structure. These results show that the fibers allow the panel to absorb and dissipate more energy, as well as maintain the structural integrity of the specimen. Figure 6.12 displays the ability of the fibers to bridge the cracks in the tension face which helps absorb energy and reduce the spalling nature of the concrete which could be potentially fatal to an at-risk building occupant.

Figure 6.10. Top of I-2-6F-2 after testing

Figure 6.11. Bottom of I-2-6F-2 after testing

Figure 6.12. Fibers bridging bottom crack of I-2-6F-2

Figure 6.13 displays the data collected by the Synergy system for measured impact force versus drop height for each of the impact specimens. As expected, this curve shows that with an increase in drop height, there is an increase in the impact force imparted on the specimen. The sharp "jumps" in the data are most likely due to the steel impact weight not striking the load cell in an exactly concentric manner.

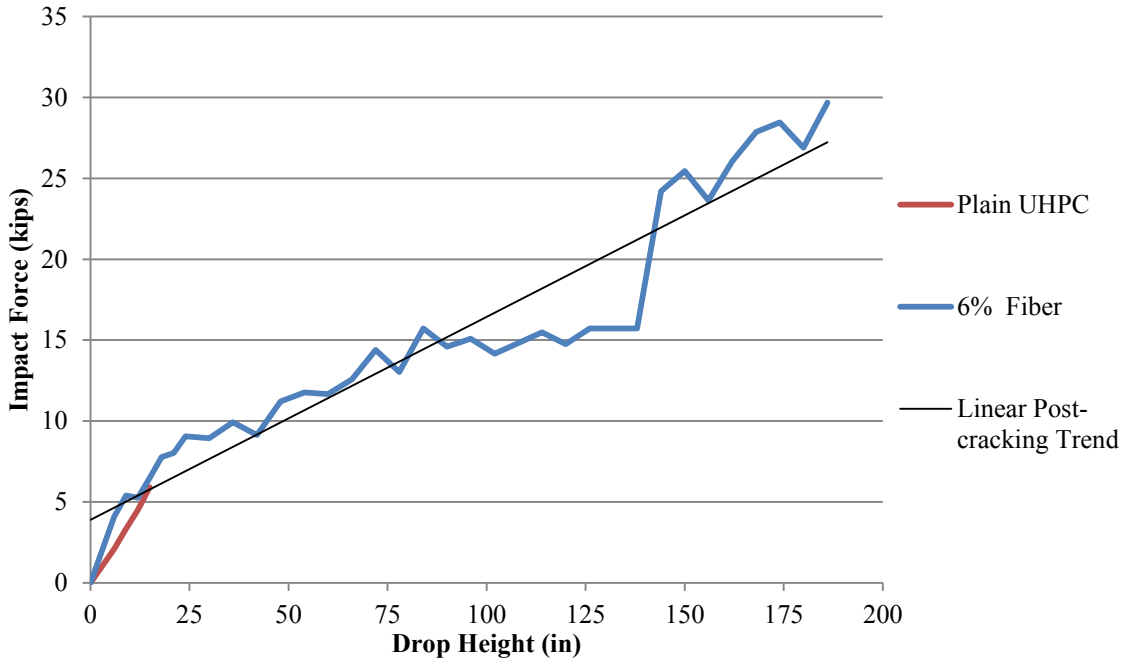

Figure 6.13. Force vs. drop height for impact specimens

Figure 6.14 shows impact force versus specimen deflection for the impact panels tested. The data trend for the plain UHPC panel shows what would be expected for a typical unreinforced concrete panel. This curve is representative of a brittle material in which little plastic deflection/deformation occurs before failure. The data shows a liner-elastic trend until cracking height (just before failure), and then takes on a more inelastic trend. The data for the panel with 6% fiber shows a less brittle trend and more

representative of what would be expected for a reinforced concrete specimen. For the specimen with fibers, the trend again begins linear-elastic until 6-in (152.4 mm), and then takes on a slope indicating an inelastic response. The inelastic behavior does not align with the drop height at which cracking was seen on the panel. This indicates that a softening of the system was taking place from the inside before the cracks were observed on the specimen surface. This softening means that as the fibers were absorbing energy during the impact, micro cracks were most likely opening inside the panel. A trendline was added to this data set because after a certain drop height (force) the deflection readings began to misrepresent the actual performance of the panel. The reason the deflection data "jumps" around is because the physical panel was absorbing enough energy that it experienced a "bouncing" reaction when impact occurred. This is because the test set-up did not restrain the specimen from moving in the vertical upward direction. The data trends shown in Figure 6.14 are consistent with the trends found by Gliha (2011), except that the 6% fiber panel in this study never reached true "failure".

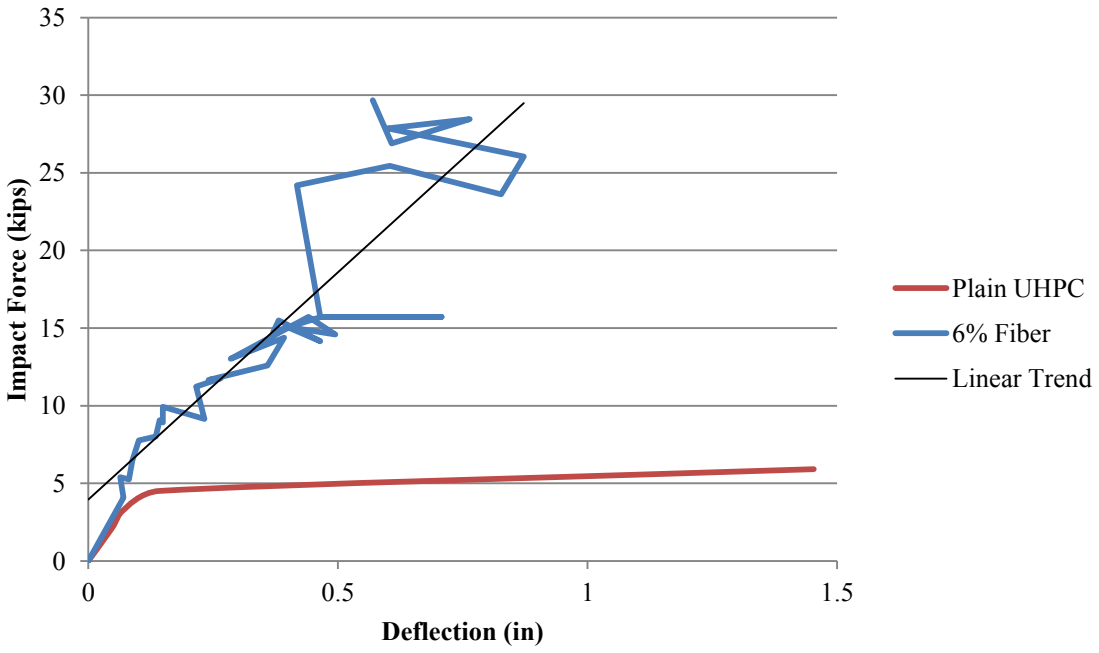

Figure 6.14. Force vs. deflection for impact specimens

6.3. BLAST TESTING

6.3.1. Full Panel Specimen Testing. Table 6.7 shows the testing matrix for the results of the full panel specimens that are shown in this section. The descriptions for the various levels of damage are shown in Appendix D. The definitions come from the PDC-TR 06-08 Rev 1 "Single Degree of Freedom Structural Response Limits for Antiterrorism Design".

Table 6.7. Full panel blast test matrix

Specimen	Detonation	Charge Weight (lb)	Standoff Distance (in)
B-1-6F-3.5	1	3	36
	2	3	18
B-2-P-3.5	N/A	Broken Pre-Testing	
B-3-2F-3.5	1	3	36
	2	3	36
B-4-2F-2	1	3	12
B-5-P-2	1	0.25	72
	2	1	72
B-6-6F-2	1	3	48

Conversions: 1 lb = 0.45 kg

1-in = 25.4 mm

6.3.1.1 B-4-2F-2 results. Blast panel B-4-2F-2 shown in Figure 6.15 and Figure 6.16, exhibited typical shock wave failure. This x-pattern failure occurs when a compression wave travels through the specimen and reflects back as a tension wave. Where the tension waves meet are along the lines of the cracking pattern. One small portion dislodged from the top face of the panel, mostly as a result of the x-cracking pattern, but also slightly from a spalling behavior which is demonstrated by the angle at which the fragment broke off during the event.

Figure 6.15. Panel B-4-2F-2 before detonation.

Figure 6.16. Panel B-4-2F-2 damage after detonation

The initial weight of the specimen was 394 lbs (178.7 kg), and the final weight of the panel was 385 lbs (174.6 kg). After accounting for the accuracy of the load cell, the mass loss of this panel was roughly 1%.

6.3.1.2 B-3-2F-3.5 results. Blast panel 2 shown in Figure 6.17 showed minimal damage after the first blast event. Hairline flexural cracking developed on the front and back edges, as well as the bottom (tension face) of the panel as shown in Figure 6.18 and Figure 6.19. No spalling, fragmentation, or major cracking was observed. The residual deflection after this event was 0.375-in (9.5 mm) at the center of the specimen.

Figure 6.17. Panel B-3-2F-3.5 before detonation

Figure 6.18. Top face of B-3-2F-3.5 after detonation

Figure 6.19. Bottom face of B-3-2F-3.5 after detonation

Due to the minimal damage observed, the panel was set to experience a second blast event of the same magnitude. Ideally, a new panel would have been tested to ensure that damage was not being compounded from each event, however due to budget restraints; specimen re-use was permitted to investigate blast mitigation behavior. Although extensive cracking may not be seen on the exterior faces of the panels, interior damage may have occurred such as interior micro-cracking and fiber pull-out. It should be noted that while testing a specimen for a second time will affect the results due to a softening of the panel system, the testing results still hold value.

After the second detonation, a small hairline crack had developed along the centerline of the top face, and a larger crack 0.25-in (6.4 mm) wide had opened on the back (tension) face of the panel. Again, no spalling, or fragmentation was observed, and the residual deflection after this event was 1.375-in (34.9 mm) at the center of the panel. The damage after this event is pictured in Figure 6.20 through Figure 6.22. The initial weight of the panel was 636.5 lbs (288.7 kg), and the final weight of the panel was 634.0 lbs (287.6 kg) for a total of 2.5 lbs (1.1 kg) of mass lost after the two events. The accuracy of the load cell used to weigh the specimens was +/- 5 lbs (2.3 kg), and since no spalling or fragmentation was noted, statistically the 2.5 pound (1.1 kg) difference in weight does not suggest mass loss.

Figure 6.20. Panel B-3-2F-3.5 top face damage after 2nd detonation

Figure 6.21. Panel B-3-2F-3.5 vertical crack on front edge after 2nd detonation

Figure 6.22. Panel B-3-2F-3.5 bottom face damage after both blast events

6.3.1.3 B-1-6F-3.5 results. Blast panel B-1-6F-3.5 showed minimal damage after the first blast event. The specimen had no cracking on the top face, and no cracking along the tension face other than a small crack 0.02-in (0.5 mm) wide that began on the front edge of the panel. There were no signs of spalling and no mass lost after this blast event. There was a residual deflection of 0.125-in (3.2 mm) along the center of the panel. Photographs of the panel before and after testing are shown in Figure 6.23 through Figure 6.26

Figure 6.23. Panel B-1-6F-3.5 before testing

Figure 6.24. Top face of B-1-6F-3.5 after first detonation

Figure 6.25. Bottom face of B-1-6F-3.5 after first detonation

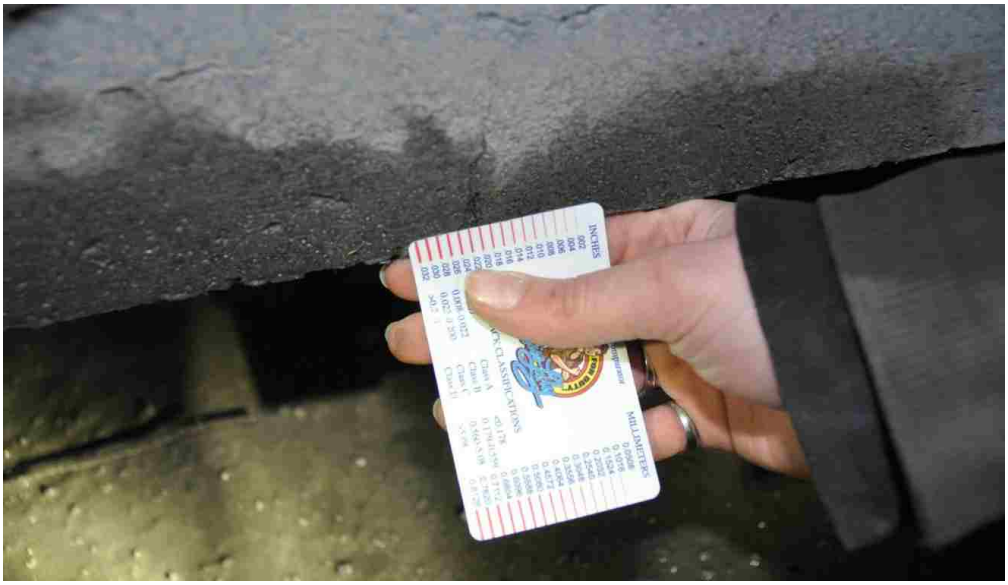

Figure 6.26. Crack development on front edge of B-1-6F-3.5 after first detonation

Due to the minimal damage observed after the first blast event, the panel was set to experience a second event using the same charge weight, but a 50% reduction in

standoff distance. The goal was to achieve the same level of damage as panel B-3-2F-3.5. After the second event, the panel had developed a crack along the tension face measuring 0.375-in (9.5 mm) at the front edge, and 0.25-in (6.4 mm) at the back edge. A fine hairline crack developed along the top face of the panel. There was a residual deflection of 1-in (25.4 mm) at the center of the panel. Figure 6.27and Figure 6.28 display the resulting damage visually. The initial weight of the panel was 704 lbs (319.3 kg), and the final weight of the panel was 699 lbs (317.1 kg) for a total of 5 pounds (2.3 kg) of mass lost after the two events. The accuracy of the load cell used to weigh the specimens was +/- 5 lbs (2.3 kg), and since no spalling or fragmentation was noted, statistically the 5 pound (2.3 kg) difference in weight does not suggest mass loss.

Figure 6.27. Top face of B-1-6F-3.5 after second detonation

Figure 6.28. Cracking on the tension face after testing

6.3.1.4 B-2-P-3.5 results. The 3.5-in (89 mm) thick panel with no fibers broke before testing. The three thicker panels were stacked on a pallet for storage, and when the top 3.5-in (89 mm) panel was being loaded, the forks of the bobcat caught the hooks of the middle panel. The panel detached after the corner was lifted approximately 1-in (25.4 mm) in the air and the fall broke this panel which sat at the bottom of the stack. The broken panel is shown in Figure 6.29.

Figure 6.29. Broken 3.5-in plain UHPC panel

6.3.1.5 B-6-6F-2 results. Blast panel B-6-6F-2, showed heavy damage after the first blast event. After detonation, the panel had developed a thin crack along the top face, and a significant crack along the tension face of the panel that measured 0.375-in (9.5 mm) wide at the back edge, and 0.1875-in (4.8 mm) wide at the front edge. The residual deflection was 2-in (50.8 mm) along the center of the panel, front to back. The initial weight of this specimen was 358.5 lbs (162.6 kg), and the final weight was 346.5 lbs (157.2 kg). There was no observed spalling or fragmentation, and after accounting for the accuracy of the load cell, the mass loss for this specimen was 4.7%. The CEDAW prediction for this event is shown in Figure 6.30. The pressure-impulse curves produced by CEDAW display a green line to indicate the upper bound of superficial damage, a light blue line to indicate the upper bound of moderate damage, a red line to indicate the upper bound of heavy damage, and a dark blue line to indicate the onset of blowout failure. It also shows both the incident load from the user inputs (the triangle point) and the reflected load from the threat (diamond point). The diamond point indicates the overall category the specimen should fall in after the threat. For instance, for the threat B-6-6F-2 was exposed to (3 lb (1.36 kg) charge at 48-in (1.2 m) standoff), the

P-i curve in Figure 6.30 shows that this event should cause results in the heavy damage range, which is what is displayed in Figure 6.31 through Figure 6.35.

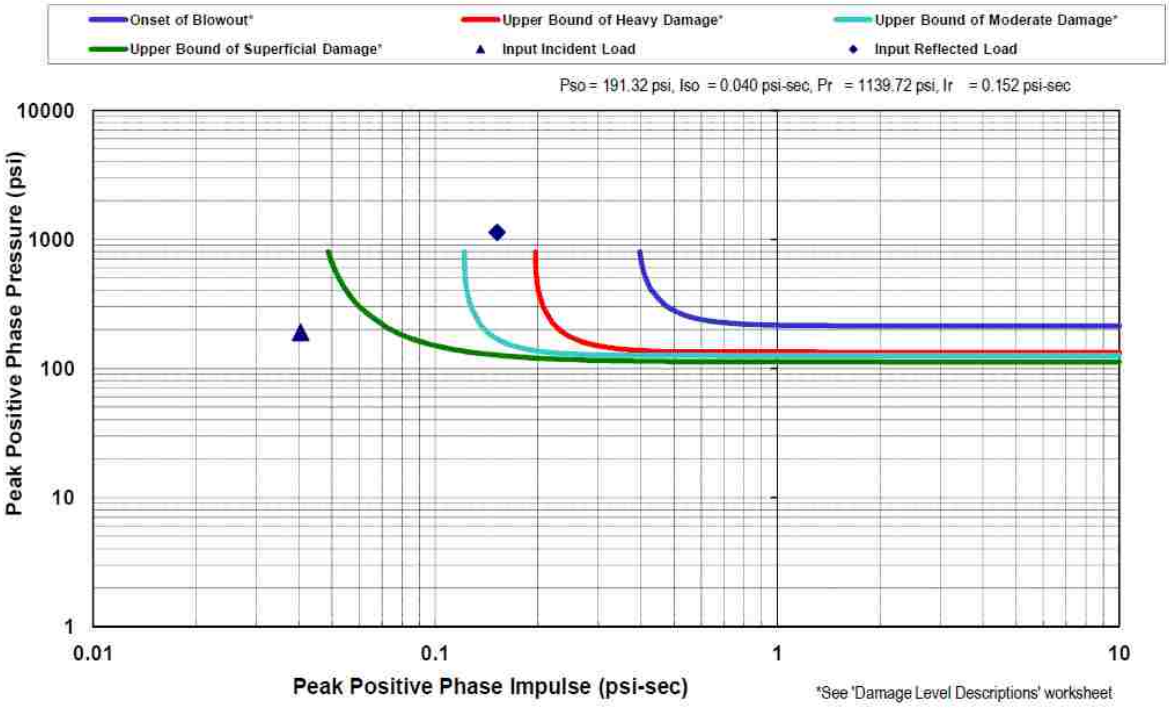

Figure 6.30. CEDAW P-i curves for 3 lb (1.36 kg) at 48-in (1.2 m) blast event

Figure 6.31. Panel B-6-6F-2 before detonation

Figure 6.32. Top face of B-6-6F-2 after detonation

Figure 6.33. Crack development after detonation

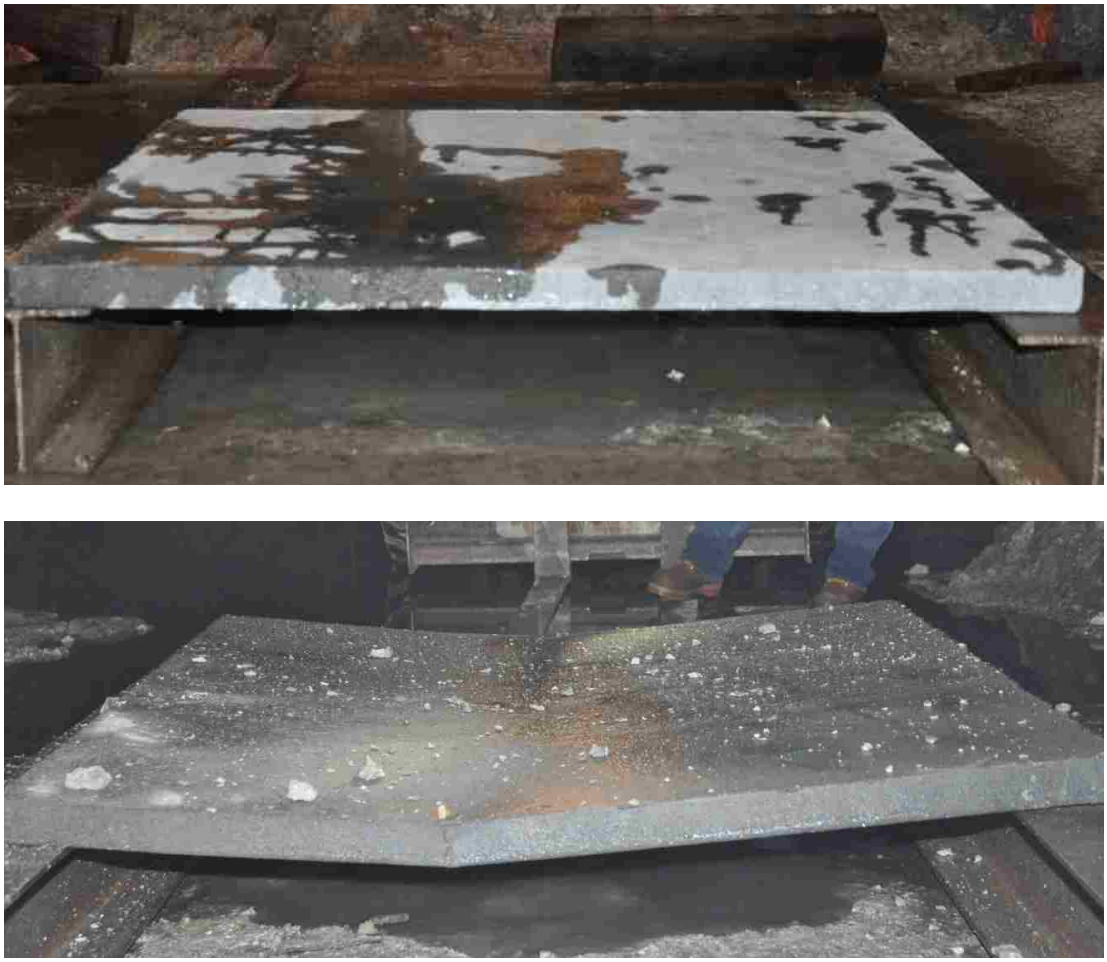

Figure 6.34. Deflection of B-6-6F-2 before (top) and after (bottom) detonation

Figure 6.35. Tension face cracking of B-6-6F-2 after detonation

6.3.1.6 B-5-P-2 results. After review of the impact data of the failure load on the comparable impact panel specimen, it was determined that roughly 10 psi (0.069 MPa) of pressure should fail panel B-5-P-2 shown in Figure 6.37. Using this information, a series of CEDAW analyses were studied to estimate the type of blast event that would bring the panel close to failure without failing it in a catastrophic way which would provide no valuable data. The CEDAW results are shown in Appendix E, Figure 7-44 through Figure 7-54. After the first blast event (0.25 lb (0.11 kg) C-4 at 36-in (0.9 m) standoff), minimal damage was observed on both the top and bottom faces of the specimen. No cracking or fragmentation was observed, and a residual deflection of 0.125-in (3.2 mm) was measured at the center of the panel. The CEDAW prediction for this event is shown in Figure 6.36. It shows that this event should cause damage in the superficial damage range, which is what is displayed in Figure 6.38.

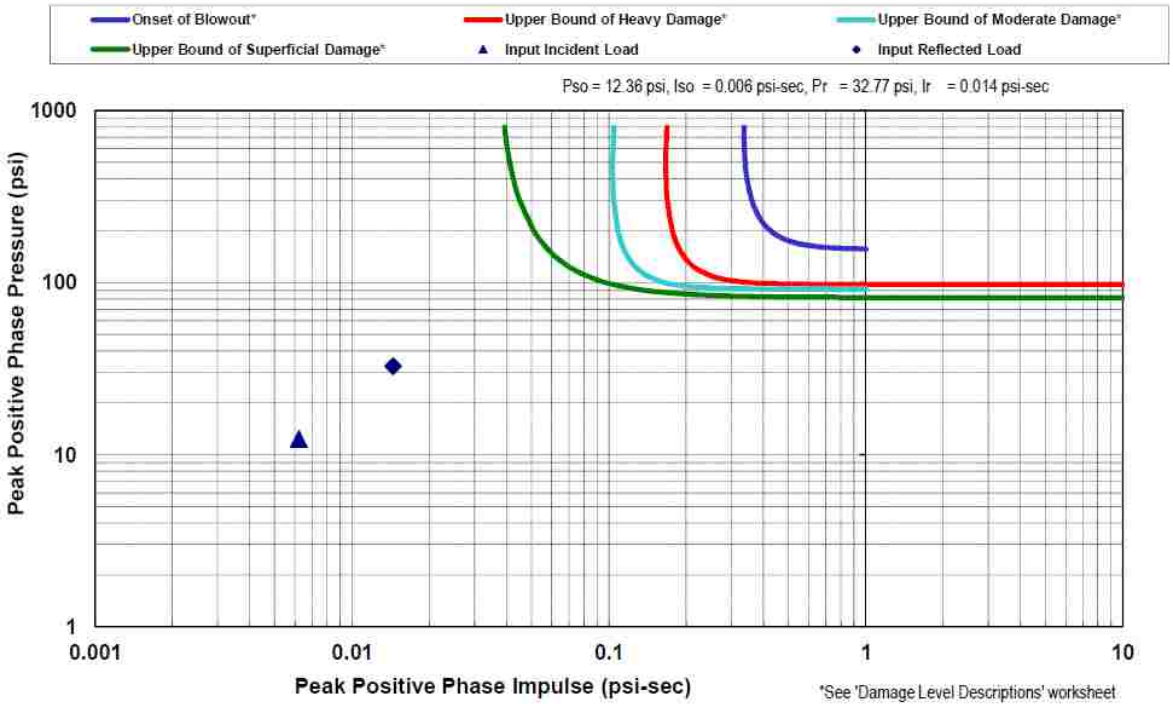

Figure 6.36. CEDAW P-i curves for 0.25 lb (0.11 kg) at 72-in (1.8 m) blast event

Figure 6.37. Panel B-5-P-2 before detonation

Figure 6.38. Panel B-5-P-2 after first detonation

Due to the minimal damage seen after the first blast event, the panel was set to undertake a second blast event at the same standoff distance, but the charge weight was increased to 1 lb (0.45 kg) of C-4 explosive. According to a CEDAW prediction shown in Figure 6.39, this blast event was still in the "Superficial Damage" zone of this specimen's predicted strength, however, after the detonation the failure shown in Figure 6.40 was observed. The panel broke into four pieces, but it did not display the typical shock wave failure.

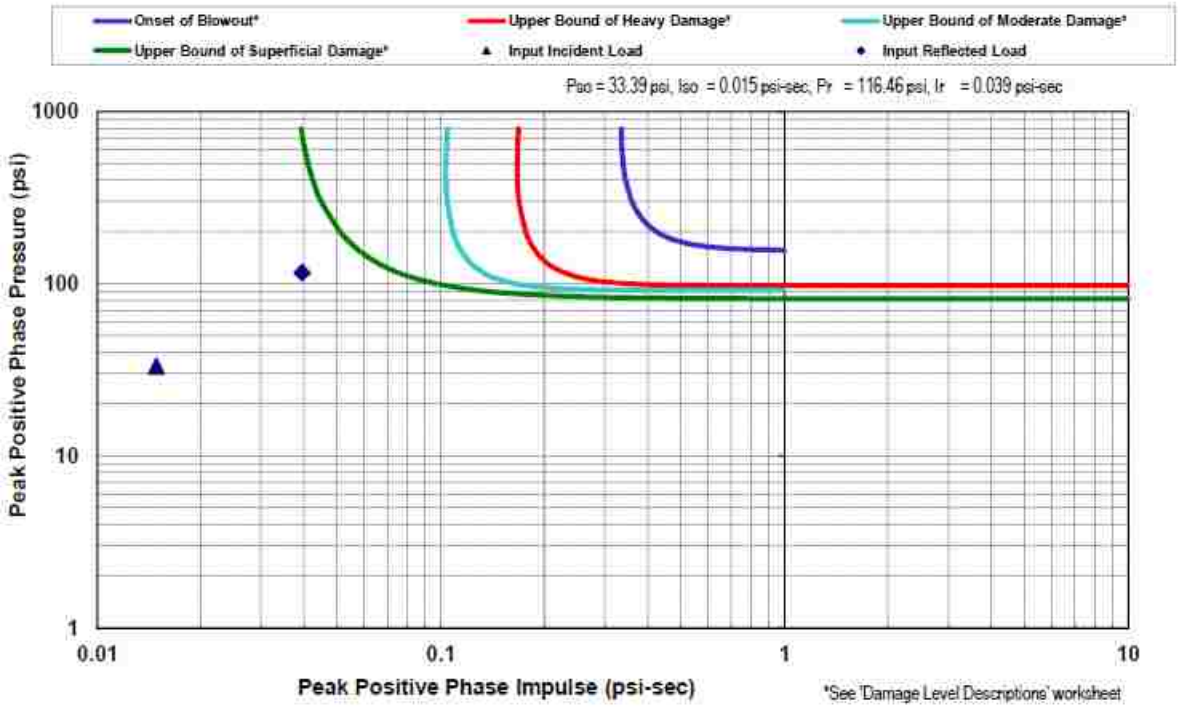

Figure 6.39. CEDAW P-I curves for 1 lb (0.45 kg) at 72-in (1.8 m) blast event

Figure 6.40. Panel B-5-P-2 after second detonation

6.3.1.7 Full panel testing summary. The following discussion is a summary of the full panel blast test results that are discussed in detail previously in this section.

Table 6.8 and Table 6.9 are summaries of theoretical pressures and observed damages for each of the tested 3.5-in thick (89 mm), and 2-in (50.8 mm) thick blast panels respectively. For each specimen type, the theoretical blast pressure is shown next to the corresponding damage that was observed. The theoretical pressures come from values predicted by ConWep analyses that are shown in Appendix F. The actual pressures were not measured because previous research had not been successful in collecting usable data without destroying the pressure sensing equipment.

Table 6.8. Summary of full, 3.5-in, blast specimen results

Full 3.5-in Thick Panels					
6% Fiber		2% Fiber		No Fiber	
Pressure[1] (psi)	Damage[2]	Pressure[1] (psi)	Damage[2]	Pressure[1] (psi)	Damage[2]
	None		None		None
1550	Superficial		Superficial		Superficial
	Moderate	1550	Moderate		Moderate
7663	Heavy	1550	Heavy		Heavy
	Hazardous Failure		Hazardous Failure	30*	Hazardous Failure
	Blowout		Blowout		Blowout

[1] Pressures predicted using ConWep

[2] Damage definitions from PDC-TR 06-08 Rev 1

* Pressure estimated based on comparable impact testing results

Conversion: 1 psi = 0.006895 MPa

Table 6.9. Summary of full, 2-in, blast specimen results

Full 2-in Thick Panels					
6% Fiber		2% Fiber		No Fiber	
Pressure[1] (psi)	Damage[2]	Pressure[1] (psi)	Damage[2]	Pressure[1] (psi)	Damage[2]
	None		None		None
	Superficial		Superficial	21.4	Superficial
	Moderate		Moderate		Moderate
708	Heavy		Heavy		Heavy
	Hazardous Failure		Hazardous Failure		Hazardous Failure
	Blowout	15800	Blowout	71.6	Blowout

[1] Pressures predicted using ConWep

[2] Damage definitions from PDC-TR 06-08 Rev 1

Conversion: 1 psi = 0.006895 MPa

As discussed in section 6.3.1.4, the plain 3.5-in (89 mm) thick UHPC panel broke before testing. The value shown for this panel was estimated based on the results of the 2-in (50.8 mm) plain UHPC panel that underwent impact testing. The value was estimated by the force it took to fail the impact specimen, and dividing that by the area at which the force impacted the panel.

Table 6.8 and Figure 6.41 are an easy way to show the general results of the blast testing of these specimens. They show that for the same blast event, in this case a blast event causing a peak pressure of 1550 psi (10.7 MPa), the panel with 6% fiber out-performed the specimens with only 2% fiber. It also shows that for the 6% fiber panel to sustain the same level of damage as the panel with 2% fiber, it took 7663 psi (52.8 MPa) of pressure compared to 1550 psi (10.7 MPa) of pressure. The figure and table also show the drastic difference in performance between the panels with fiber, and the plain UHPC panel with no fiber.

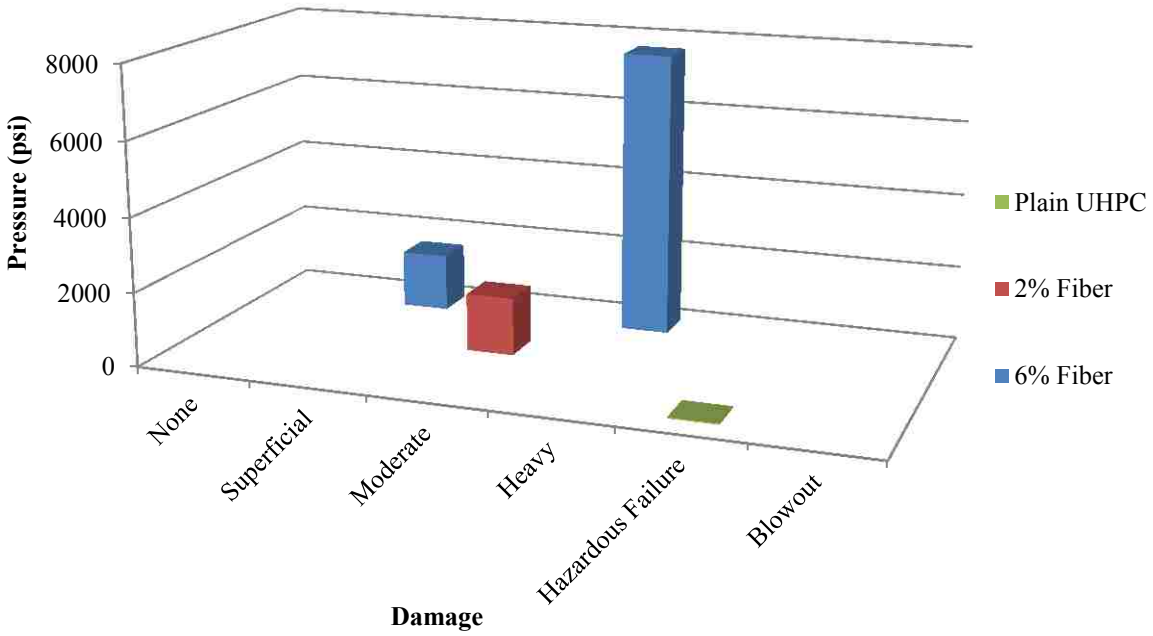

Conversion: 1 psi = 0.006895 MPa

Figure 6.41. Graphic summary of full, 3.5-in (89 mm), blast specimen results

Table 6.9 and Figure 6.42 show that very little pressure causes superficial damage in a plain UHPC panel, and only slightly more pressure can cause blowout of the same panel. Both of these pressures are extremely small in comparison to the 708 psi (4.9 MPa) of pressure that caused "heavy" damage in the 6% fiber panel. The peak pressure value for the 2% fiber panel is so high because that was the first panel that was tested, and it was set to experience the same event as the study from Wulfers (2012). This event caused blowout failure of the panel, and this outcome is what led to the additional use of ConWep and CEDAW to create blast events that would yield more useful data.

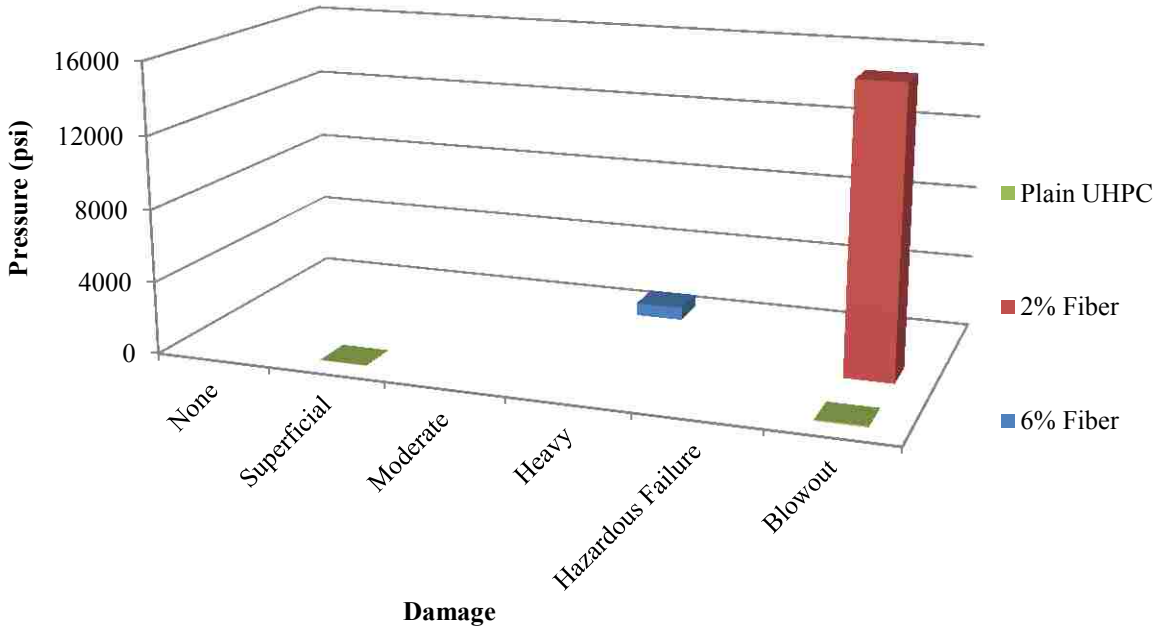

Conversion: 1 psi = 0.006895 MPa

Figure 6.42. Graphic summary of full, 2-in (50.8 mm), blast specimen results

Figure 6.43 is a graphic representation of the full blast panel specimen results. The chart shows both the peak pressure and average impulse predicted by ConWep, as well as the level of damage as described for CEDAW for each full panel specimen tested.

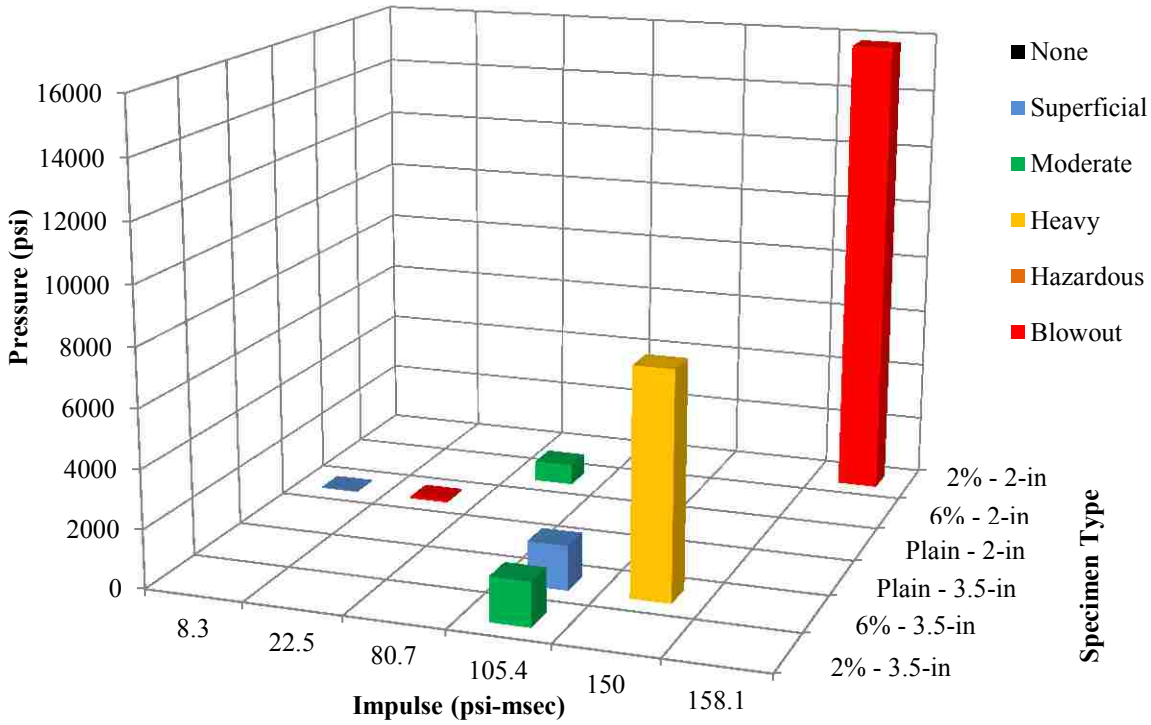

Conversion: 1 psi = 0.006895 MPa

Figure 6.43. Full blast specimen results

6.3.2. Half Panel Specimen Testing Set #1. The goal of this round of testing was to investigate the cratering and spalling behaviors of this material by specifically trying to create these failure modes. As mentioned in Section 5.5.2.2, the testing matrix was developed based on a series of ConWep breaching predictions. These predictions are shown in Appendix F. Table 6.10 shows the testing matrix for the half panel specimens that are shown in this section.

Table 6.10. Test matrix for half panel specimen set #1

Specimen	Charge Weight (lb)	Standoff Distance (in)
H-1-2F-3.5	3	36
H-2-6F-3.5	3	36
H-3-6F-3.5	0.5	2.25
H-4-P-3.5	3	36

Conversions: 1 lb = 0.45 kg

1 in = 25.4 mm

Panels are designated with an 'H' to indicate they are half size specimens, and the number following H indicates in what order the panels were tested. The other portions of the specimen designation remain the same as the full panel specimens. This naming convention continues to the second set of half panel testing.

6.3.2.1 H-3-2F-3.5 results. The first panel tested had a fiber content of 2%. After detonation, the panel displayed small cracking on the front face, and major cracking on the back (tension) face. The major crack on the back face measured 0.5-in (12.7 mm) wide. The other cracking shown on the back face in Figure 6.45 are mostly from when the specimen was tested as a full panel. Cracks that were not visible when the panel was tested the first time likely had their roots from the aftermath of the full panel blast event. The residual deflection of this panel was 0.25-in (6.4 mm). Its initial weight was 317 lb (143.8 kg) and its final weight was 317 lb (143.8 kg) which resulted in 0% mass loss. ConWep's breaching software predicted 0.688-in (17.5 mm) of breaching, and 0.3352-in (8.5 mm) of spalling for this blast event. As shown in Figure 6.44 and Figure 6.45, no spalling or breaching was observed.

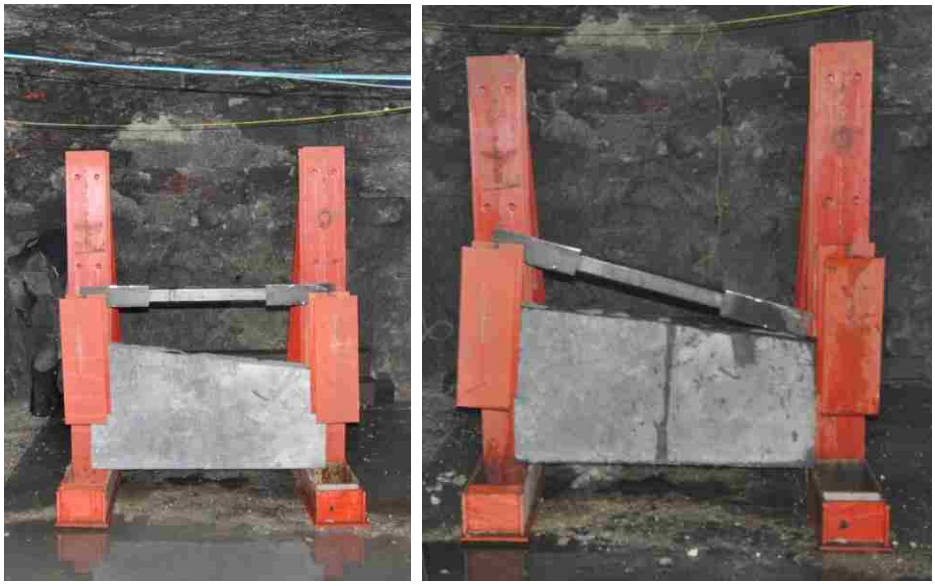

Figure 6.44. Front face of H-1-2F-3.5 before (left) and after (right) detonation

Figure 6.45. Back face of H-1-2F-3.5 after detonation

6.3.2.2 H-2-6F-3.5 results. The second panel tested had a fiber content of 6%. After detonation, the panel displayed hairline cracking on the front face, and no cracking on the back (tension) face. There was no residual deflection after this blast event. Its initial weight was 383 lb (173.7 kg) and its final weight was 383 lb (173.7 kg) which resulted in 0% mass loss. ConWep's breaching software predicted 0.6474-in (16.4 mm) of breaching, and 0.3044-in (7.7 mm) of spalling for this blast event. The before and after testing photographs are shown below in Figure 6.46 through Figure 6.49. As shown in Figure 6.49, no spalling or breaching was observed.

Figure 6.46. Front of H-2-6F-3.5 before detonation

Figure 6.47. Back of H-2-6F-3.5 before detonation

Figure 6.48. Front of H-2-6F-3.5 after detonation

Figure 6.49. Back of H-2-6F-3.5 after detonation

As mentioned in the test set-up portion of this report, this panel had so little damage after detonation, it was reset for a close range trial blast event to determine the testing setup for the next group of panels. After this close range trial detonation, the panel had successfully displayed spalling and cratering behavior as shown in Figure 6.50 through Figure 6.52. The panel incurred a crater roughly 3-in (76.2 mm) in diameter and 0.25-in (6.4 mm) deep on the front face, and spalling of roughly 11-in (0.28 m) in diameter and 1-in (25.4 mm) deep on the back (tension) face. The initial weight was 383 lb (173.7 kg), and the final weight was 364 lb (165.1 kg). After taking into account the accuracy of the load cell, the panel experienced roughly 4% mass loss after this event.

Figure 6.50. Cratering on front face of H-3-6F-3.5 after detonation

Figure 6.51. Spalling on tension face of H-3-6F-3.5 after detonation

Figure 6.52. Close-up of spalling on H-3-6F-3.5

6.3.2.3 H-4-P-3.5 results. The last panel tested in the first half-specimen set had no fiber reinforcement and is shown in Figure 6.53. After detonation, the specimen was in many large fragmented pieces due to experiencing blowout failure. The initial weight of this panel was 306.5 lb (139.0 kg), and the final weight of the collected pieces was 298 lb (135.2 kg). This final weight was dependent on the amount of fragments that could be recovered after the failure. The final mass of the fragments was found by weighing the pieces atop a pallet, and then subtracting the weight of the pallet. After taking into account the accuracy of the load cell, roughly 4.5% mass loss was recorded. ConWep's breaching software predicted 0.7984-in (20.3 mm) of breaching, and 0.4246-in (10.8 mm) of spalling for this blast event. As shown in Figure 6.54, the entire specimen was breached, however upon collection of the fragments, no evidence of spalling or cratering was observed meaning the damage is due to structural blowout.

Figure 6.53. Front (left) and back (right) of H-4-P-3.5 before detonation

Figure 6.54. Panel H-4-P-3.5 after detonation

6.3.2.4 Half panel testing summary. The following discussion is a summary of the first set of half panel blast test results that are discussed in detail previously in this section. Although this set of tests was aimed at investigating spalling and breaching behavior, the results were more similar to what was seen in the full panel tests. Therefore the results will be presented in the same manner.

Table 6.11 is a summary of theoretical pressures and observed damages for each of the tested 3.5-in (89 mm) thick blast panels. The theoretical pressures come from values predicted by ConWep analyses that are shown in Appendix F. As stated before, the actual pressures were not measured because previous research had not been successful in collecting usable data without destroying the pressure sensing equipment.

Table 6.11. Summary of half, 3.5-in (89 mm) thick, blast panel results

Half Panels, 3.5-in Thick, Set #1					
6% Fiber		2% Fiber		No Fiber	
Pressure[1] (psi)	Damage[2]	Pressure[1] (psi)	Damage[2]	Pressure[1] (psi)	Damage[2]
	None		None		None
1550	Superficial		Superficial		Superficial
	Moderate		Moderate		Moderate
	Heavy	1550	Heavy		Heavy
	Hazardous Failure		Hazardous Failure		Hazardous Failure
	Blowout		Blowout	1550	Blowout

[1] Pressures predicted using Conwep

[2] Damage definitions from PDC-TR 06-08 Rev 1

Conversion: 1 psi = 0.006895 MPa

Table 6.11 and Figure 6.55 show that for the same blast event, in this case a blast event causing a peak pressure of 1550 psi (10.7 MPa) and an average impulse of 105.4 psi-msec (0.73 MPa-msec), the panel with 6% fiber out-performed the other

specimens with lower fiber contents. The figure shows that the same event caused a blowout of the plain UHPC panel, heavy damage to the 2% fiber panel, and very little damage to the panel with 6% fiber content. This result clearly shows the improved performance of the panel solely due to an increase in fiber content.

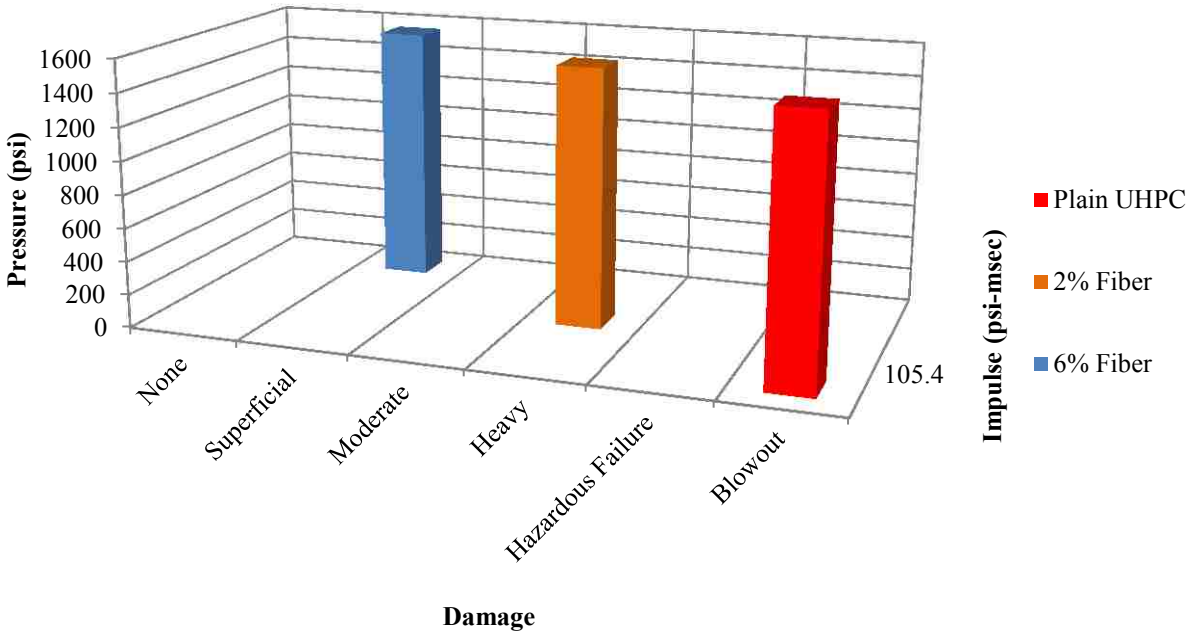

Conversion: 1 psi = 0.006895 MPa

Figure 6.55. Graphic summary of half, 3.5-in (89 mm) thick, blast panel results

6.3.3. Half panel specimen testing set #2. The goal of this set of testing was to again investigate the cratering and spalling behaviors of this material by specifically trying to create these failure modes. As shown in the previous results, the first attempt to create this failure was unsuccessful; therefore a new test matrix was used for this set of tests. As mentioned in Section 5.5.2.2, the testing matrix was developed based on a trial

detonation that was performed on one of the panels in the first set of half-size specimen testing. Table 6.12 shows the testing matrix for the half panel specimens that are shown in this section. The panel designation labels follow the same format as the test matrix shown in section 6.3.2.

Table 6.12. Testing matrix for half panel specimen set #2

Specimen	Charge Weight (lb)	Standoff Distance (in)
H-5-2F-3.5	0.5	2.25
H-6-P-3.5	0.5	2.25
H-7-6F-3.5	0.5	2.25

Conversions: 1 lb = 0.45 kg

1-in = 25.4 mm

6.3.3.1 H-5-2F-3.5 results. The first panel tested had a fiber content of 2%. After this close range detonation, the panel had successfully displayed spalling and cratering behavior as pictured in Figure 6.56 and Figure 6.57. The panel incurred a crater roughly 3.5-in (89 mm) in diameter and 0.25-in (6.35 mm) deep on the front face, and spalling of roughly 11-in (0.28 m) in diameter and 1-in (25.4 mm) deep on the back (tension) face. The initial weight was 320 lb (145.2 kg), and the final weight was 308 lb (139.7 kg). After taking into account the accuracy of the load cell, the panel experienced roughly 2% mass loss after this event. Roughly 3 lb (1.4 kg) of fragmentation was recovered.

Figure 6.56. Front face of H-5-2F-3.5 before (left) and after (right) detonation

Figure 6.57. Back (tension) face of H-5-2F-3.5 after detonation

6.3.3.2 H-6-P-3.5 results. The second panel in this set contained no fibers. After the close range detonation, the panel displayed blowout failure behavior with many small fragments. The initial weight of this panel was 347 lb (157.4 kg), and the final weight of

the collected pieces was 311 lb (141.1 kg). This final weight was dependent on the amount of fragments that could be recovered after the failure. The final mass of the fragments was found by weighing the pieces atop a pallet, and then subtracting the weight of the pallet. After taking into account the accuracy of the load cell, roughly 9% mass loss was recorded. Photographs of the threat damage are displayed below as Figure 6.58 and Figure 6.59.

Figure 6.58. Panel H-6-P-3.5 before (left) and after (right) detonation

Figure 6.59. Collected fragments of H-6-P-3.5 after detonation

6.3.3.3 H-7-6F-3.5 results. The final panel tested contained 6% fiber. After detonation, the panel displayed cratering and spalling failures as shown in Figure 6.60 and Figure 6.61. The panel incurred a crater roughly 3-in (76.2 mm) in diameter and 0.25-in (6.35 mm) deep on the front face, and spalling of roughly 11-in (0.28 m) in diameter and 1.5-in (38.1 mm) deep on the back (tension) face. The initial weight was 332 lb (150.6 kg), and the final weight was 322.5 lb (146.3 kg). After taking into account the accuracy of the load cell, the panel experienced roughly 1.5% mass loss after this event.

Figure 6.60. Panel H-7-6F-3.5 before (left) and after (right) detonation

Figure 6.61. Tension face of panel H-7-6F-3.5 after detonation

7. CONCLUSIONS AND RECOMMENDATIONS

7.1. CONCLUSIONS

The following is a summary of general conclusions that can be made based on the results and discussion presented in section 6 of this report.

Creep and Shrinkage Behavior

- The superior performance of the UHPC in creep and shrinkage is due to the material density and particle packing nature, as well as its high cement content and low w/cm ratio.
- Heat curing is instrumental in the ability of UHPC to minimize the creep and shrinkage strains that develop, however, the results also show that ambient air cured UHPC still achieves favorable creep and shrinkage behavior relative to conventional concrete.
- The heat curing process has the ability to reduce the post curing creep and shrinkage behavior of the material to an extremely small amount.

Impact Behavior

- The favorable performance of the impact panels tested suggests that traditional continuous steel reinforcement is not required for UHPC designed for use in impact situations. This is because the impulse load is able to be handled mostly by the material strength.
- The superior performance of the specimen with 6% fiber relative to the plain UHPC panel is due to the fact that the fibers allow the specimen to dissipate the impact energy without failing the concrete panel.
- No spalling or fragmentation was observed at the peak drop height and showed superior performance to all other concrete mixture materials tested previously at Missouri S&T.

Blast Behavior

- The performance of the blast panels suggest that continuous reinforcement is necessary to prevent fracture of panels. This is to help distribute the blast load through the panel since the fiber reinforcement is discontinuous.
- UHPC panels under blast loading show minimal to no spalling and fragmentation, even when the panels fractured. This is very beneficial compared to conventional concrete which experiences dangerous fragmentation under blast loading.
- A few conclusions can be drawn about using ConWep to predict the performance of UHPC panels by studying the results of this research. ConWep does not predict overall performance or spalling behavior well for plain UHPC panels. The software also under-predicts the capability of UHPC panels with 6% fiber. However, the testing suggests that ConWep does accurately predict the capabilities of UHPC panels with 2% fiber. Future research in this area could prove beneficial to the use of UHPC in blast design situations.
- While the testing results show improved performance with an increase in fiber content, further investigations should include balancing the performance benefit of the increased fiber content and the material cost.

7.2. RECOMMENDATIONS

The following is a summary of general recommendations in areas that could have potential for improvements or could benefit from future studies based on the results presented from this work.

Mix Design:

- Try the use of rubber fibers or a hybrid mix of rubber and steel fibers for possible system pseudo-ductility.
- Grade the sand for more consistent results.
- Investigate if the lime water curing had any effect on cube specimen strength.
- Explore the use of ice in the mix to reduce fresh concrete temperature and possibly increase strength.

Creep and Shrinkage:

- Investigate the length of heat curing on creep and shrinkage behavior.
- Put specimens in a temperature and humidity controlled environment to reduce variables affecting creep and shrinkage.

Impact Performance:

- Increase the weight of the steel rod used for impact to induce failure on the steel fiber reinforced UHPC panel.
- Restrain the upward "bouncing" of the panel.
- Investigate the effect of changing the aspect ratio of the steel fibers.
- Explore the "self-healing" nature of the material indicated by the lack of failure and ability to continue to absorb energy.
- Study the cause of the cross pattern cracking experienced in this testing, as well as Gliha's testing for unreinforced panels.
- Study the effect of fiber content on impact performance.

Blast Mitigation:

- Add WWR continuous reinforcement to blast panels to provide some minimum continuous reinforcing.
- Investigate hybrid panels with WF-FA, plain concrete, or polyurea.
- Investigate material cost vs. material performance.
- Studies should be conducted without repeat testing to ensure the resulting damage is not compounded with each blast event.
- Increase in accuracy of software predictions for UHPC panel systems possibly through use of combining experimental data with material modeling.

APPENDIX A

PANEL SPECIMEN BATCH INFORMATION

Conversions: 1 lb/yd^3 = 0.59 kg/m^3

1 lb = 0.45 kg

Table A.1. Impact panel #1 batch weights

UHPC Composition			
Material	Amount (lb/yd^3)	Percent by Weight (%)	Batch Weight** (lb)
Type V Portland Cement	1324	29.6	191.3
Fine Sand	1896	42.3	273.8
Silica Fume	432	9.6	62.4
Ground Quartz	390	8.7	56.4
Glenium 3030NS Superplasticizer	56	1.2	8.1
Rheocrete CNI Accelerator	N/A	N/A	N/A
Steel Fibers	N/A	N/A	N/A
Water*	382	8.5	50.8

*Water adjusted on mix date to account for sand moisture content

**Batch Volume = 3.9 ft^3

Table A.2. Impact panel #2 batch weights

UHPC Composition			
Material	Amount (lb/yd^3)	Percent by Weight (%)	Batch Weight** (lb)
Type V Portland Cement	1324	27.8	224.0
Fine Sand	1896	39.8	320.7
Silica Fume	432	9.1	73.1
Ground Quartz	390	8.2	66.0
Glenium 3030NS Superplasticizer	56	1.2	9.4
Rheocrete CNI Accelerator	N/A	N/A	N/A
Steel Fibers	288	6.0	48.7
Water*	382	8.0	64.7

*Water adjusted on mix date to account for sand moisture content

**Batch Volume = 4.6 ft^3

Table A.3. Blast Panel #1 Batch Weights

UHPC Composition			
Material	Amount (lb/yd^3)	Percent by Weight (%)	Batch Weight** (lb)
Type V Portland Cement	1324	27.8	285.6
Fine Sand	1896	39.8	408.8
Silica Fume	432	9.1	93.2
Ground Quartz	390	8.2	84.2
Glenium 3030NS Superplasticizer	56	1.2	12.0
Rheocrete CNI Accelerator	N/A	N/A	N/A
Steel Fibers	288	6.0	62.1
Water*	382	8.0	79.8

*Water adjusted on mix date to account for sand moisture content

**Batch Volume = 5.8 ft^3

Table A.4. Blast panel #2 batch weights

UHPC Composition			
Material	Amount (lb/yd^3)	Percent by Weight (%)	Batch Weight** (lb)
Type V Portland Cement	1324	29.6	274.8
Fine Sand	1896	42.3	393.4
Silica Fume	432	9.6	89.7
Ground Quartz	390	8.7	81.0
Glenium 3030NS Superplasticizer	56	1.2	11.6
Rheocrete CNI Accelerator	N/A	N/A	N/A
Steel Fibers	N/A	N/A	N/A
Water*	382	8.5	76.8

*Water adjusted on mix date to account for sand moisture content

**Batch Volume = 5.6 ft^3

Table A.5. Blast panel #3 batch weights

UHPC Composition			
Material	Amount (lb/yd^3)	Percent by Weight (%)	Batch Weight** (lb)
Type V Portland Cement	1324	29.0	254.8
Fine Sand	1896	41.5	364.8
Silica Fume	432	9.4	83.2
Ground Quartz	390	8.5	75.1
Glenium 3030NS Superplasticizer	56	1.2	10.7
Rheocrete CNI Accelerator	N/A	N/A	N/A
Steel Fibers	93	2.0	17.9
Water*	382	8.4	71.2

*Water adjusted on mix date to account for sand moisture content

**Batch Volume = 5.2 ft^3

Table A.6. Blast panel #4 batch weights

UHPC Composition			
Material	Amount (lb/yd^3)	Percent by Weight (%)	Batch Weight** (lb)
Type V Portland Cement	1324	29.0	164.6
Fine Sand	1896	41.5	235.6
Silica Fume	432	9.4	53.7
Ground Quartz	390	8.5	48.5
Glenium 3030NS Superplasticizer	56	1.2	6.9
Rheocrete CNI Accelerator	N/A	N/A	N/A
Steel Fibers	93	2.0	11.6
Water*	382	8.4	46.0

*Water adjusted on mix date to account for sand moisture content

**Batch Volume = 3.4 ft^3

Table A.7. Blast panel #5 batch weights

UHPC Composition			
Material	Amount (lb/yd^3)	Percent by Weight (%)	Batch Weight** (lb)
Type V Portland Cement	1324	29.6	239.8
Fine Sand	1896	42.3	343.2
Silica Fume	432	9.6	78.2
Ground Quartz	390	8.7	70.7
Glenium 3030NS Superplasticizer	56	1.2	10.1
Rheocrete CNI Accelerator	N/A	N/A	N/A
Steel Fibers	N/A	N/A	N/A
Water*	382	8.5	67.0

*Water adjusted on mix date to account for sand moisture content

**Batch Volume = 4.9 ft^3

Table A.8. Blast panel #6 batch weights

UHPC Composition			
Material	Amount (lb/yd^3)	Percent by Weight (%)	Batch Weight** (lb)
Type V Portland Cement	1324	27.8	221.4
Fine Sand	1896	39.8	316.9
Silica Fume	432	9.1	72.2
Ground Quartz	390	8.2	65.2
Glenium 3030NS Superplasticizer	56	1.2	9.3
Rheocrete CNI Accelerator	N/A	N/A	N/A
Steel Fibers	288	6.0	48.2
Water*	382	8.0	61.8

*Water adjusted on mix date to account for sand moisture content

**Batch Volume = 4.5 ft^3

APPENDIX B

CREEP AND SHRINKAGE DATA AND RESULTS

The following tables contain a summary of the creep and shrinkage data from the specimen readings. The tables are broken down into total strain, shrinkage strain, elastic strain, creep strain, and finally, the creep coefficient.

Table B.1. Creep and shrinkage data for plain UHPC, air cured specimens

Mix	Curing Condition	Strain	Age of Testing (days)												
			4	5	6	7	8	10	12	13	19	32	49	57	79
Plain UHPC (P)	Air Cured (A)	Total (in/in)	-0.00569	-0.00736	-0.00899	-0.01037	-0.01126	-0.01306	-0.01439	-0.01537	-0.0181	-0.02112	-0.02197	-0.02383	-0.02386
		Shrinkage (in/in)	-0.00905	-0.01098	-0.0123	-0.01401	-0.01482	-0.01667	-0.01824	-0.01955	-0.02198	-0.02542	-0.02634	-0.02822	-0.02831
		Elastic (in/in)	-0.00456	-0.00456	-0.00456	-0.00456	-0.00456	-0.00456	-0.00456	-0.00456	-0.00456	-0.00456	-0.00456	-0.00456	-0.00456
		Creep (in/in)	0.003359	0.003614	0.003306	0.003646	0.003569	0.003616	0.003847	0.004187	0.003878	0.004302	0.004376	0.004391	0.004451
		Creep Coefficient	-0.73739	-0.79324	-0.72577	-0.80038	-0.78345	-0.79378	-0.84456	-0.91917	-0.85116	-0.94442	-0.96049	-0.96393	-0.97713

Table B.2. Creep and shrinkage data for plain UHPC, heat cured specimens

Mix	Curing Condition	Strain	Age of Testing (days)												
			4	5	6	7	8	10	12	13	19	32	49	57	79
Plain UHPC (P)	Heat Cured (H)	Total (in/in)	0.252587	0.253872	0.254218	0.254349	0.254372	0.254303	0.25421	0.254241	0.253441	0.252733	0.252641	0.251749	0.252003
		Shrinkage (in/in)	-0.00419	-0.00278	-0.00237	-0.0023	-0.00224	-0.00238	-0.00251	-0.0027	-0.00331	-0.00387	-0.00405	-0.00508	-0.00477
		Elastic (in/in)	0.390203	0.390203	0.390203	0.390203	0.390203	0.390203	0.390203	0.390203	0.390203	0.390203	0.390203	0.390203	0.390203
		Creep (in/in)	0.256777	0.25665	0.256584	0.256644	0.256608	0.25668	0.256717	0.256937	0.256748	0.256605	0.256689	0.256832	0.256769
		Creep Coefficient	0.65806	0.657734	0.657566	0.65772	0.657629	0.657813	0.657908	0.65847	0.657987	0.657621	0.657836	0.658203	0.658039

Table B.3. Creep and shrinkage data for 6% fiber UHPC, air cured specimens

Mix	Curing Condition	Strain	Age of Testing (days)												
			4	5	6	7	8	10	12	13	19	32	49	57	79
6% Fiber (F)	Air Cured (A)	Total (in/in)	-0.03933	-0.04156	-0.04273	-0.0442	-0.04504	-0.04684	-0.04793	-0.04916	-0.05144	-0.0542	-0.05473	-0.05696	-0.05651
		Shrinkage (in/in)	0.00377	-0.01979	-0.02107	-0.02231	-0.02307	-0.02578	-0.02662	-0.02753	-0.02994	-0.03296	-0.03365	-0.03542	-0.03526
		Elastic (in/in)	-0.03902	-0.03902	-0.03902	-0.03902	-0.03902	-0.03902	-0.03902	-0.03902	-0.03902	-0.03902	-0.03902	-0.03902	-0.03902
		Creep (in/in)	-0.0431	-0.02177	-0.02166	-0.02189	-0.02197	-0.02106	-0.02131	-0.02163	-0.0215	-0.02124	-0.02108	-0.02154	-0.02125
		Creep Coefficient	1.104594	0.557897	0.555049	0.561029	0.563022	0.53973	0.546222	0.554195	0.551063	0.544229	0.540243	0.551917	0.544514

Table B.4. Creep and shrinkage data for 6% fiber UHPC, heat cured specimens

Mix	Curing Condition	Strain	Age of Testing (days)												
			4	5	6	7	8	10	12	13	19	32	49	57	79
6% Fiber (F)	Heat Cured (H)	Total (in/in)	-0.0212	-0.01998	-0.01975	-0.01962	-0.02009	-0.02026	-0.02064	-0.02071	-0.02102	-0.02195	-0.02164	-0.02266	-0.02255
		Shrinkage (in/in)	-0.0169	-0.01546	-0.0154	-0.01513	-0.0153	-0.01573	-0.01509	-0.01536	-0.01583	-0.0161	-0.01638	-0.0173	-0.01688
		Elastic (in/in)	-0.02064	-0.02064	-0.02064	-0.02064	-0.02064	-0.02064	-0.02064	-0.02064	-0.02064	-0.02064	-0.02064	-0.02064	-0.02064
		Creep (in/in)	-0.0043	-0.00451	-0.00435	-0.00449	-0.00479	-0.00454	-0.00555	-0.00535	-0.00519	-0.00585	-0.00527	-0.00536	-0.00568
		Creep Coefficient	0.208172	0.218601	0.210863	0.217726	0.231855	0.219879	0.269062	0.25897	0.251636	0.283528	0.255135	0.259845	0.275051

APPENDIX C

IMPACT TESTING RESULTS

This appendix contains the collected data from the impact tests performed in this study. Each figure represents the force and deflection vs. time data for one drop height only. Since the linear potentiometer was removed for the last 3 repetitions of the 186-in (4.7 m) drop test, the data from those tests is not shown in this appendix.

Note that for both test specimens, the first drop height at 3-in (0.07 m) was not captured by the data acquisition system, however testing proceeded as to not affect the data for the following drop heights. Since this data was not captured, it is not present in the following figures. For specimen I-2-6F-2, the same phenomena occurred for the 108-in (2.7 m) drop height, and as a result, this data is missing from the appendix.

Conversions: 1 lb = 0.45 kg

1-in = 25.4 mm

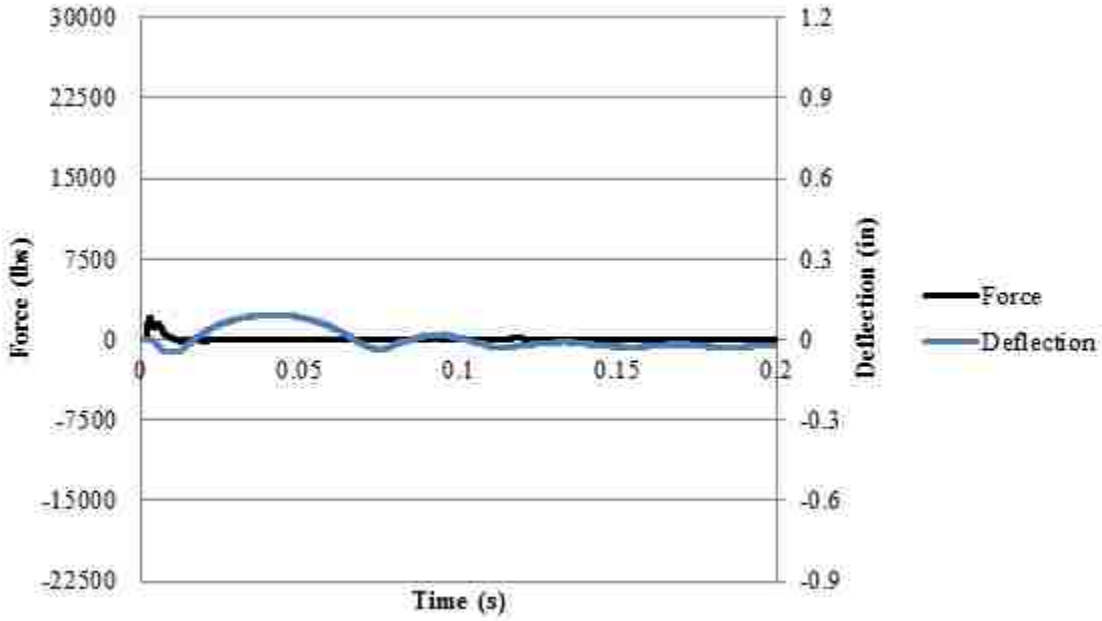

Figure C.1. Force and deflection vs. time for I-1-P-2 at 6-in (0.15 m)

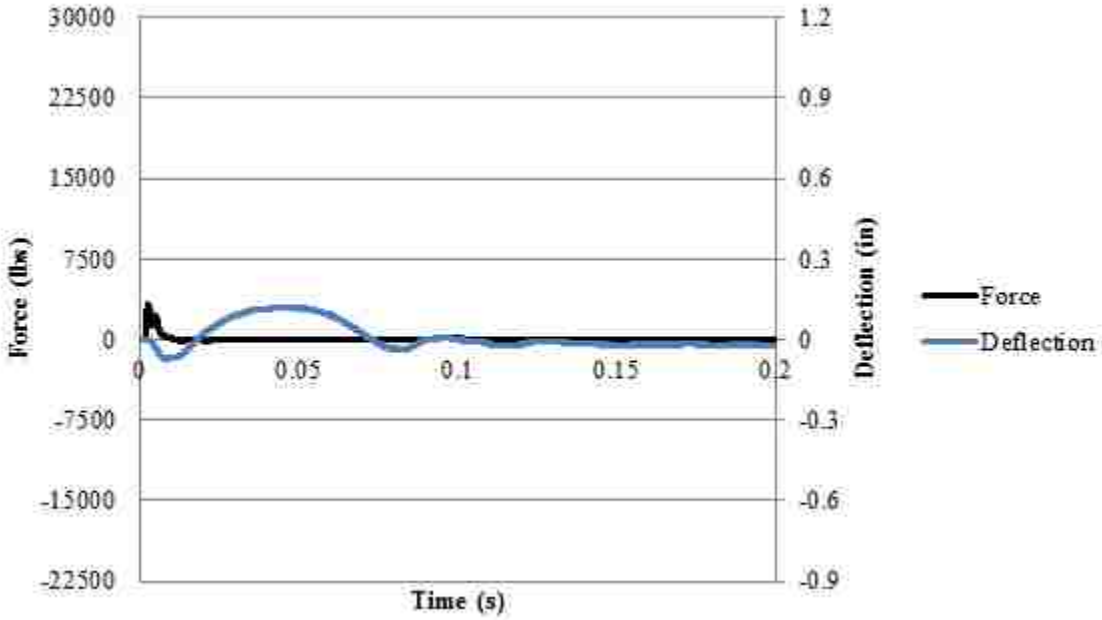

Figure C.2. Force and deflection vs. time for I-1-P-2 at 9-in (0.2 m)

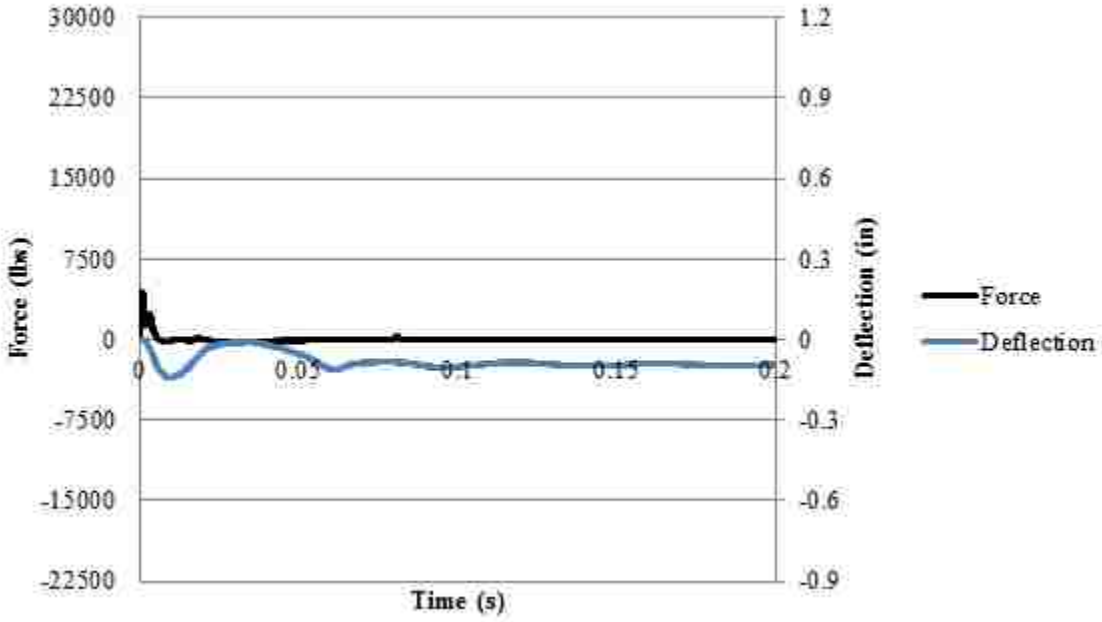

Figure C.3. Force and deflection vs. time for I-1-P-2 at 12-in (0.3 m)

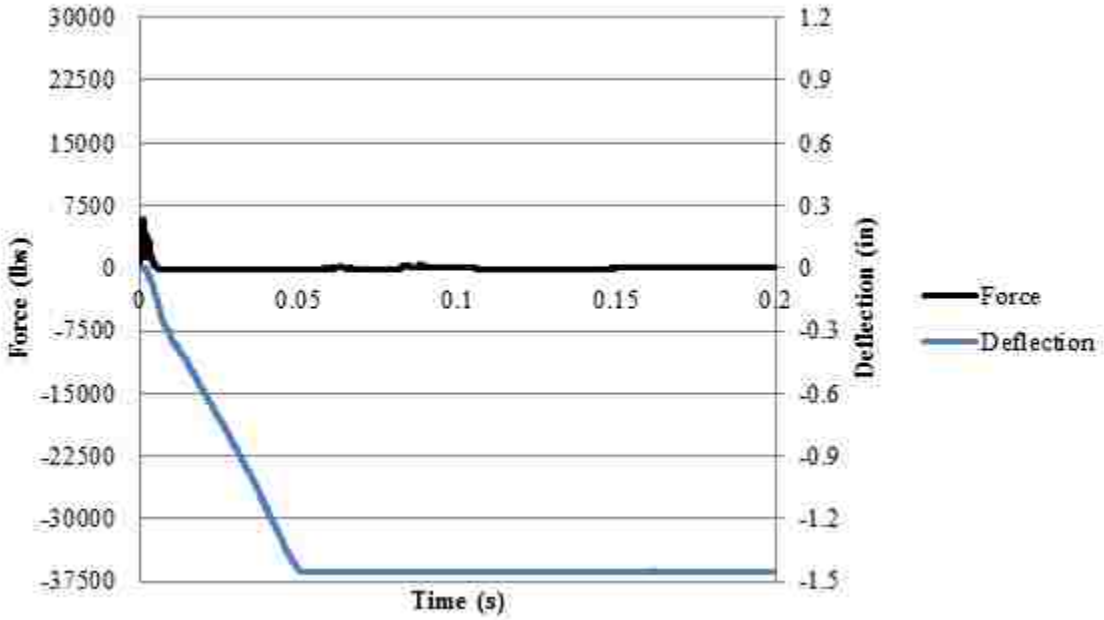

Figure C.4.Force and deflection vs. time for I-1-P-2 at 15-in (0.38 m)

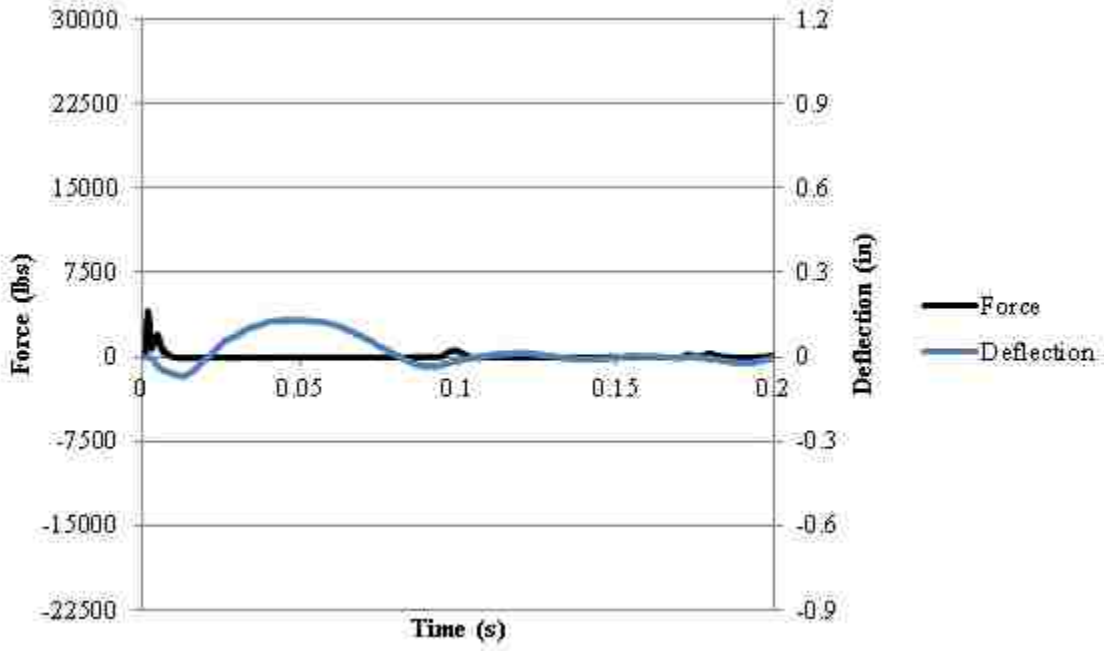

Figure C.5. Force and deflection vs. time for I-2-6F-2 at 6-in (0.15 m)

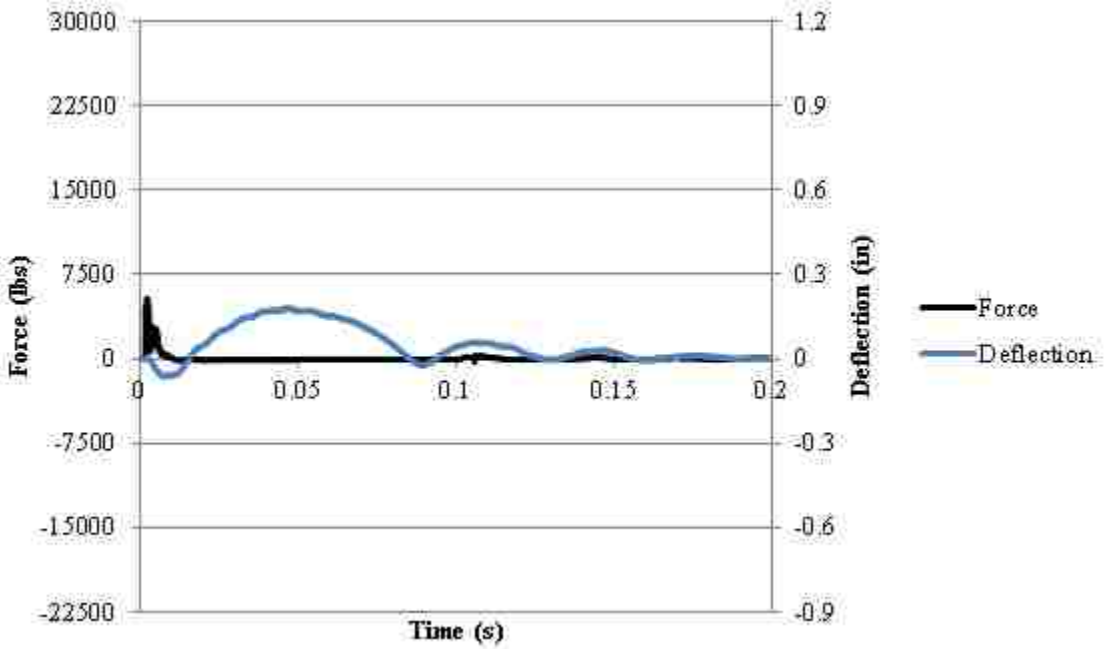

Figure C.6. Force and deflection vs. time for I-2-6F-2 at 9-in (0.2 m)

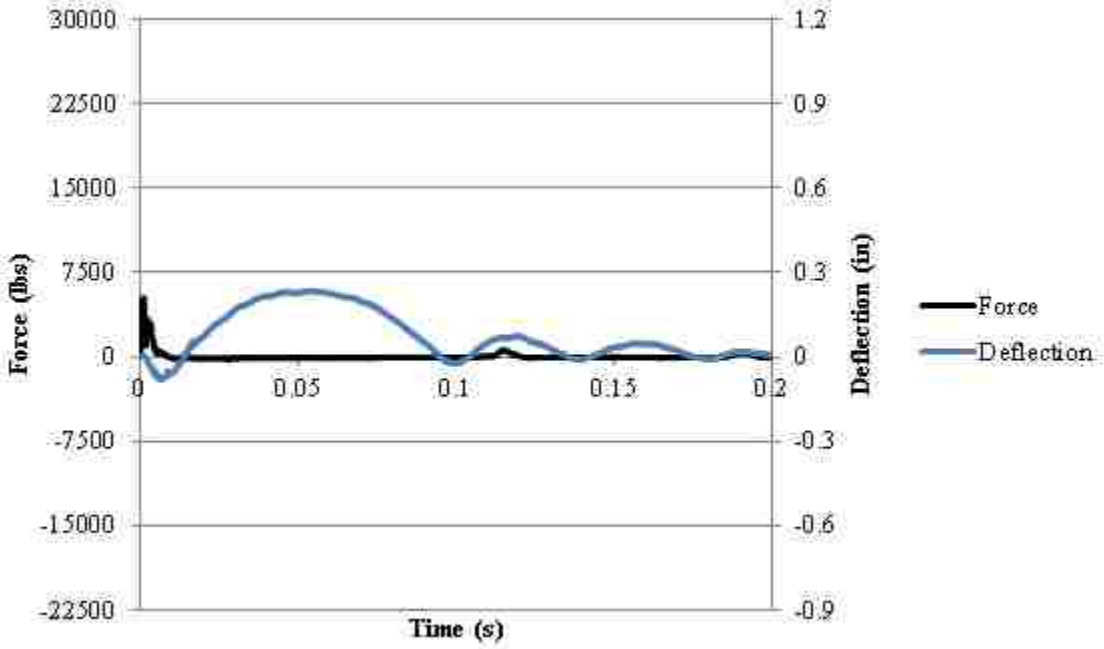

Figure C.7. Force and deflection vs. time for I-2-6F-2 at 12-in (0.3 m)

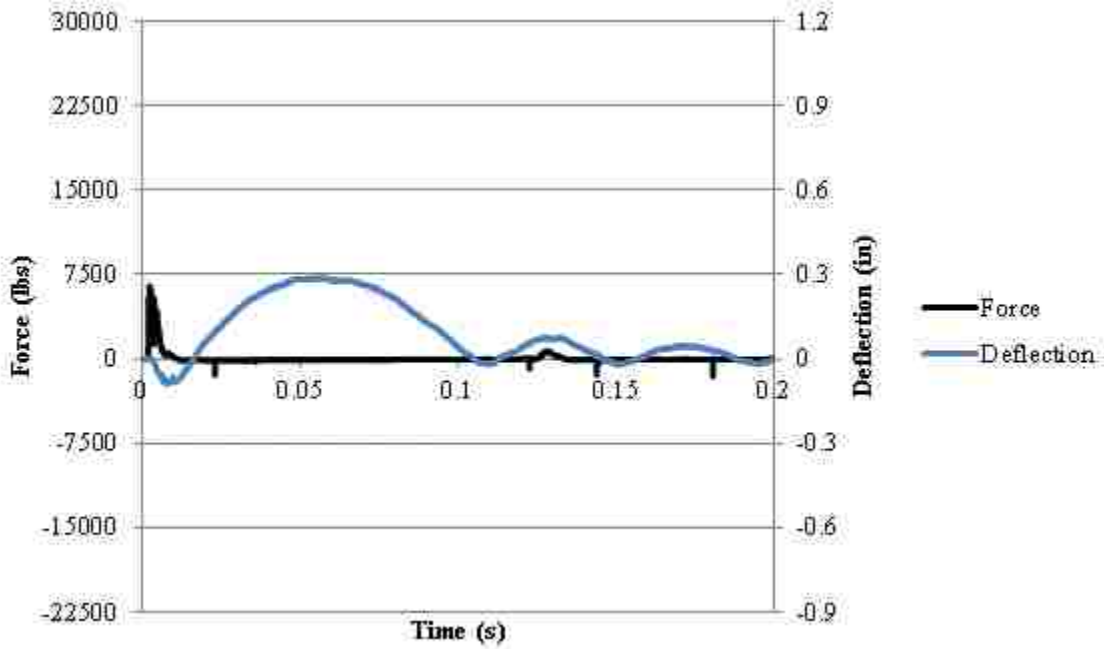

Figure C.8. Force and deflection vs. time for I-2-6F-2 at 15-in (0.38 m)

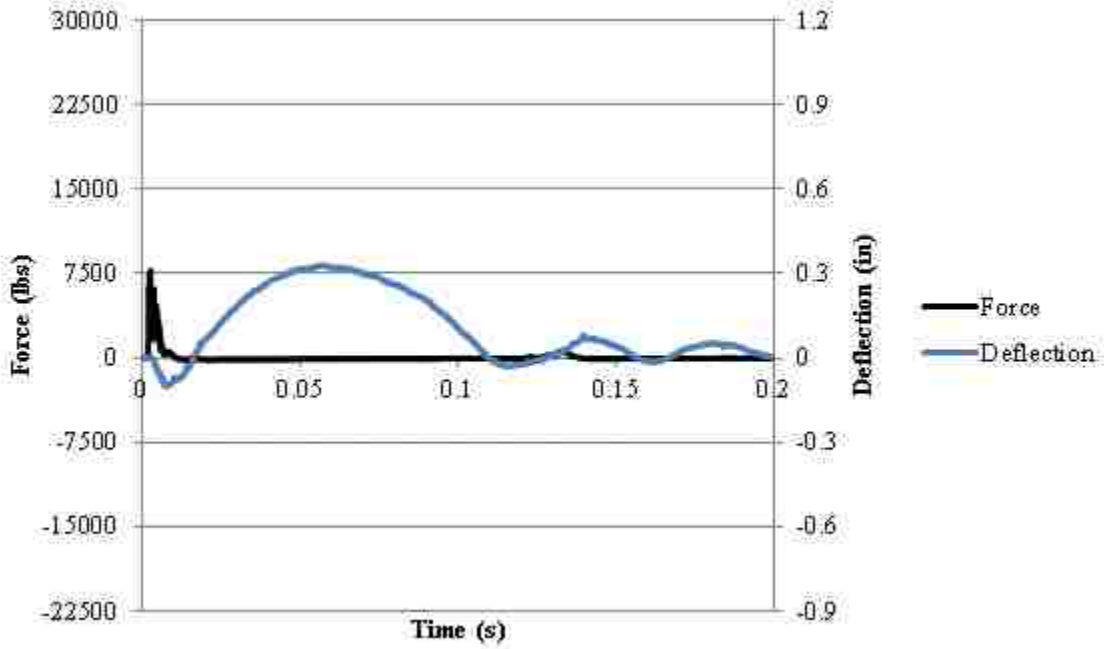

Figure C.9. Force and deflection vs. time for I-2-6F-2 at 18-in (0.46 m)

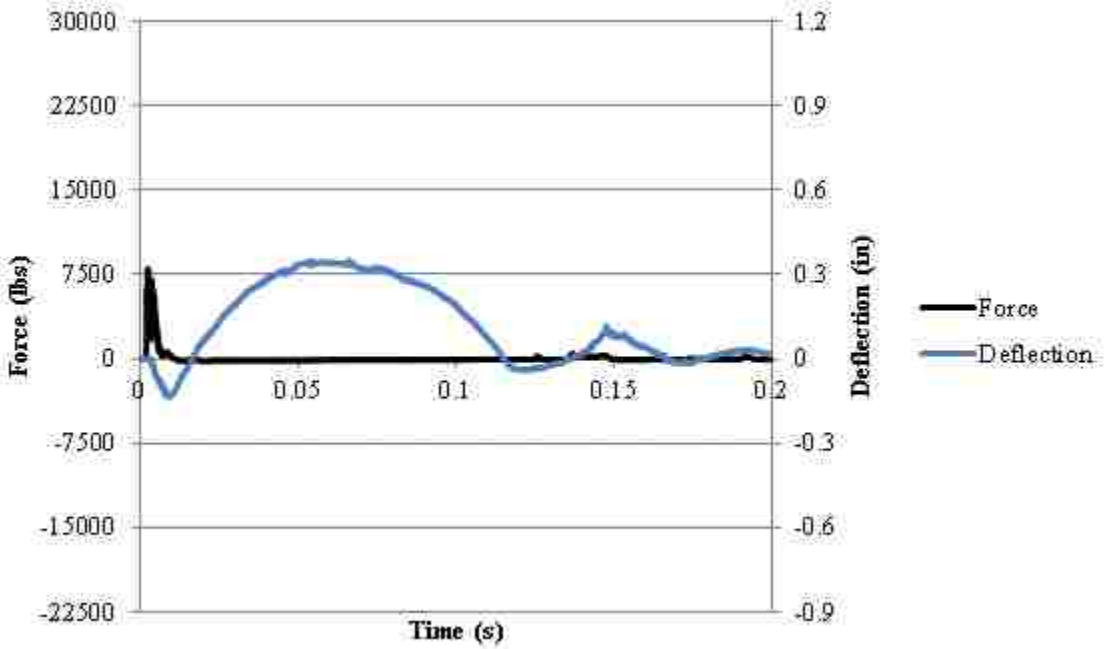

Figure C.10. Force and deflection vs. time for I-2-6F-2 at 21-in (0.5 m)

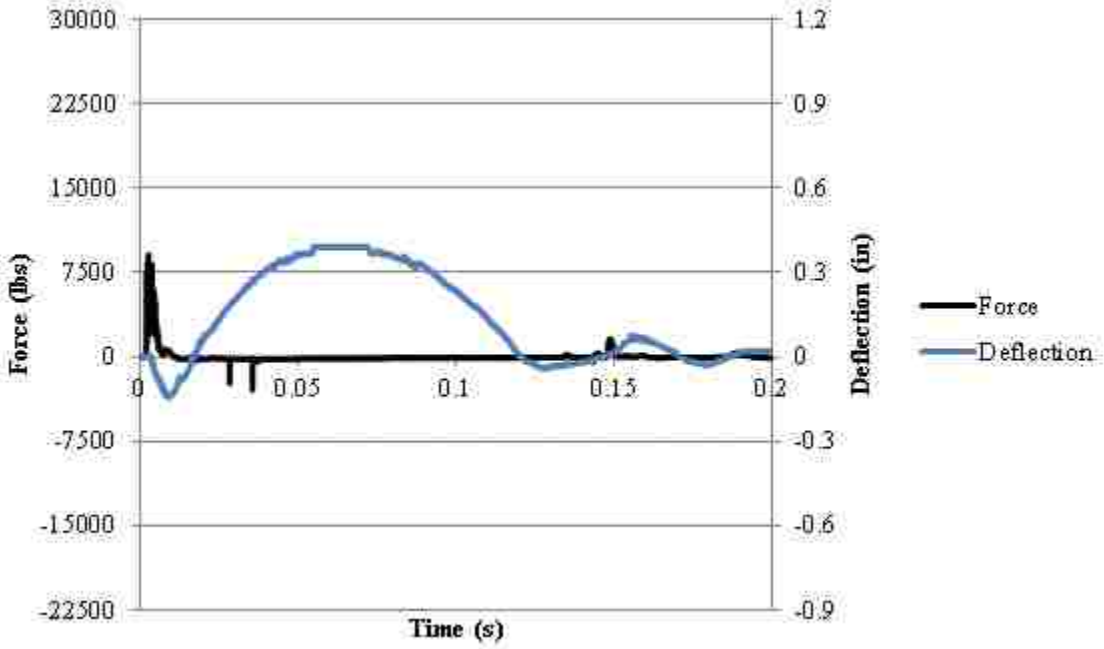

Figure C.11. Force and deflection vs. time for I-2-6F-2 at 24-in (0.6 m)

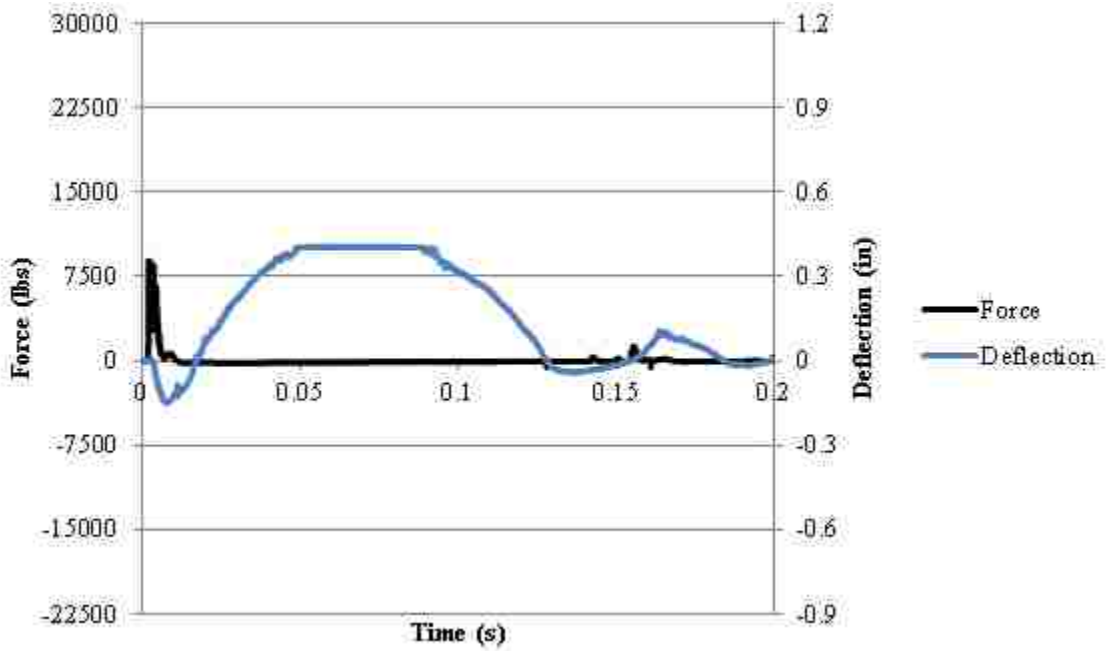

Figure C.12. Force and deflection vs. time for I-2-6F-2 at 30-in (0.8 m)

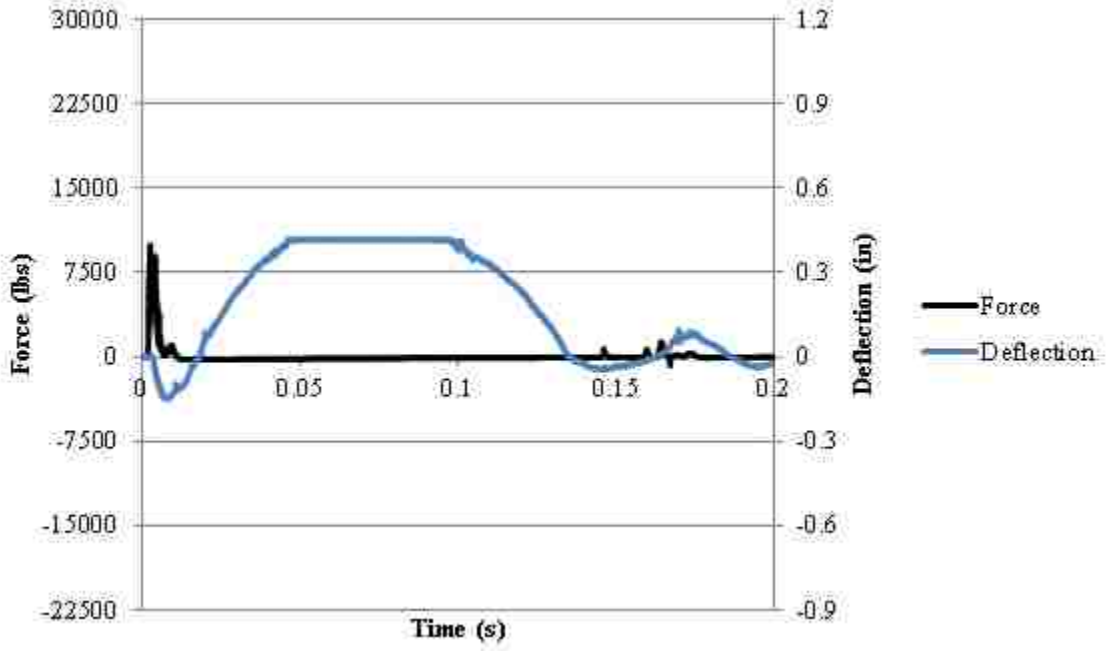

Figure C.13. Force and deflection vs. time for I-2-6F-2 at 36-in (0.9 m)

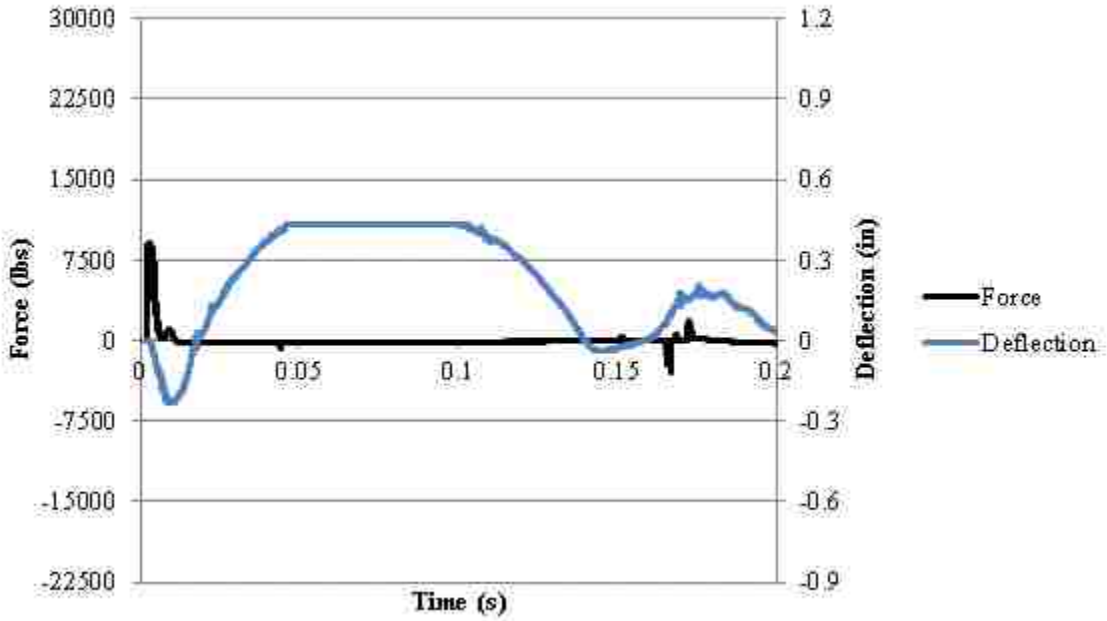

Figure C.14. Force and deflection vs. time for I-2-6F-2 at 42-in (1.1 m)

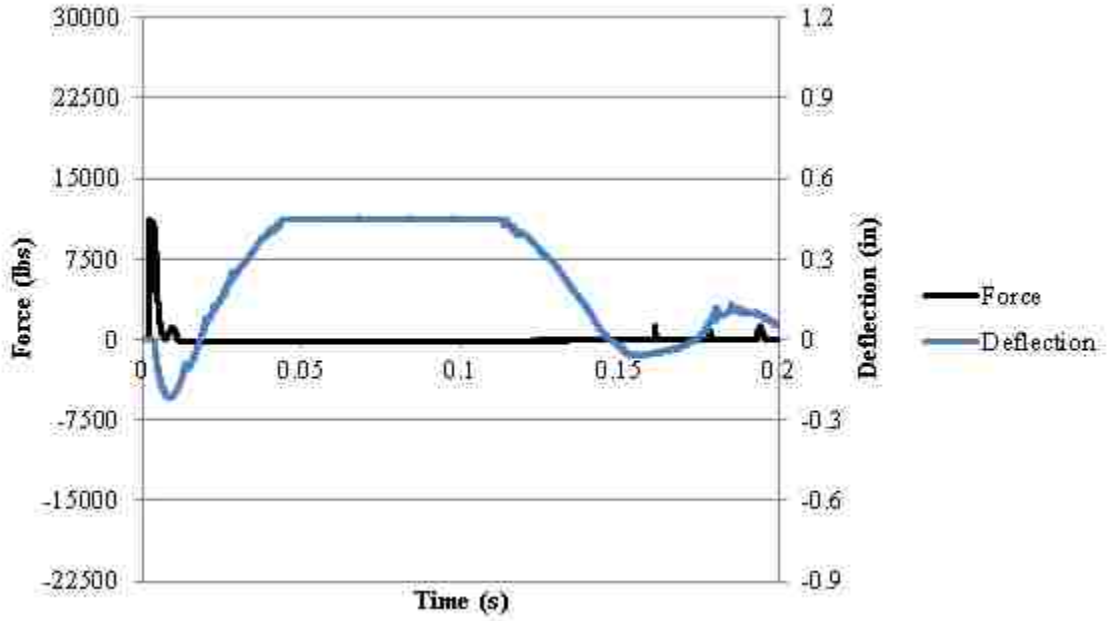

Figure C.15. Force and deflection vs. time for I-2-6F-2 at 48-in (1.2 m)

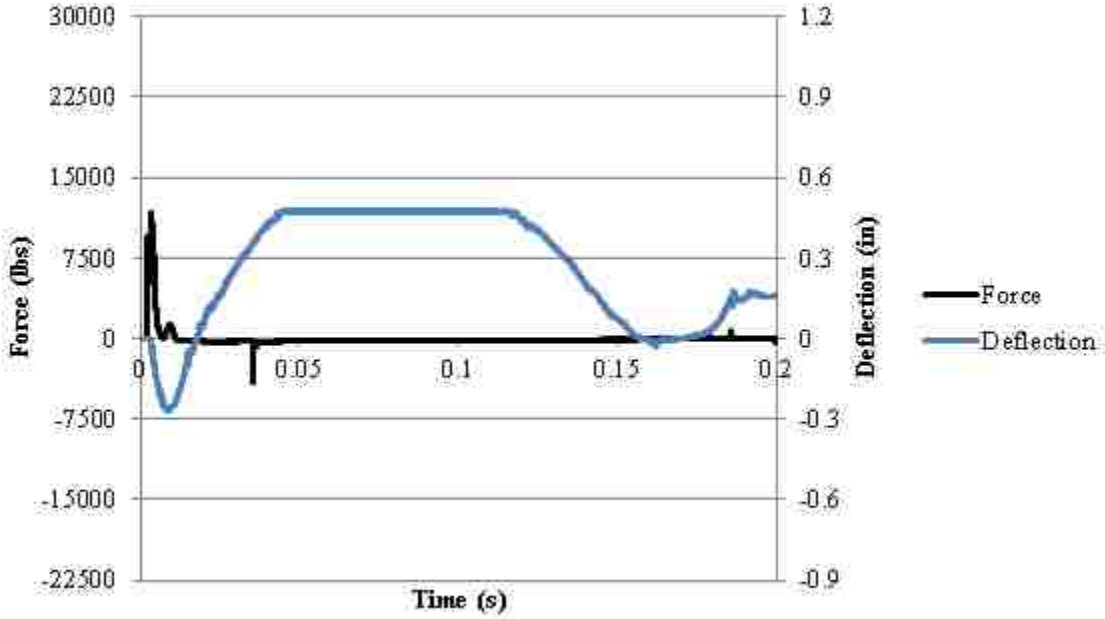

Figure C.16. Force and deflection vs. time for I-2-6F-2 at 54-in (1.4 m)

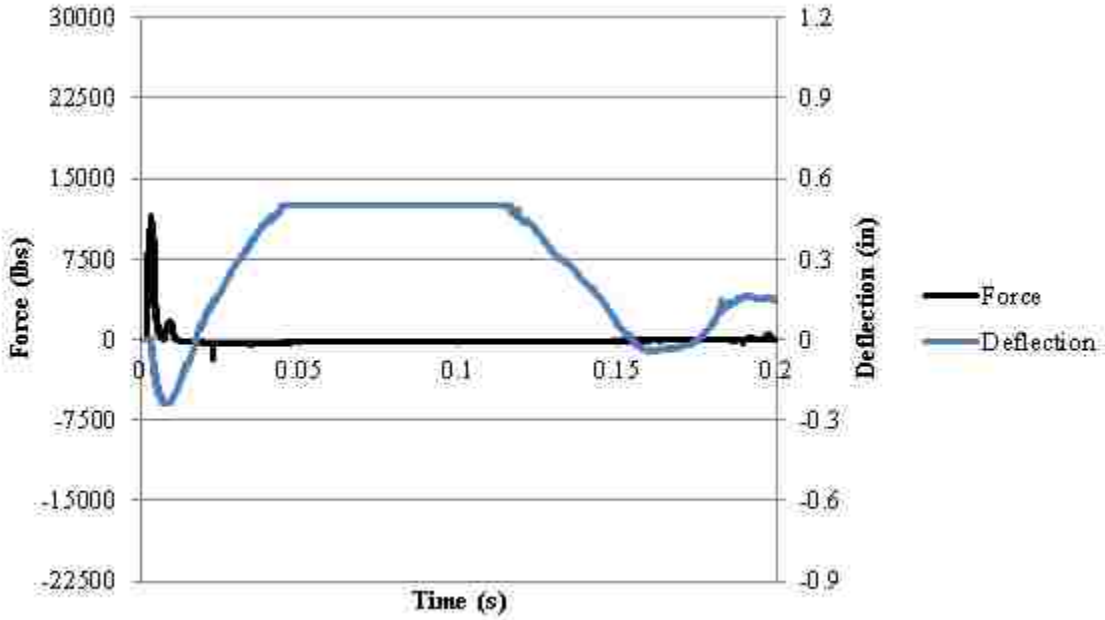

Figure C.17. Force and deflection vs. time for I-2-6F-2 at 60-in (1.5 m)

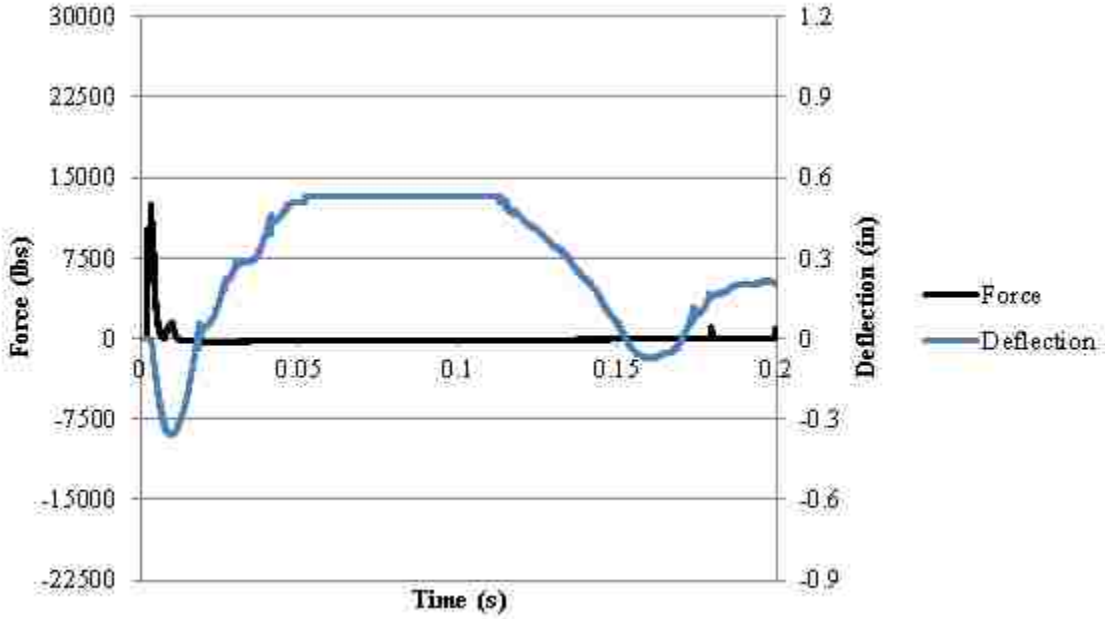

Figure C.18. Force and deflection vs. time for I-2-6F-2 at 66-in (1.7 m)

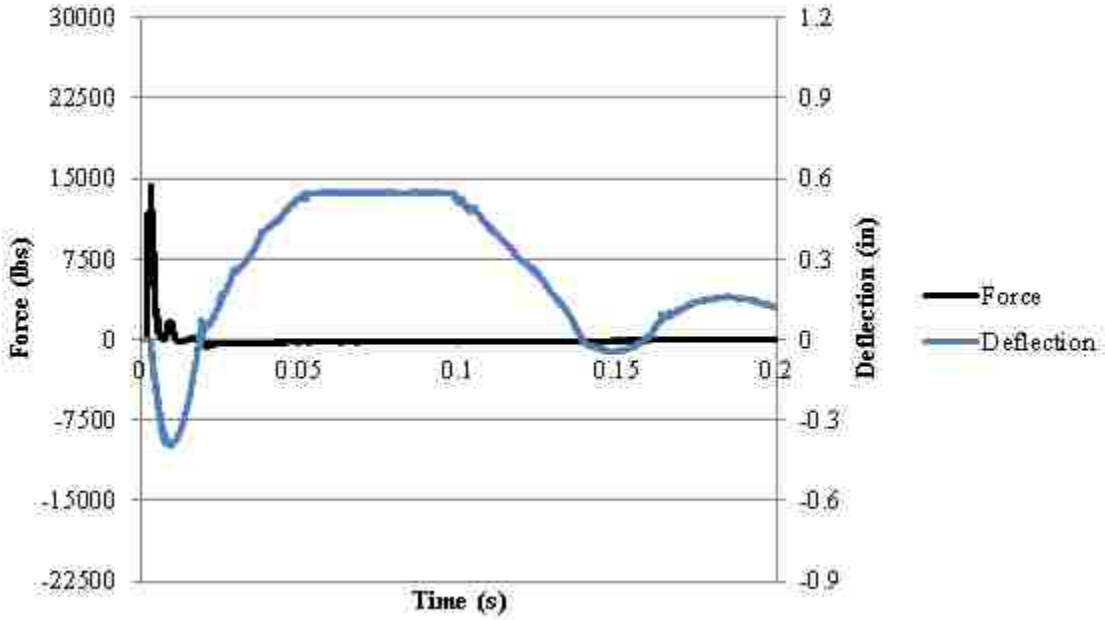

Figure C.19. Force and deflection vs. time for I-2-6F-2 at 72-in (1.8 m)

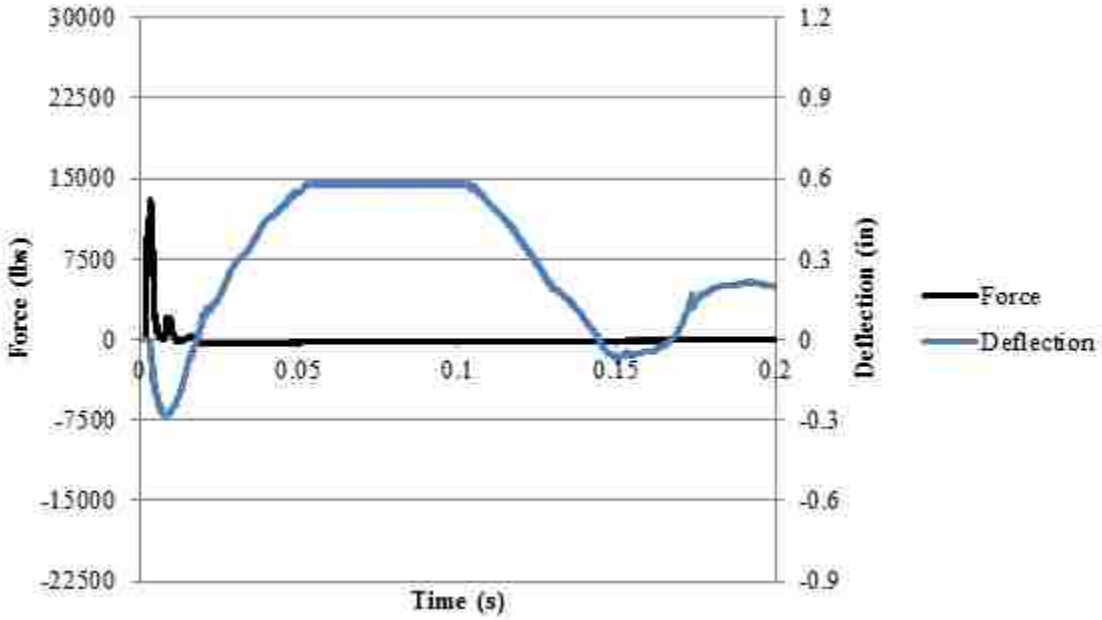

Figure C.20. Force and deflection vs. time for I-2-6F-2 at 78-in (1.9 m)

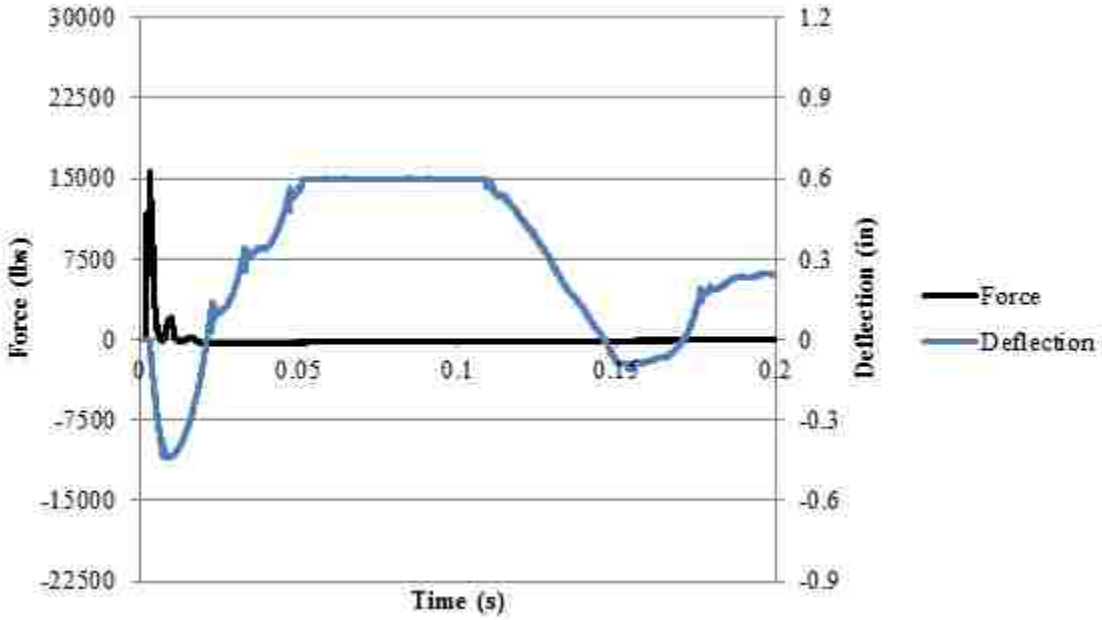

Figure C.21. Force and deflection vs. time for I-2-6F-2 at 84-in (2.1 m)

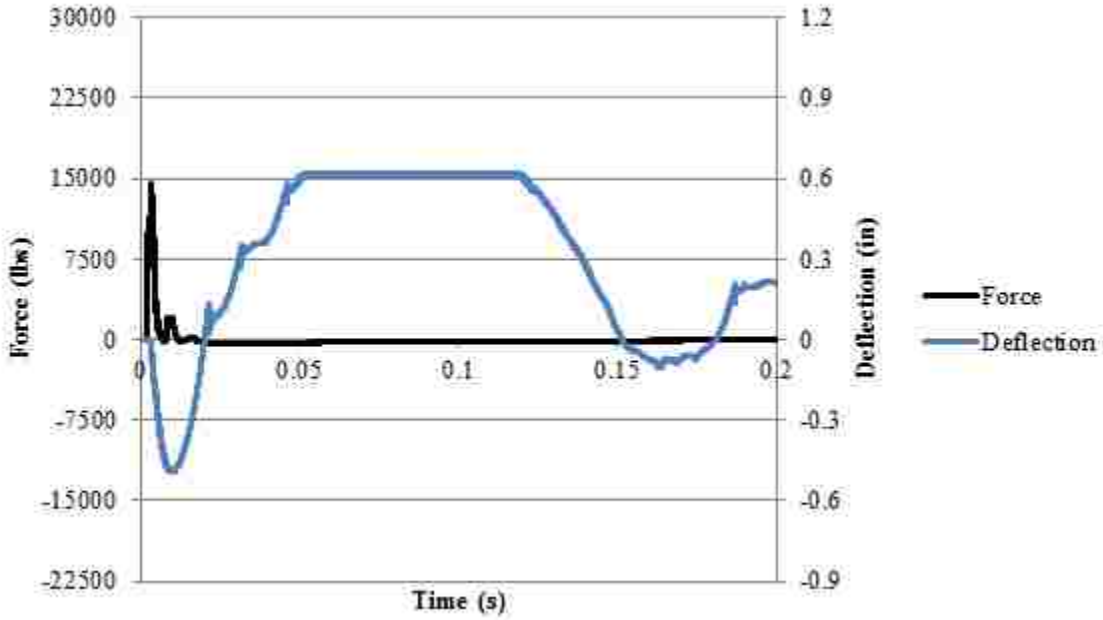

Figure C.22. Force and deflection vs. time for I-2-6F-2 at 90-in (2.3 m)

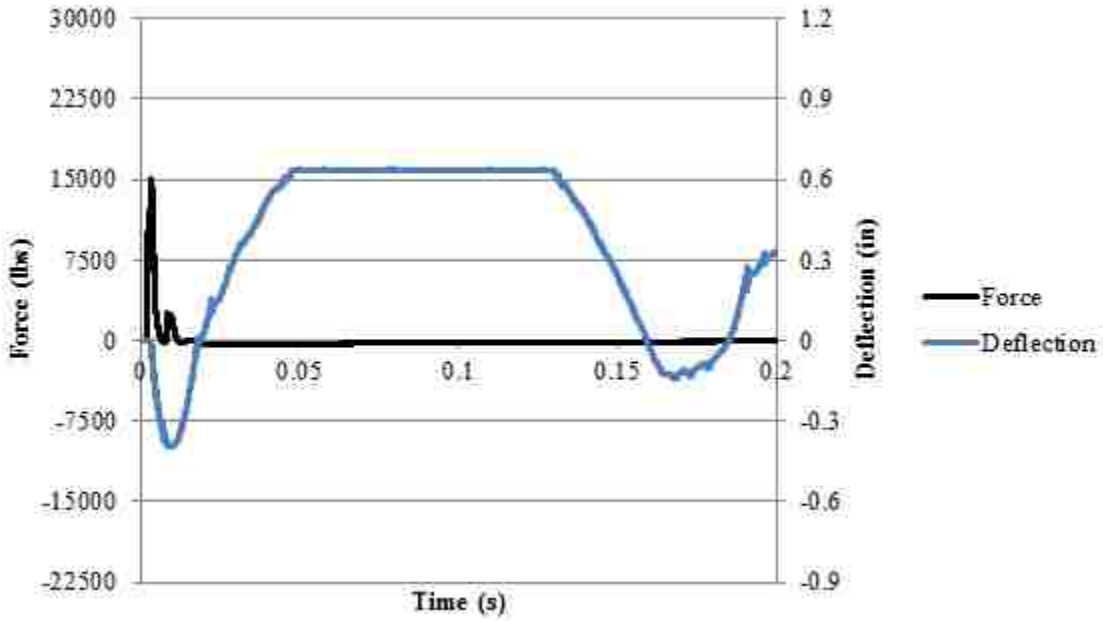

Figure C.23. Force and deflection vs. time for I-2-6F-2 at 96-in (2.4 m)

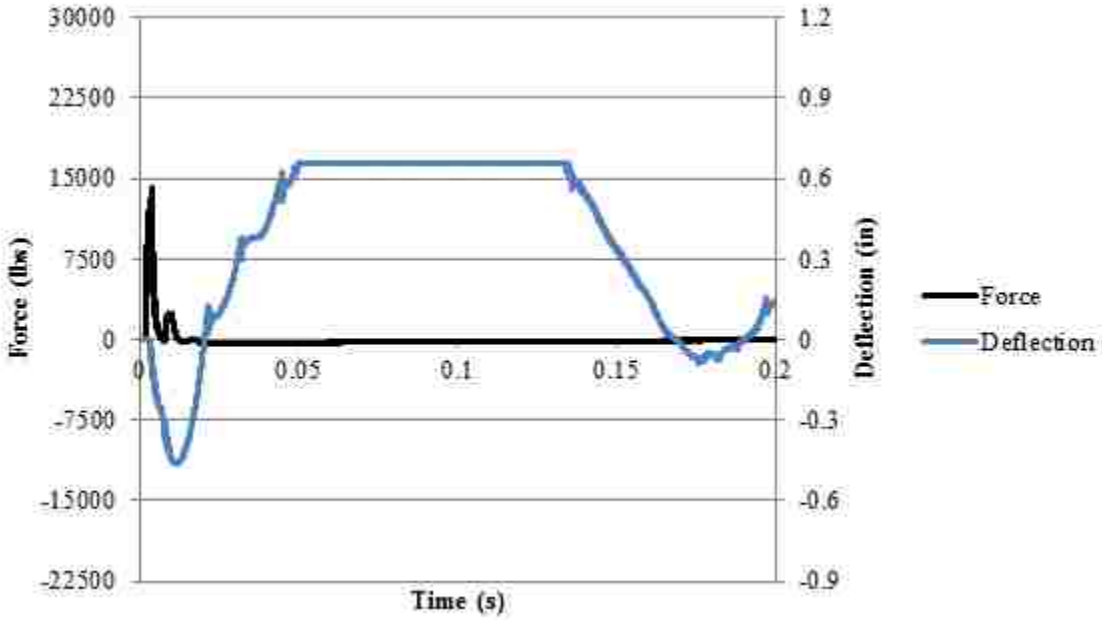

Figure C.24. Force and deflection vs. time for I-2-6F-2 at 102-in (2.6 m)

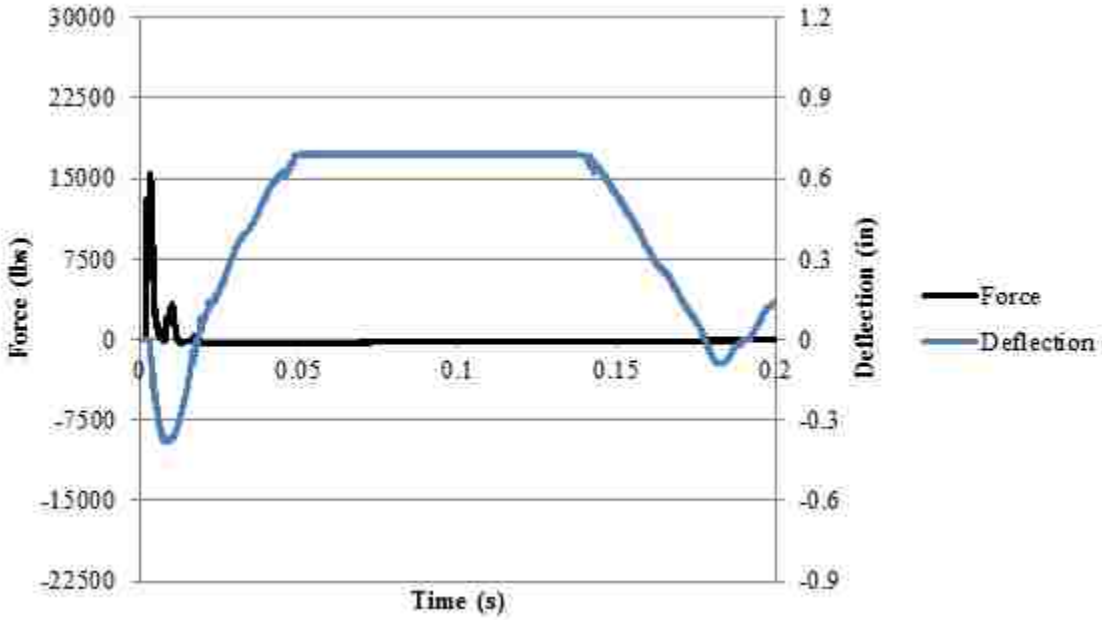

Figure C.25. Force and deflection vs. time for I-2-6F-2 at 114-in (2.9 m)

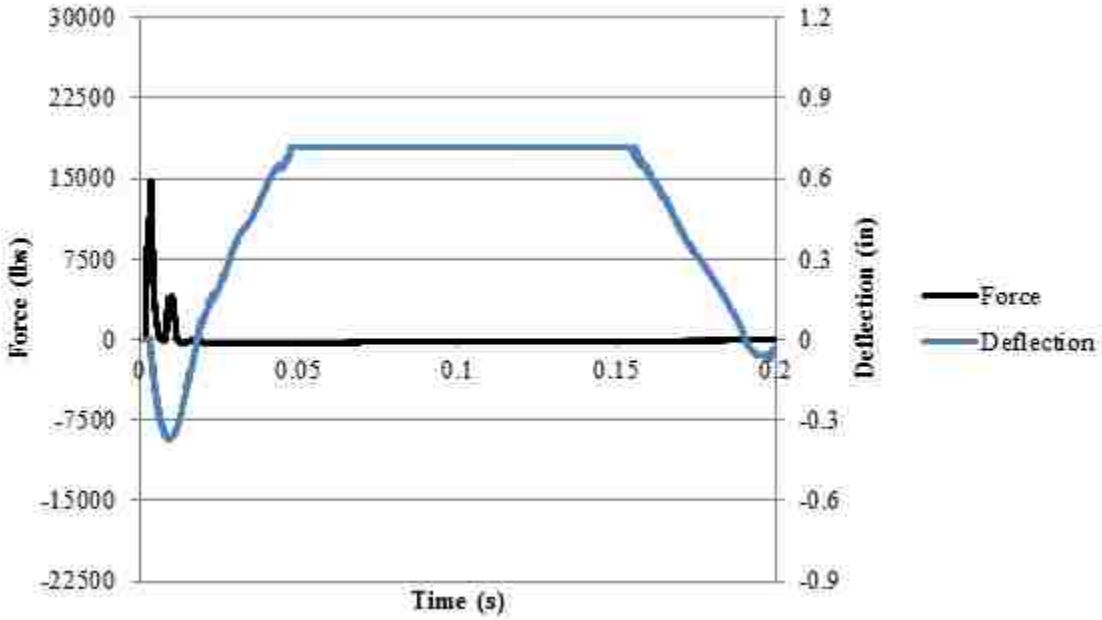

Figure C.26. Force and deflection vs. time for I-2-6F-2 at 120-in (3.0 m)

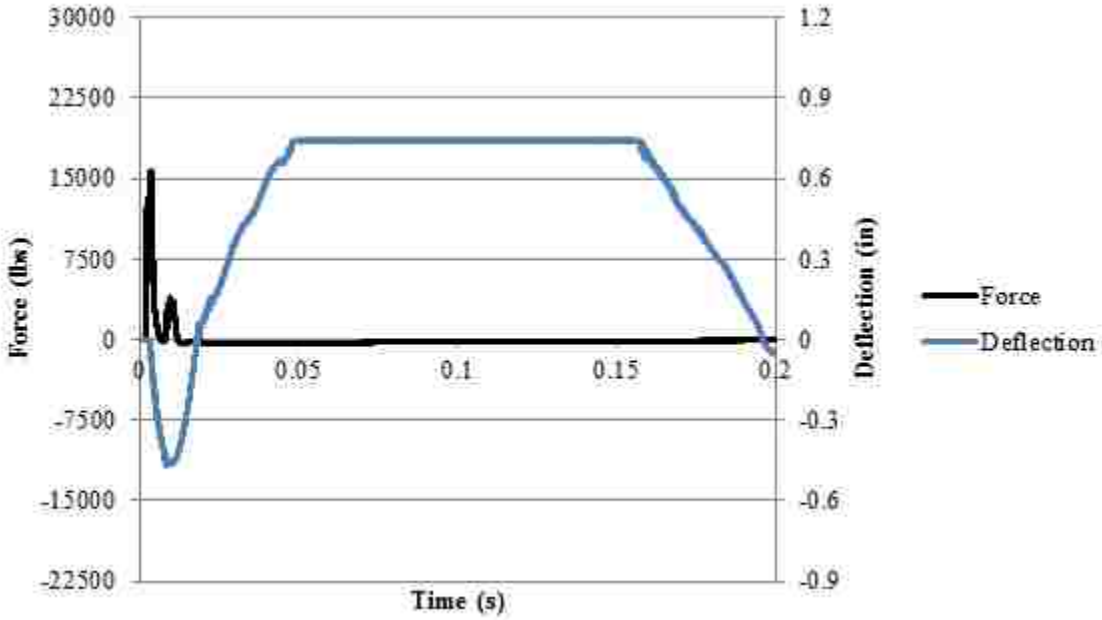

Figure C.27. Force and deflection vs. time for I-2-6F-2 at 126-in (3.2 m)

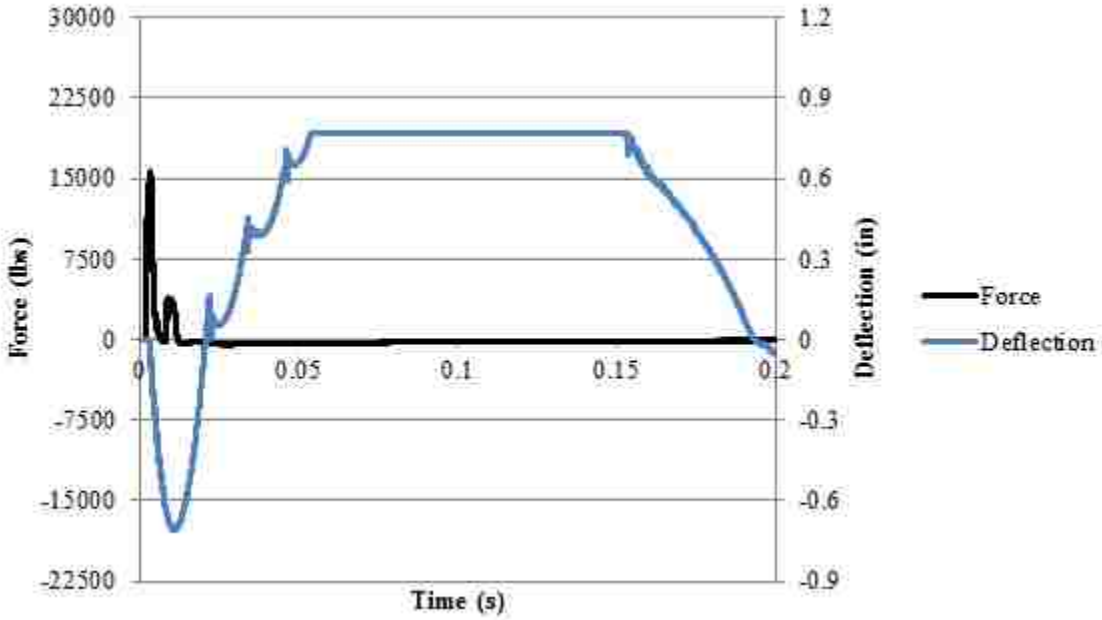

Figure C.28. Force and deflection vs. time for I-2-6F-2 at 132-in (3.4 m)

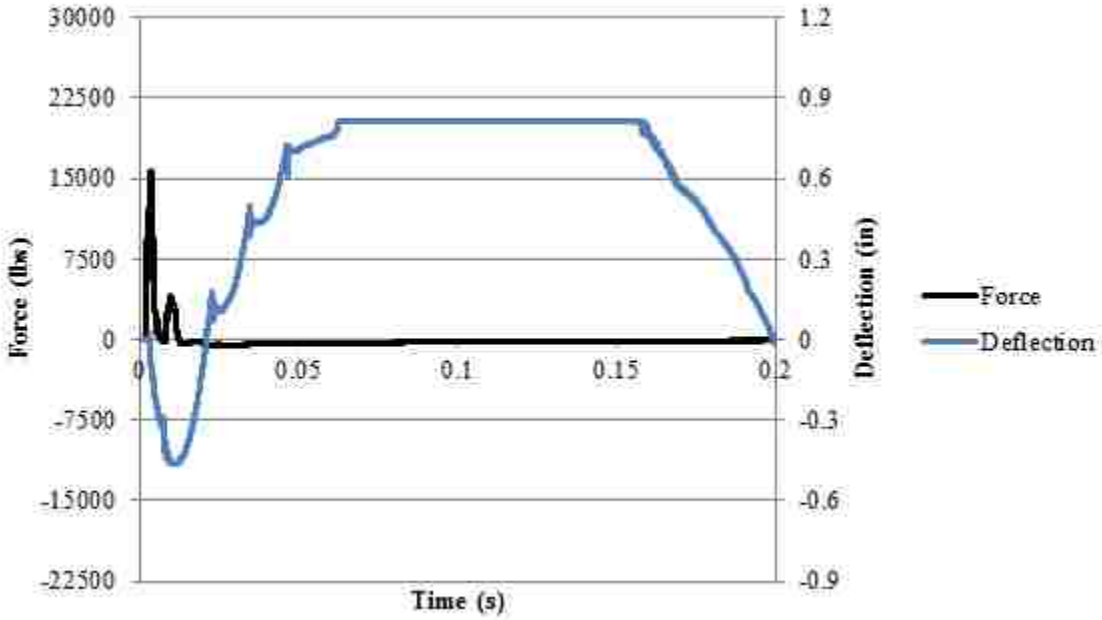

Figure C.29. Force and deflection vs. time for I-2-6F-2 at 138-in (3.5 m)

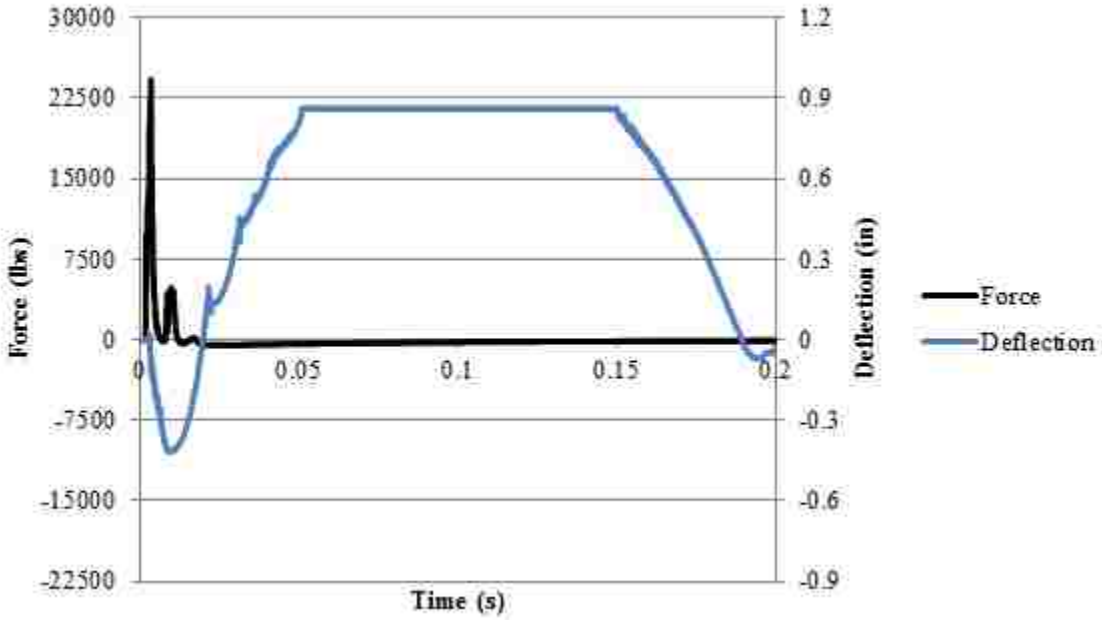

Figure C.30. Force and deflection vs. time for I-2-6F-2 at 144-in (3.7 m)

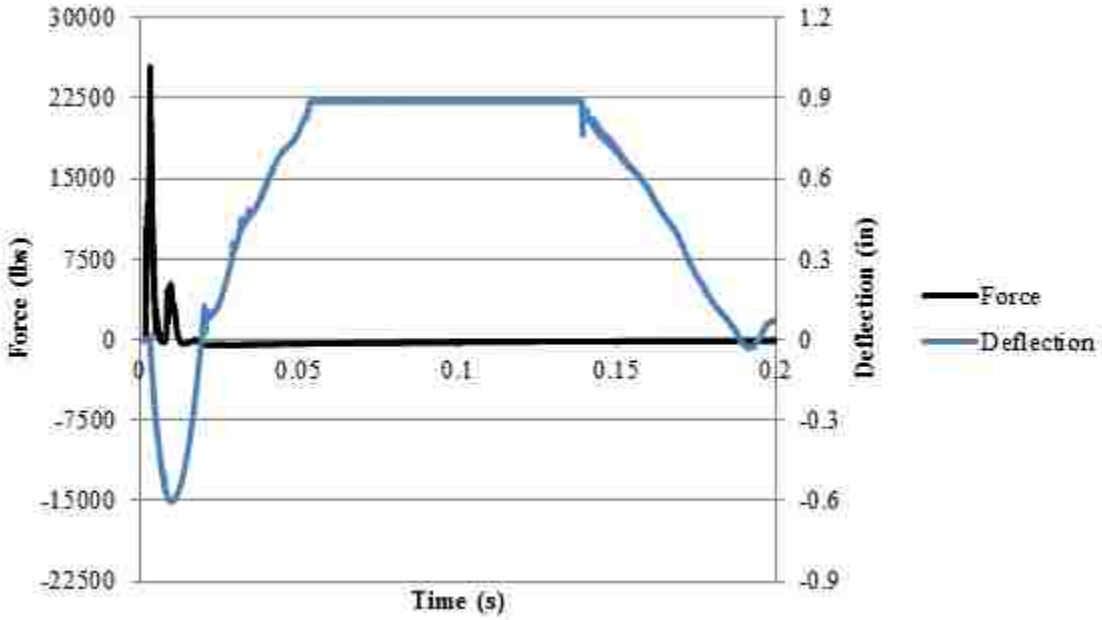

Figure C.31. Force and deflection vs. time for I-2-6F-2 at 150-in (3.8 m)

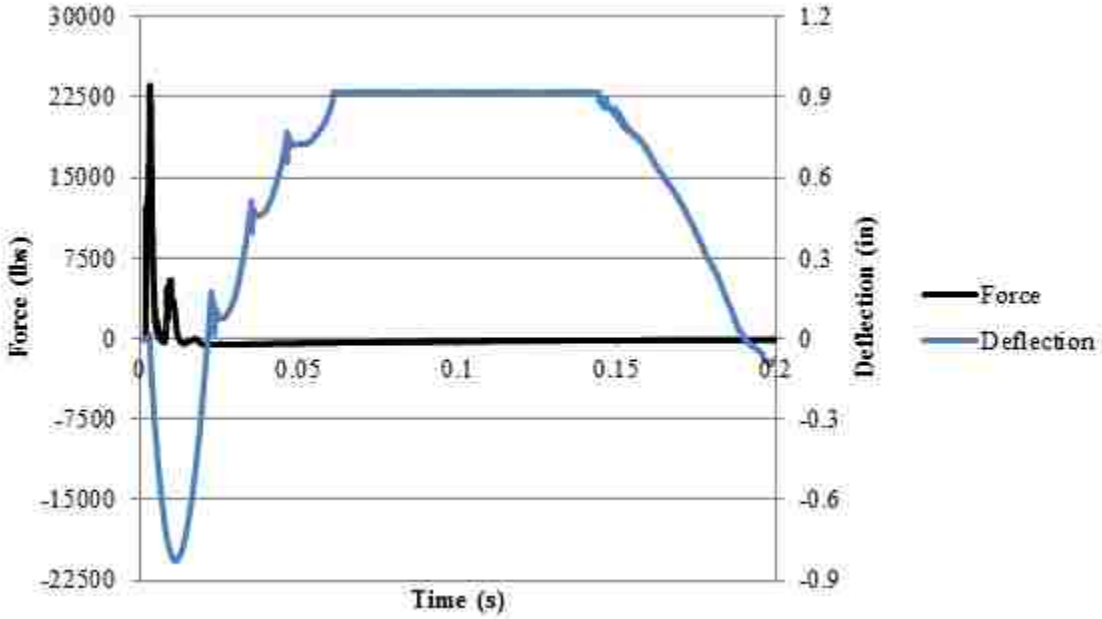

Figure C.32. Force and deflection vs. time for I-2-6F-2 at 156-in (3.9 m)

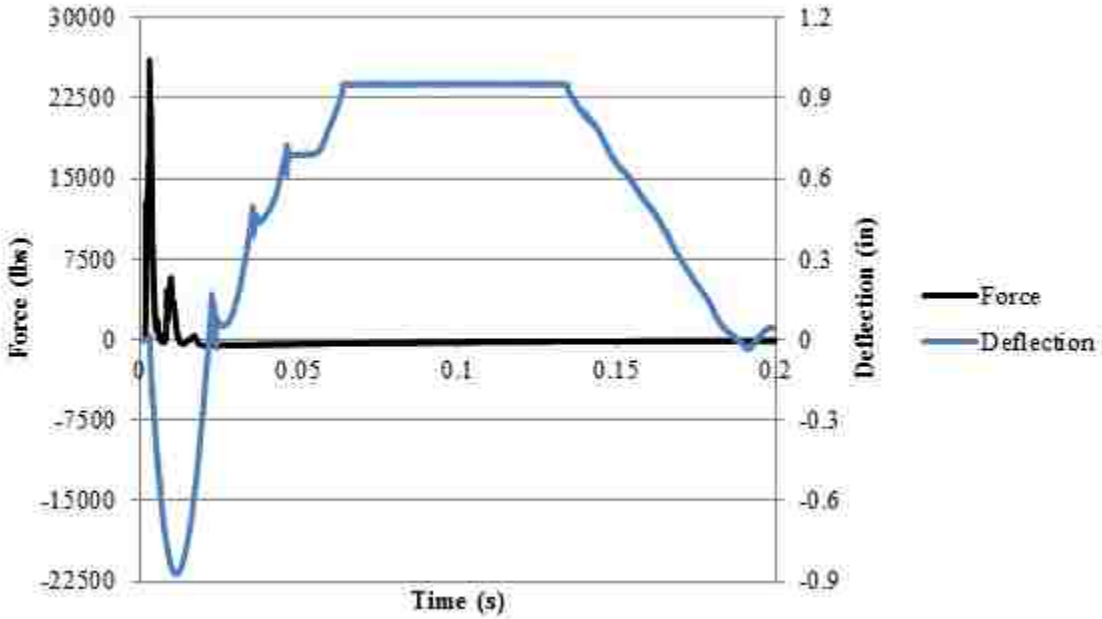

Figure C.33. Force and deflection vs. time for I-2-6F-2 at 162-in (4.1 m)

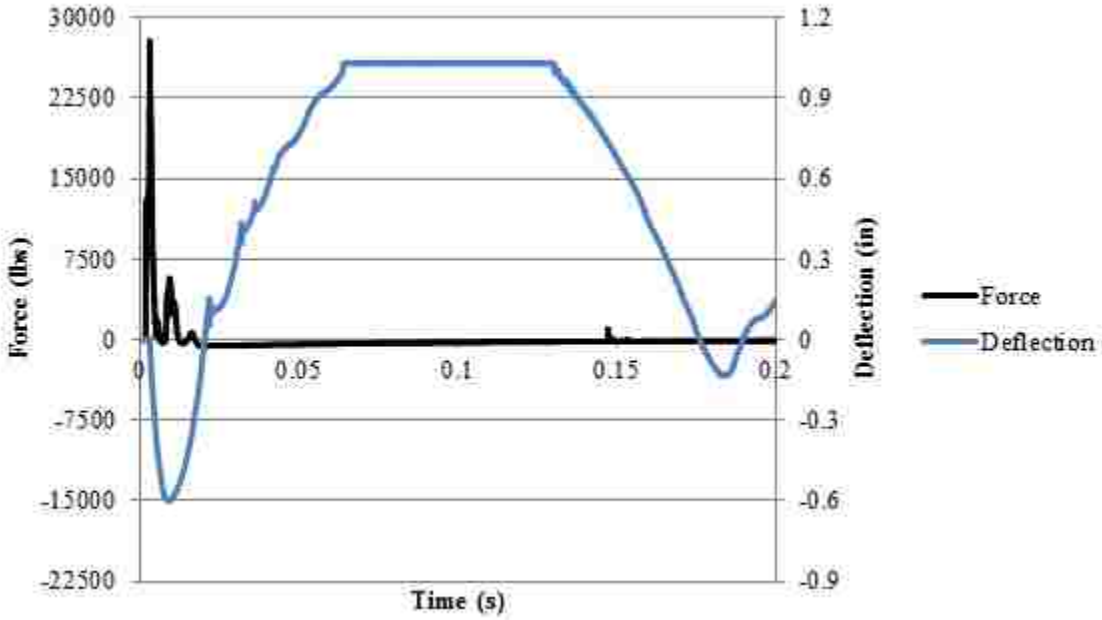

Figure C.34. Force and deflection vs. time for I-2-6F-2 at 168-in (4.3 m)

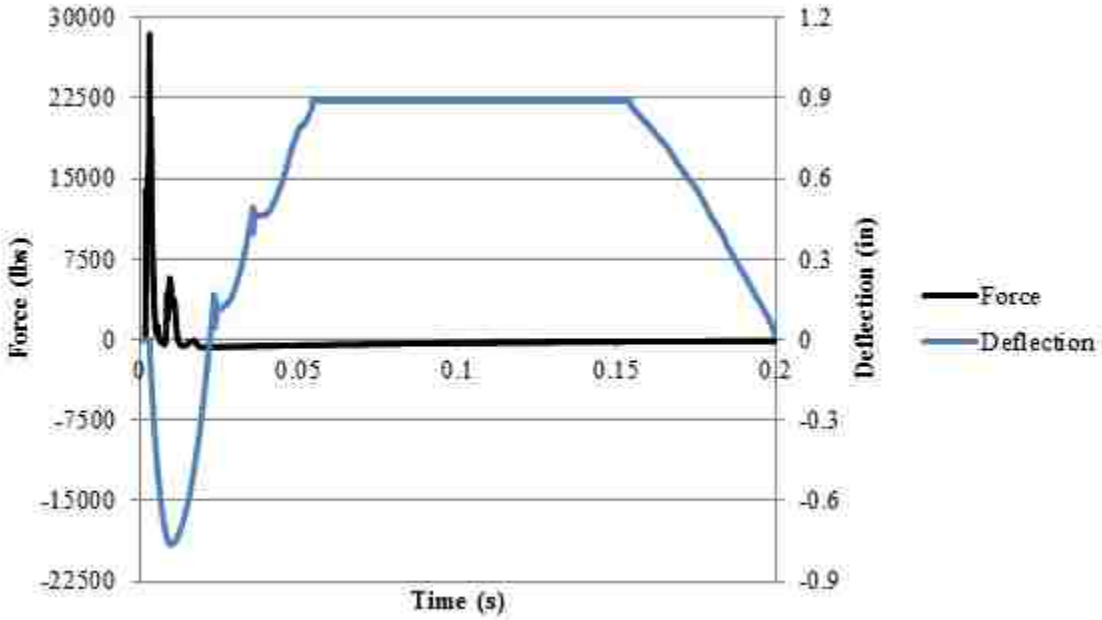

Figure C.35. Force and deflection vs. time for I-2-6F-2 at 174-in (4.4 m)

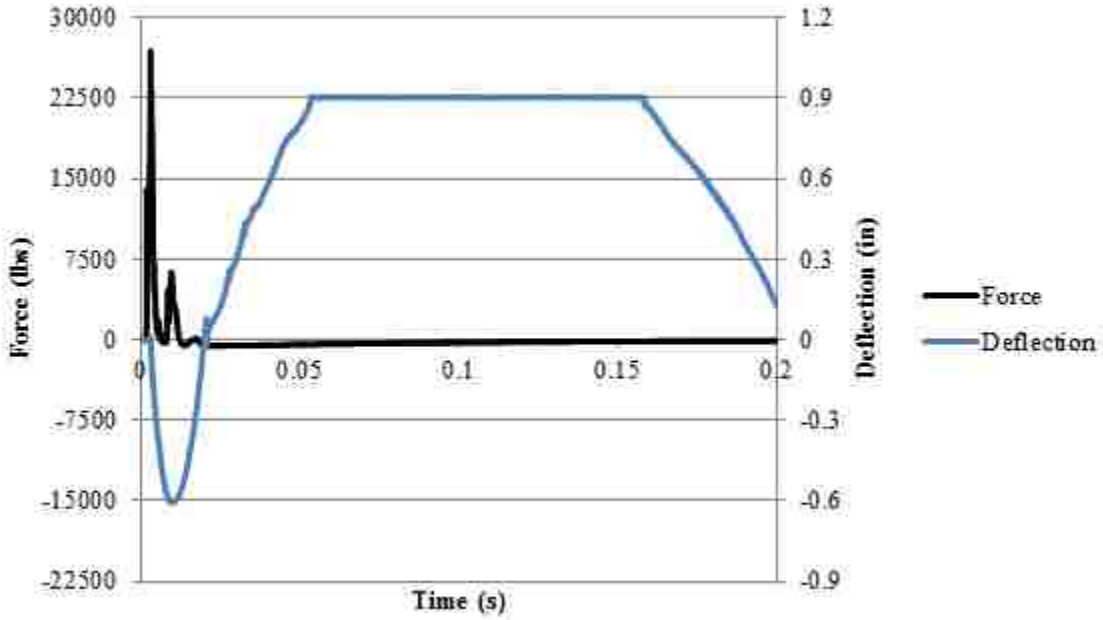

Figure C.36. Force and deflection vs. time for I-2-6F-2 at 180-in (4.6 m)

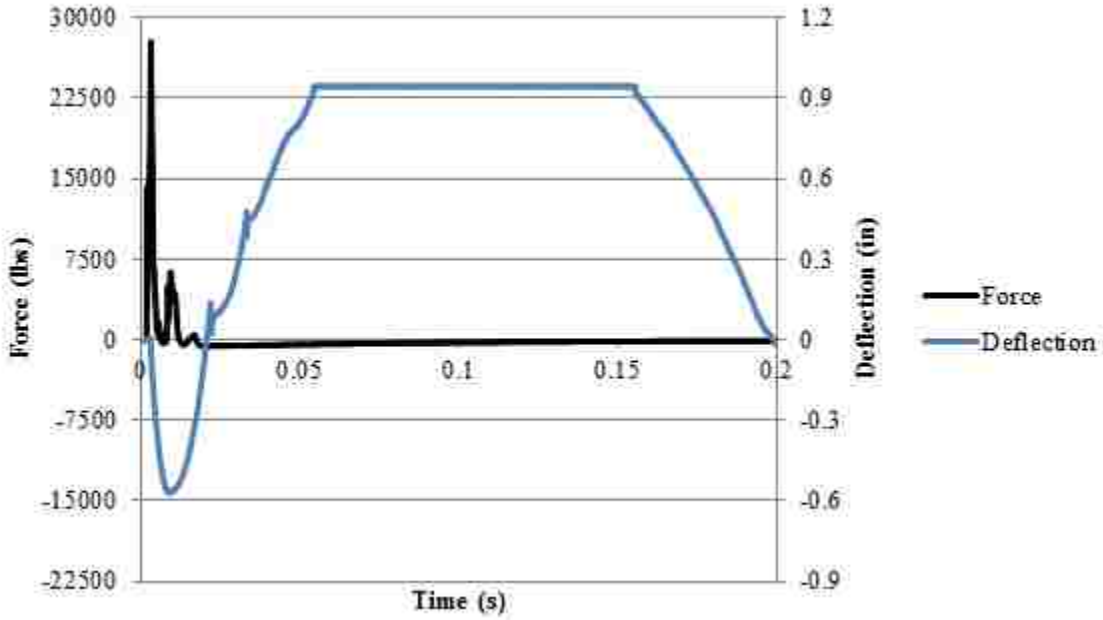

Figure C.37. Force and deflection vs. time for I-2-6F-2 at 186-in (4.7 m)

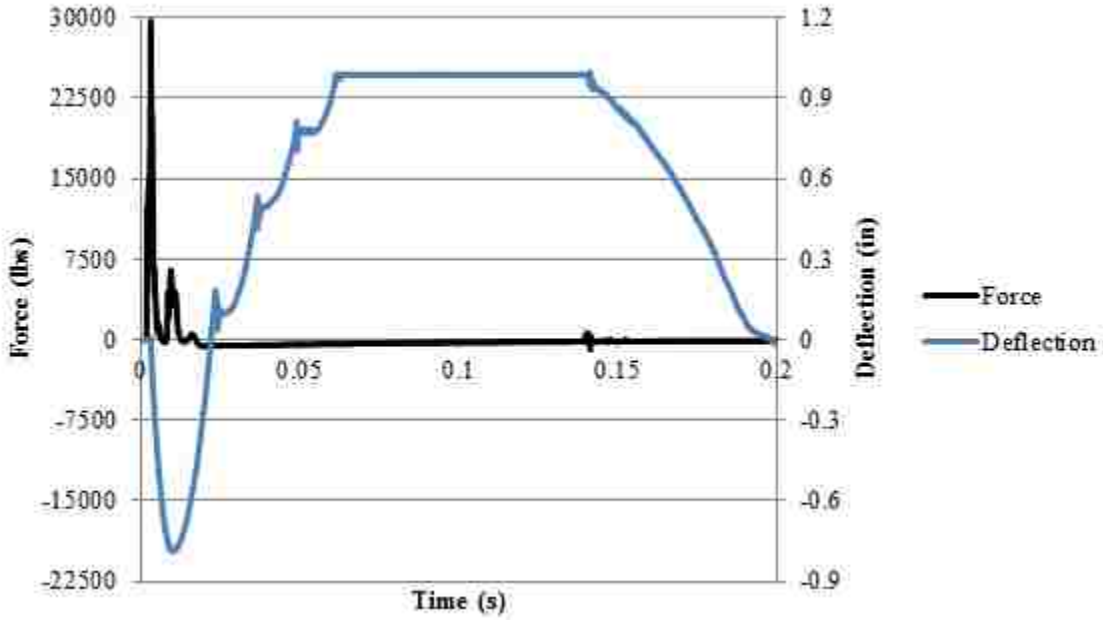

Figure C.38. Force and deflection vs. time for I-2-6F-2 at 186-in (4.7 m), 2nd repetition

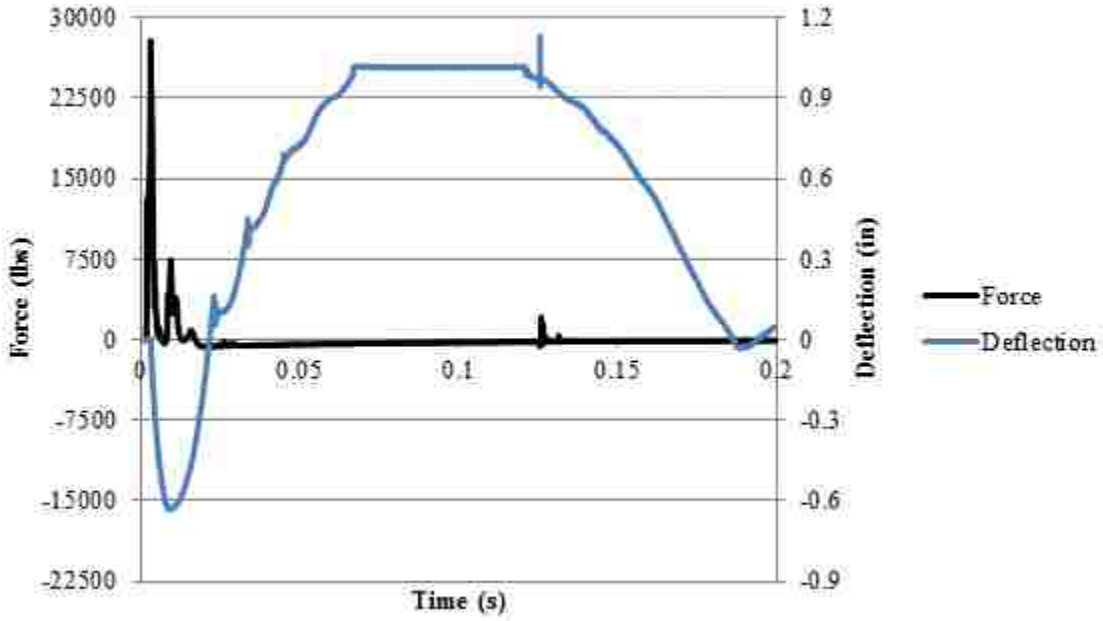

Figure C.39. Force and deflection vs. time for I-2-6F-2 at 186-in (4.7 m), 3rd repetition

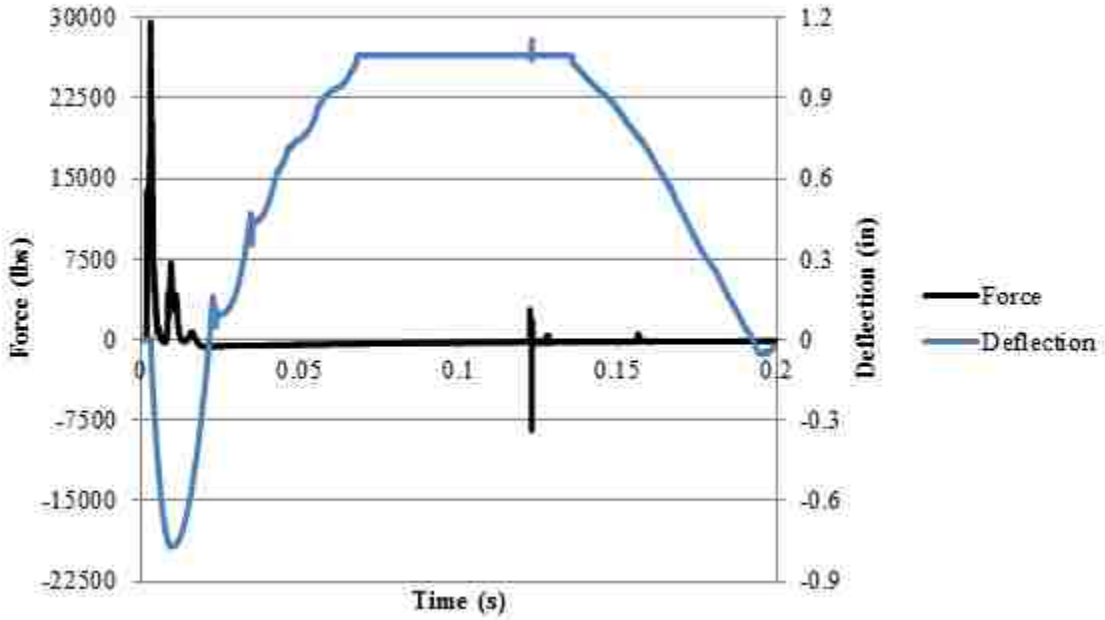

Figure C.40. Force and deflection vs. time for I-2-6F-2 at 186-in (4.7 m), 4th repetition

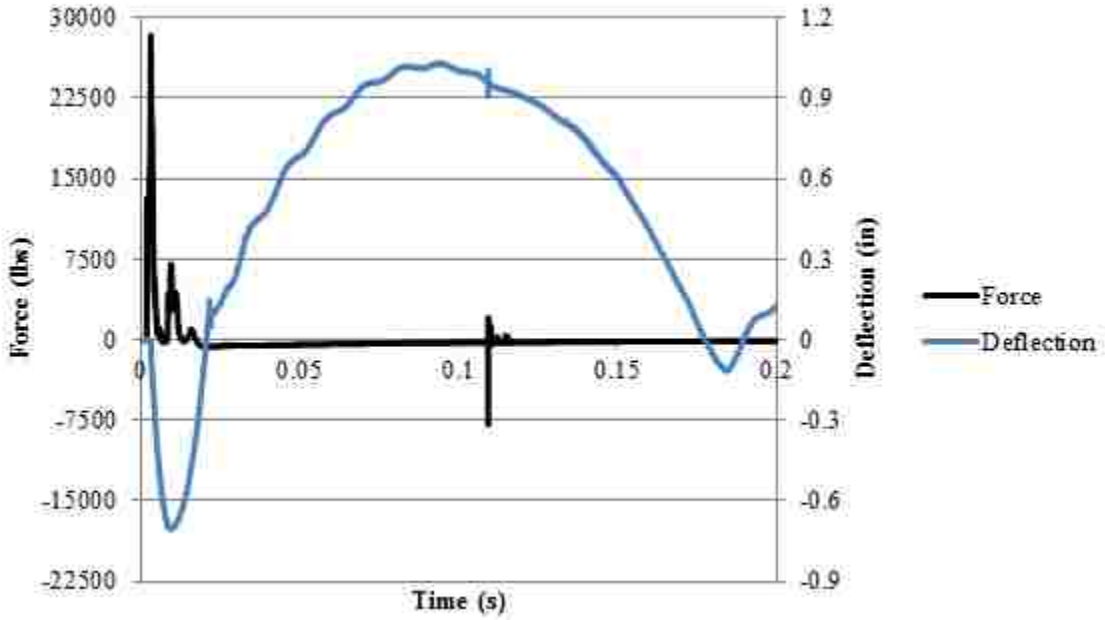

Figure C.41. Force and deflection vs. time for I-2-6F-2 at 186-in (4.7 m), 5th repetition

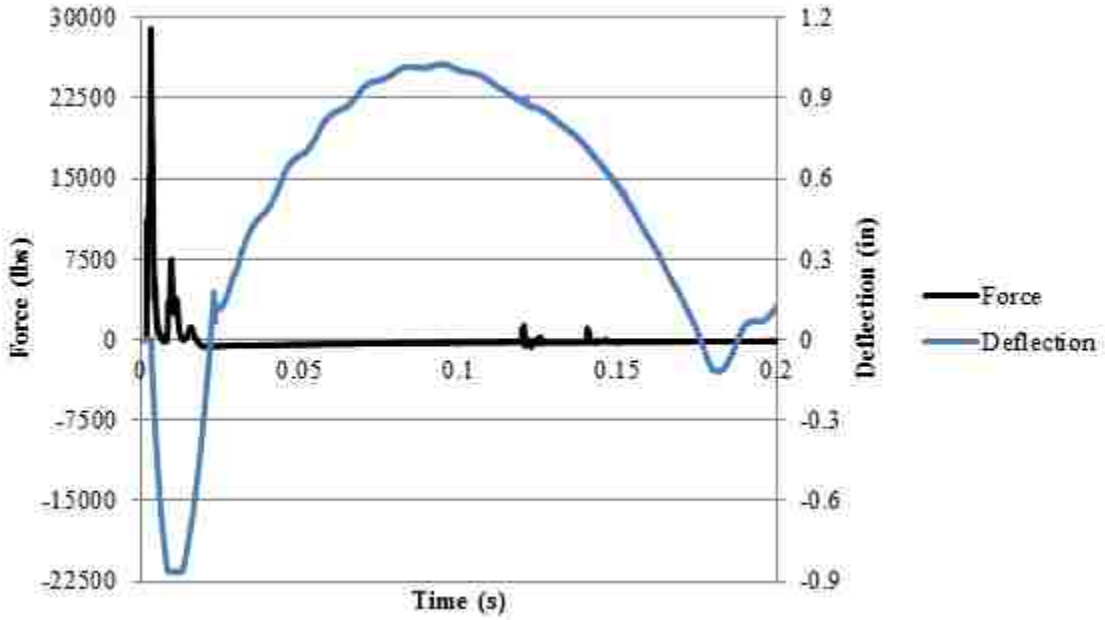

Figure C.42. Force and deflection vs. time for I-2-6F-2 at 186-in (4.7 m), 6th repetition

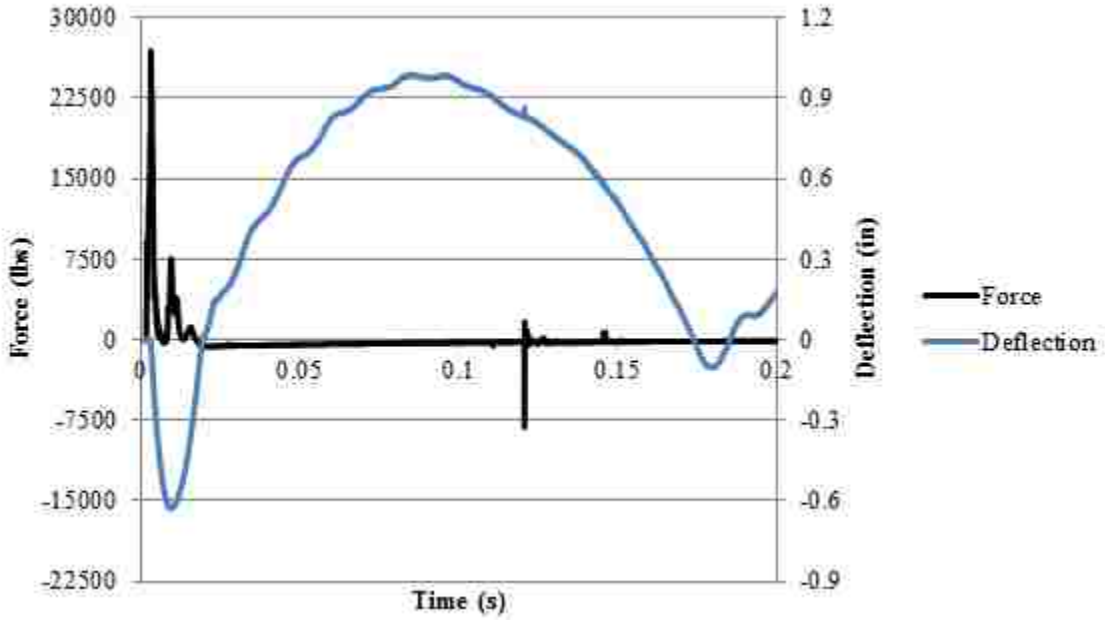

Figure C.43. Force and deflection vs. time for I-2-6F-2 at 186-in (4.7 m), 7th repetition

APPENDIX D

LEVEL OF DAMAGE DESCRIPTIONS

The table below is taken from CEDAW and contains component damage description information. This damage information is used to determine overall building level of protection (LOP) as stated in PDC-TR 06-08.

Table D.9. Component damage descriptions

Component Damage Level	Description of Component Damage*
Blowout	Component is overwhelmed by the blast load causing debris with significant velocities
Hazardous Failure	Component has failed, and debris velocities range from insignificant to very significant
Heavy Damage	Component has not failed, but it has significant permanent deflections causing it to be unreparable
Moderate Damage	Component has some permanent deflection. It is generally reparable, if necessary, although replacement may be more economical and aesthetic
Superficial Damage	Component has no visible permanent damage
* From PDC-TR 06-08 Rev 1 "Single Degree of Freedom Structural Response Limits for Antiterrorism Design"	

APPENDIX E

CEDAW ANALYSES

The following figures are pressure-impulse (P-i) diagrams from the program CEDAW that were used to assist with the blast testing analysis and test set-up. The diagrams give two predicted load points; incident load and reflected load. Since the results of this study were presented as complete damage from the blast event, the load of interest in these diagrams is the reflected load (denoted as a diamond). The definitions of the damage levels are as presented previously in Appendix D.

Conversions: 1 psi = 0.006895 MPa

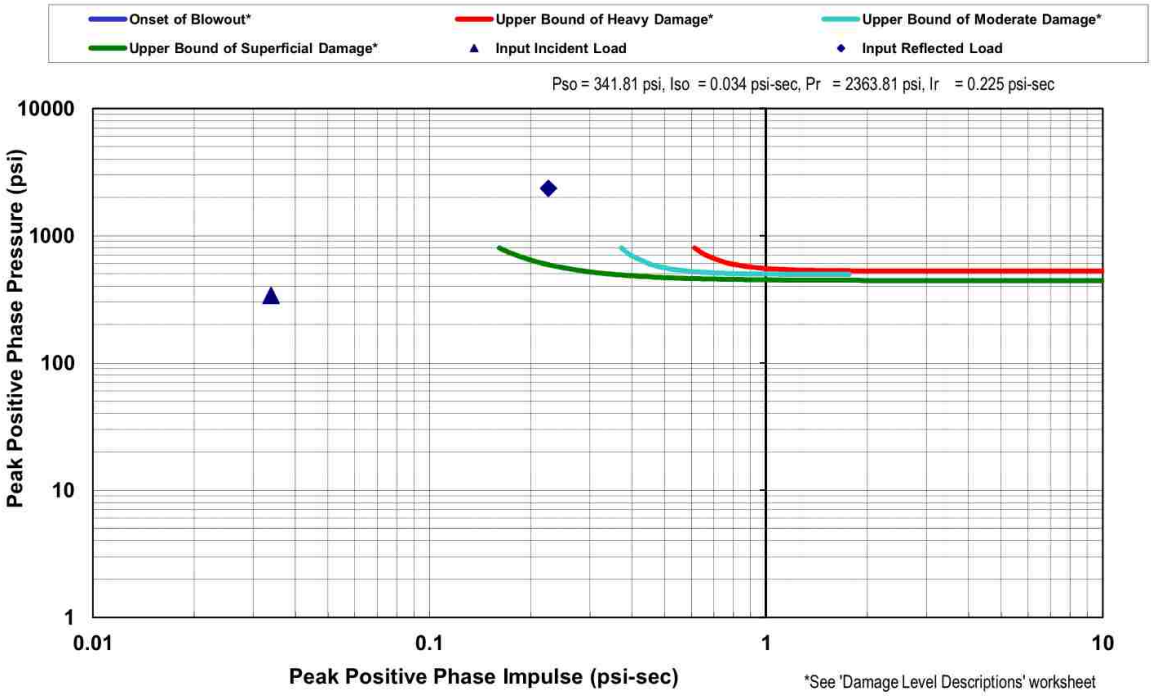

Figure E.1. P-i diagram for full 3.5-in (89 mm) panel with 6% fiber. Charge of 3 lb (1.4 kg) at 36-in (0.9 m)

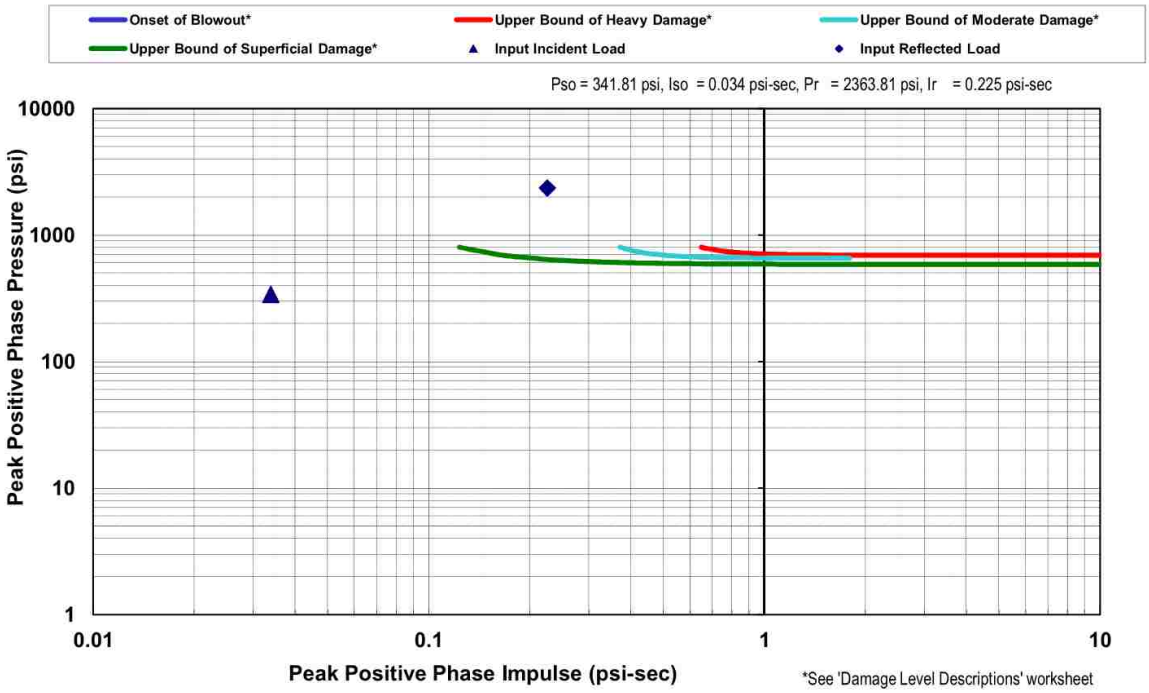

Figure E.2. P-i diagram for half 3.5-in (89 mm) panel with 0% fiber. Charge of 3 lb (1.4 kg) at 36-in (0.9 m)

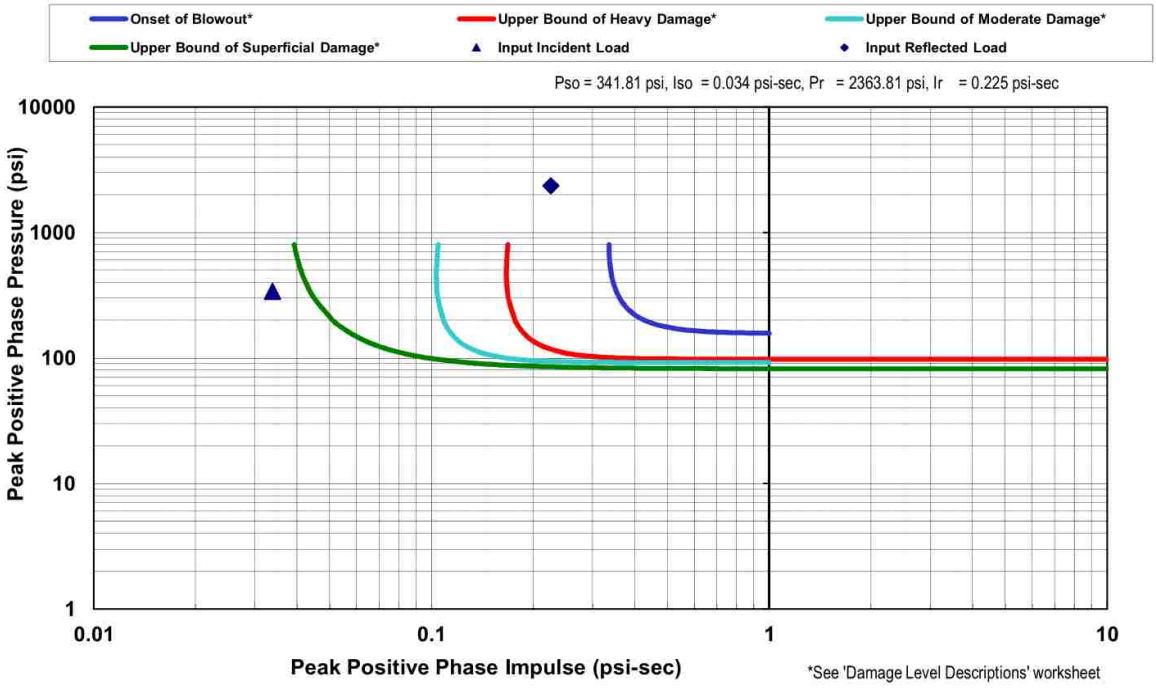

Figure E.3. P-i diagram for full 2-in (50.8 mm) panel with 0% fiber. Charge of 3 lb (1.4 kg) at 36-in (0.9 m)

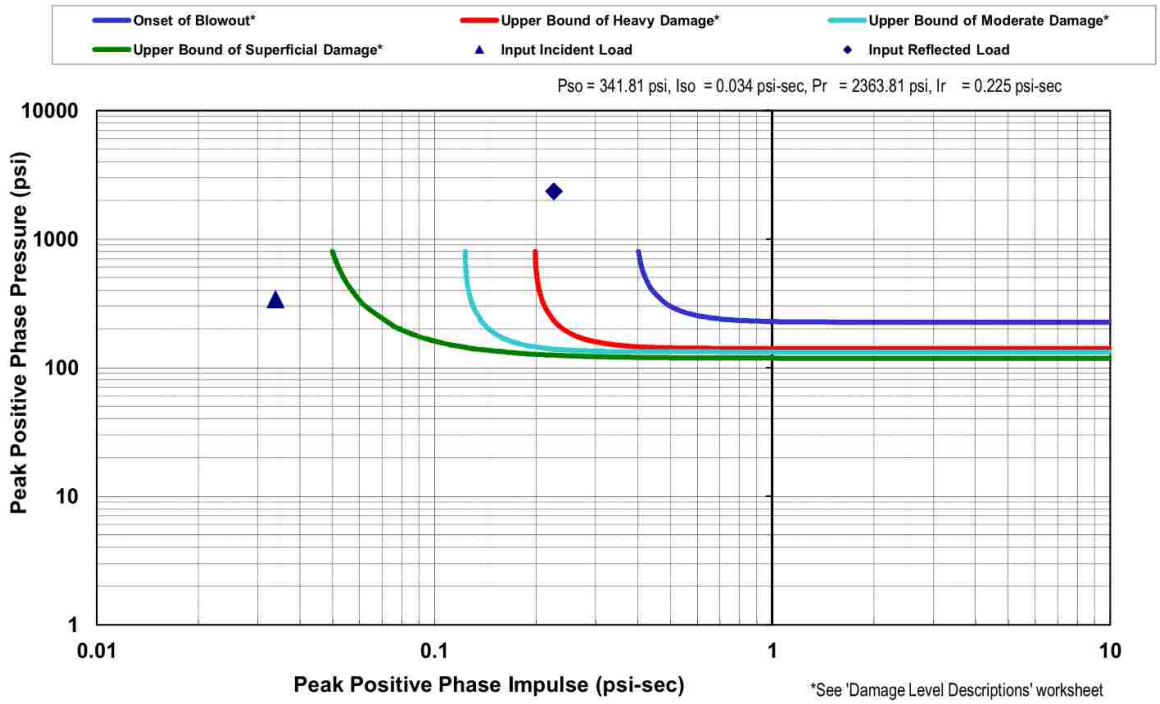

Figure E.4. P-i diagram for full 2-in (50.8 mm) panel with 2% fiber. Charge of 3 lb (1.4 kg) at 36-in (0.9 m)

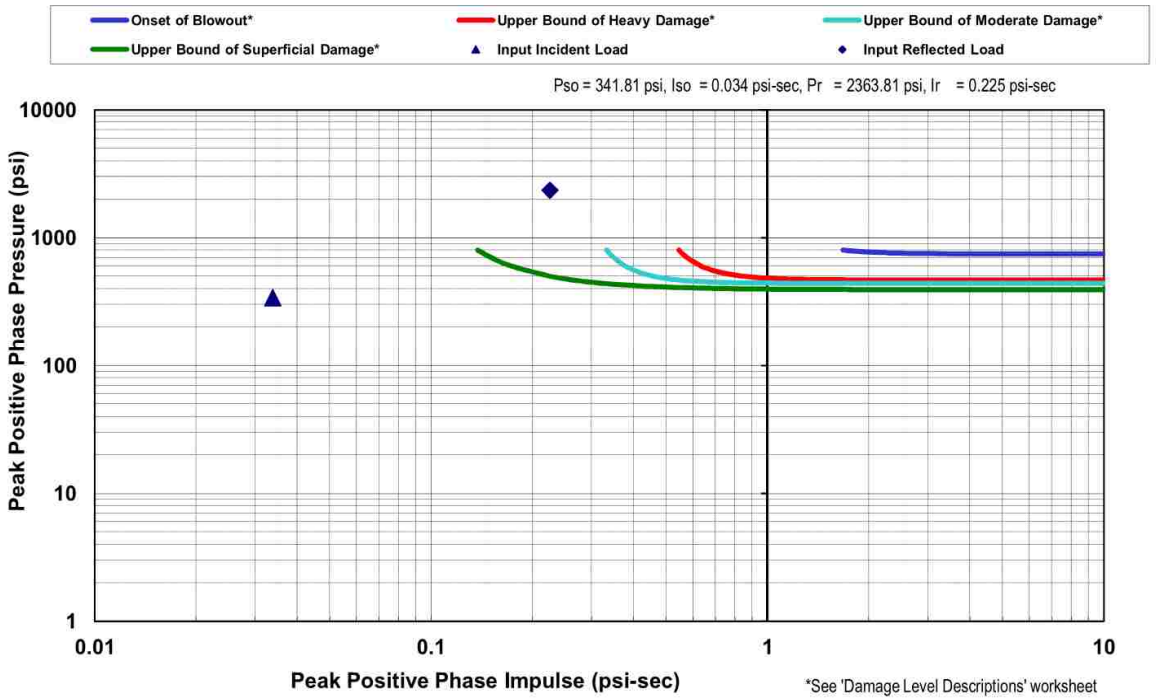

Figure E.5. P-i diagram for full 3.5-in (89 mm) panel with 2% fiber. Charge of 3 lb (1.4 kg) at 36-in (0.9 m)

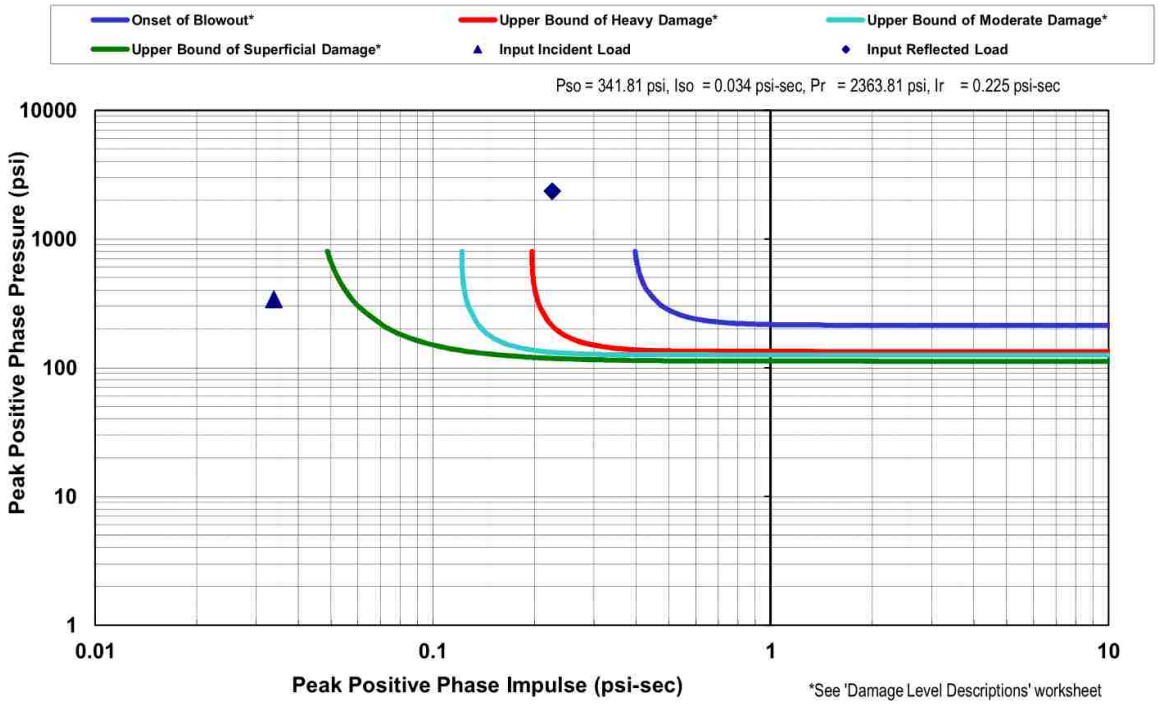

Figure E.6. P-i diagram for full 2-in (50.8 mm) panel with 6% fiber. Charge of 3 lb (1.4 kg) at 36-in (0.9 m)

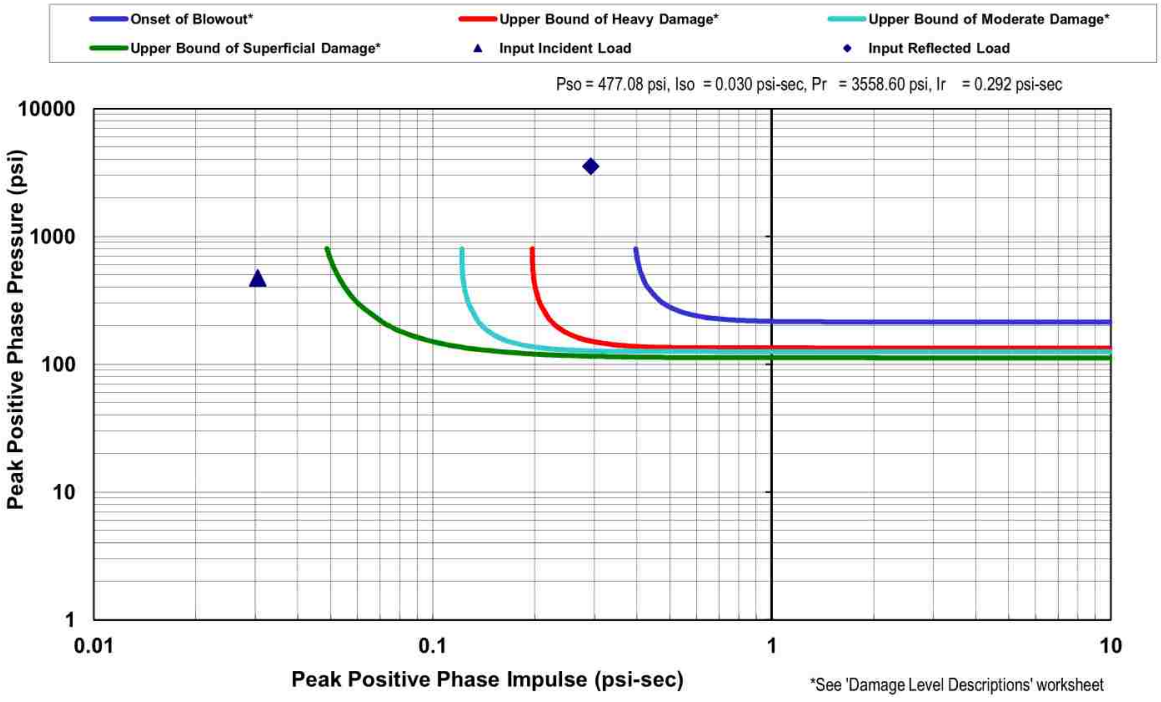

Figure E.7. P-i diagram for full 2-in (50.8 mm) panel with 6% fiber. Charge of 3 lb (1.4 kg) at 30-in (0.8 m)

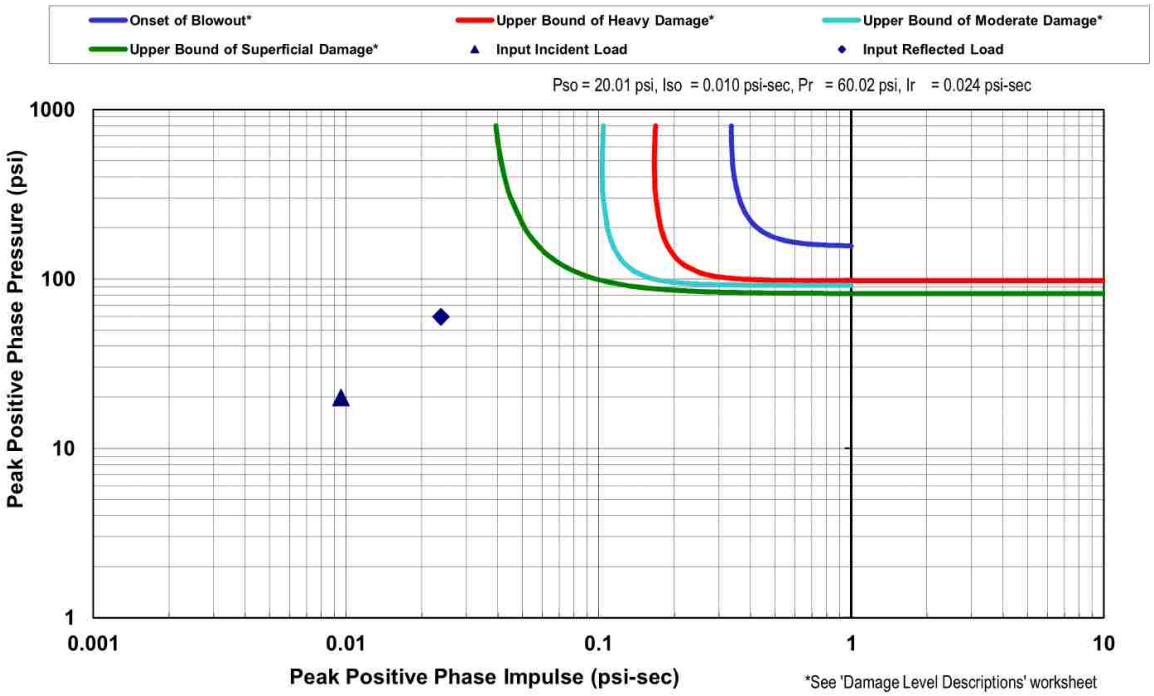

Figure E.8. P-i diagram for full 2-in (50.8 mm) panel with 0% fiber. Charge of 0.5 lb (0.23 kg) at 72-in (1.8 m)

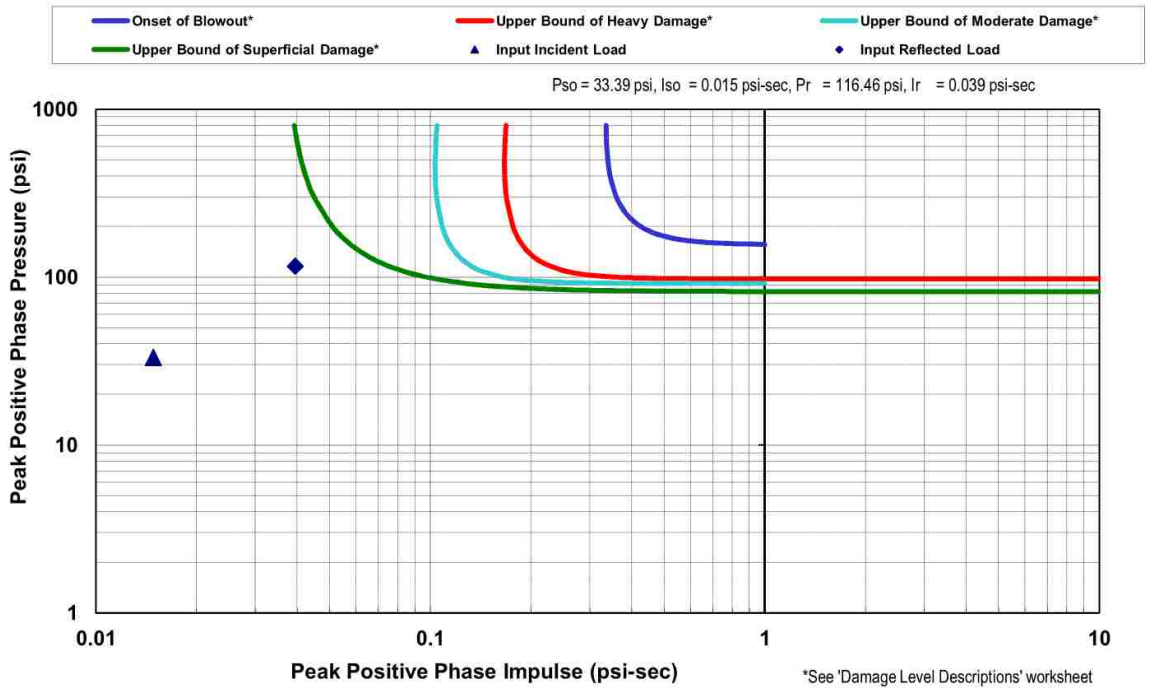

Figure E.9. P-i diagram for full 2-in (50.8 mm) panel with 0% fiber. Charge of 1 lb (0.45 kg) at 72-in (1.8 m)

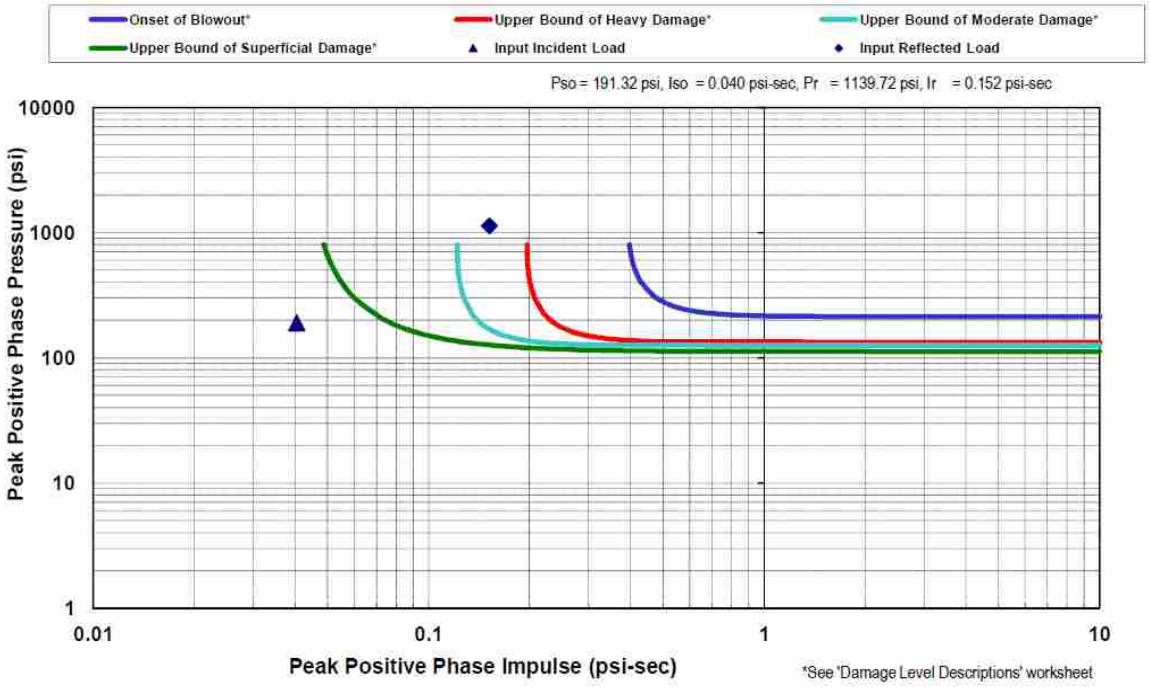

Figure E.10. P-i diagram for full 2-in (50.8 mm) panel with 6% fiber. Charge of 3 lb (1.4 kg) at 48-in (1.2 m)

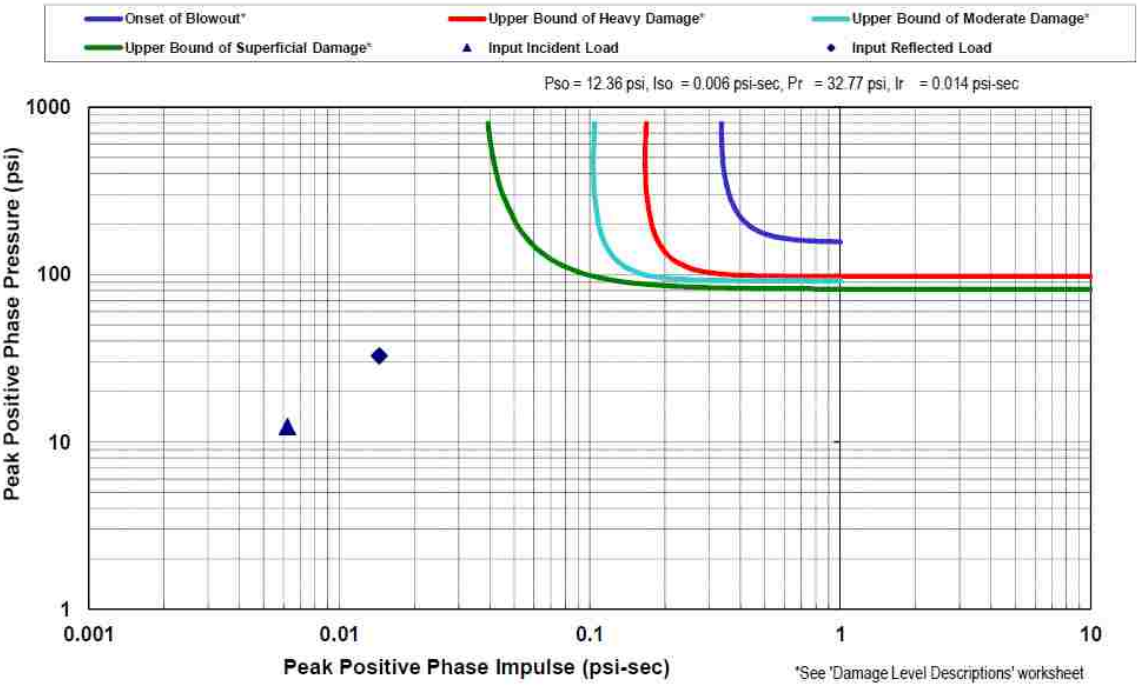

Figure E.11. P-i diagram for full 2-in (50.8 mm) panel with 0% fiber. Charge of 0.25 lb (0.11 kg) at 72-in (1.8 m)

APPENDIX F

CONWEP PREDICTIONS

The following table, labeled Table F.1, was compiled from a series of ConWep breaching analyses that were done to assist with determining the test set-up for the first set of half panel specimens that were tested. The breaching analysis in ConWep is based on the concrete strength of the specimen and does not consider the specimen size, or fiber content, therefore in Table F.1, these variables are simply shown for clarity.

In all the ConWep predictions, the charge weight remains constant at 3 lb (1.4 kg) of C-4 explosive. The standoff distance was adjusted to target a specific combined level of spalling and breaching of about 30% of the thickness of the given panel. The spalling thickness is considered as the depth of the material that is dislodged from the tension face of the specimen. The breaching thickness is considered as the cratering depth of the material that is dislodged from the face of the specimen that is directly facing the blast charge.

Table F.1. ConWep breaching predictions

Panel Type	% Fiber	f'_c (ksi)	C-4 Charge Weight (lb)	Equivalent weight of TNT (lb)	Contact detonation?	Adjusted charge mass (lb)	Standoff distance (in)	Spall threshold thickness (in)	Breach threshold thickness (in)
2" Full	0	14.5	3	3.84	No	1.92	36	0.4799	0.8623
2" Full	0	14.5	3	3.84	No	1.92	18	1.5990	1.4140
2" Full	2	20.9	3	3.84	No	1.92	36	0.3581	0.7173
2" Full	2	20.9	3	3.84	No	1.92	18	1.2080	1.1850
2" Full	6	19.8	3	3.84	No	1.92	36	0.3740	0.7372
2" Full	6	19.8	3	3.84	No	1.92	18	1.2590	1.2160
3.5" Full	0	16.9	3	3.84	No	1.92	72	0.1221	0.4661
3.5" Full	0	16.9	3	3.84	No	1.92	38	0.3854	0.7665
3.5" Full	0	16.9	3	3.84	No	1.92	36	0.4246	0.7984
3.5" Full	0	16.9	3	3.84	No	1.92	18	1.4220	1.3130
3.5" Full	2	22.7	3	3.84	No	1.92	72	0.09632	0.4002
3.5" Full	2	22.7	3	3.84	No	1.92	36	0.3352	0.6880
3.5" Full	2	22.7	3	3.84	No	1.92	18	1.1330	1.1390
3.5" Full	6	25.6	3	3.84	No	1.92	72	0.08744	0.3761
3.5" Full	6	25.6	3	3.84	No	1.92	36	0.3044	0.6474
3.5" Full	6	25.6	3	3.84	No	1.92	36	0.3352	0.6880
3.5" Full	6	25.6	3	3.84	No	1.92	34	0.3372	0.6762
3.5" Full	6	25.6	3	3.84	No	1.92	18	1.0320	1.0740

Conversions: 1 ksi = 6.895 MPa

1 lb = 0.45 kg

1-in = 25.4 mm

The ConWep software was also used to obtain theoretical pressures that would be caused by the blast testing. Figure F.1 and Figure F.2 show a representative sample of outputs that were used in this study. The set of figures show the results for a blast event with a charge weight of 3 pounds (1.4 kg) of C-4 explosive, at a standoff distance of 36-in (0.9 m) from a full panel specimen (48-in x 48-in (1.2 m x 1.2 m)). Table F.2 is a compilation of the ConWep outputs for the blast events that were simulated for this research.

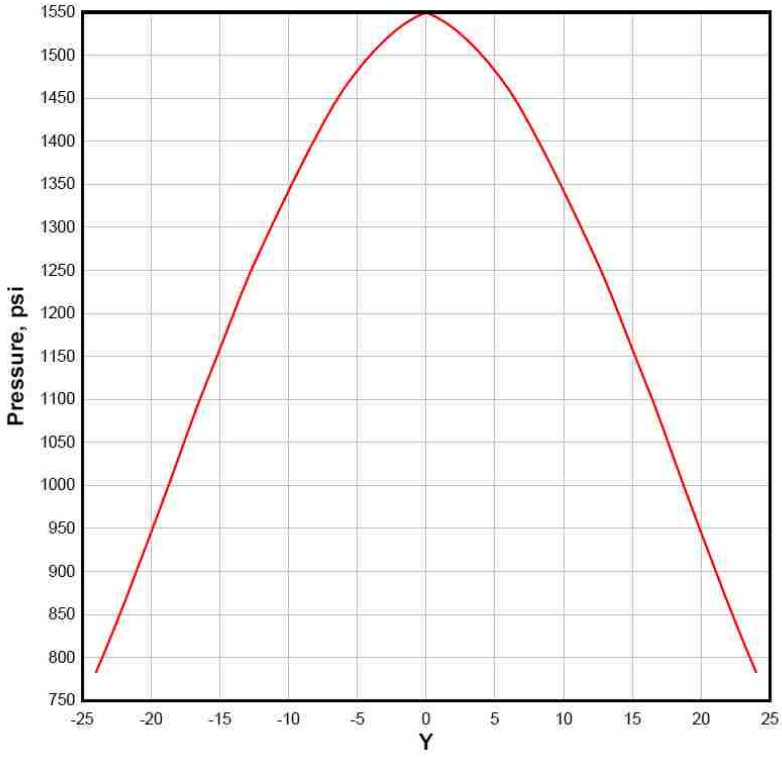

Conversion: 1 psi = 0.006895 MPa

Figure F.1. Sample ConWep peak pressure prediction output

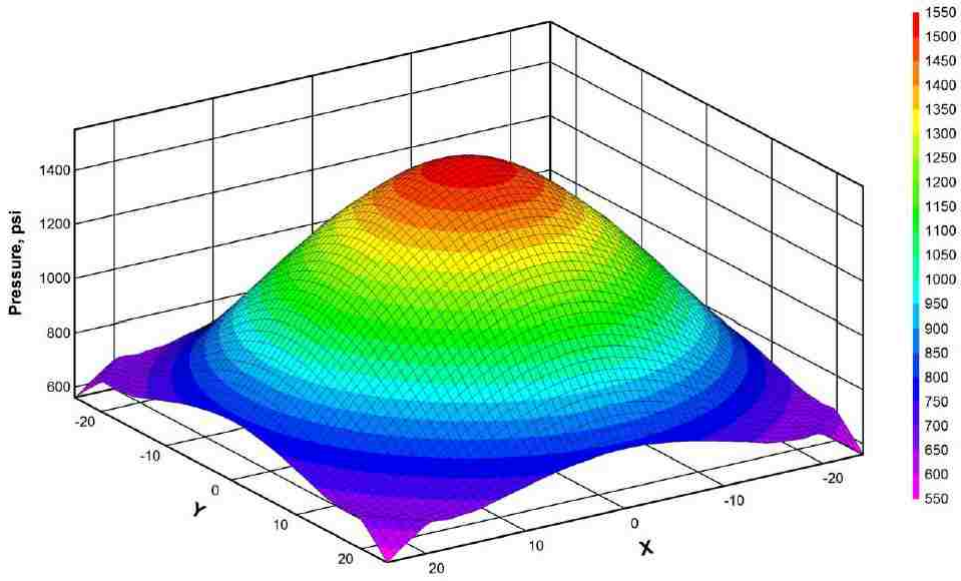

Conversion: 1 psi = 0.006895 MPa

Figure F.2. Sample ConWep pressure distribution prediction output

Table F.2. Summary of ConWep peak pressure and average impulse predictions

C-4 Charge Weight (lb)	Equivalent Weight of TNT (lb)	Standoff Distance (in)	Peak Pressure (psi)	Average Impulse (psi-msec)
3	3.84	36	1550	105.4
3	3.84	18	7663	150.0
3	3.84	48	708	80.7
3	3.84	72	21.4	8.3
3	3.84	72	71.6	22.5
3	3.84	12	15800	158.1

Conversions: 1 psi = 0.006895 MPa

1 lb = 0.45 kg

1-in = 25.4 mm

BIBLIOGRAPHY

American Concrete Institute (2000), "Cement and Concrete Terminology (ACI 116R-00)," American Concrete Institute, Farmington Hills, MI.

ACI Committee 209 (2005). "Report on Factors Affecting Shrinkage and Creep of Hardened Concrete (ACI 209.1R-05)," American Concrete Institute, Farmington Hills, MI.

ASTM C109/C109M (2011). "Standard Test Method for Compressive Strength of Hydraulic Cement Mortars (Using 2-in. or [50-mm] Cube Specimens)." American Society for Testing and Materials, West Conshohocken, Pennsylvania.

ASTM C157/C157M (2008). "Standard Test Method for Length Change of Hardened Hydraulic-Cement Mortar and Concrete." American Society for Testing and Materials, West Conshohocken, Pennsylvania.

ASTM C469/C469M (2010). "Standard Test Method for Static Modulus of Elasticity and Poisson's Ratio of Concrete in Compression." American Society for Testing and Materials, West Conshohocken, Pennsylvania.

ASTM C496/C496M (2011). "Standard Test Method for Splitting Tensile Strength of Cylindrical Concrete Specimens." American Society for Testing and Materials, West Conshohocken, Pennsylvania.

ASTM C512/C512M (2010). "Standard Test Method for Creep of Concrete in Compression." American Society for Testing and Materials, West Conshohocken, Pennsylvania.

ASTM C1437 (2007). "Standard Test Method for Flow of Hydraulic Cement Mortar." American Society for Testing and Materials, West Conshohocken, Pennsylvania.

Banthia, Nemkumar. *Impact Resistance of HPFRCC*. The University of British Columbia, Canada.

Carey, N.L., Myers, J.J., (2012) "Discrete Fiber-Reinforced Polyurea Systems for Infrastructures Strengthening and Blast Mitigation," CIES Report for Department of Defense – Awareness and Localization of Explosives-Related Threats Center of Excellence, Missouri University of Science and Technology, Rolla, Missouri, June 2012, 322 pp.

Cavill, B., Rebentrost, M., and Perry, V. "Ductal® – An Ultra-High Performance Material for Resistance to Blasts and Impacts." 1st Specialty Conference on Disaster Mitigation, Calgary, Alberta, Canada, May 23-26, 2006.

"Ductal® Characteristics." VSL International Ltd.. Web. 01 December 2011. <www.VSL.com>.

Elavenil, S., and Knight, G.M. Samuel. "Impact Response of Plates Under Drop Weight Impact Testing." *Daffodil International University Journal of Science and Technology*. 7.1 (2012).

Gliha, Benjamin. "*Long Carbon Fiber Reinforced Concrete for Impact and Blast Protection*." Master's Thesis, Civil Engineering, Missouri University of Science and Technology, Rolla, MO, 2011.

Graybeal, Benjamin. Federal Highway Administration. Office of Infrastructure Research and Development. *Material Property Characterization of Ultra-High Performance Concrete*. August 2006. Print.

Graybeal, Benjamin, and Hartmann, Joseph. "Strength and Durability of Ultra-High Performance Concrete." 2003.

Idiart, A.E. "Drying Shrinkage and Creep in Concrete: A Summary." Web. Sept 2013. <http://www.tdx.cat/bitstream/handle/10803/6263/TAEIC2de5.pdf;jsessionid=C6732436D586DF0A4690FEDE7214247E.tdx2?sequence=2>.

Loukili, A., P. Richard, and J. Lamirault. "A Study on Delayed Deformations of an Ultra High Strength Cementitious Material." *ACI Materials Journal*. 179. (1998): 929-950. Web.

Rebentrost, M. "Australian Experience with Ductal: An Ultra-high Performance Concrete," Fédération Internationale du Béton Proceedings of the 2nd International Congress, Naples, Italy, June 5-8, 2006.

Tarr, Scott M., and Farny, James A. Concrete Floors on Ground, Fourth Edition, Portland Cement Association, Skokie, Illinois, USA, 2008, 256 pages

Tinsley, M., Myers, J.J., (2007) "Investigation of a High-Volume Fly Ash-Wood Fiber Material Subjected to Low-Velocity Impact and Blast Loads," CIES Report Number 07-74, University of Missouri-Rolla, Rolla, Missouri, May 2007.

Toutlemonde, Francois, and Jacques Resplendino. *Designing and Building with UHPFRC: State of the Art and Development*. 1st ed. Hoboken, NJ: John Wiley & Sons, Inc., 2011. 4-5. Print.

United States Army Corps of Engineers (2007). *ConWep*. United States Army Corps of Engineers Protective Design Center, 07 Aug 2007. Web. 04 Nov 2013. < https://pdc.usace.army.mil/software/conwep/>.

United States Army Corps of Engineers (2008). "Single-Degree-of-Freedom Structural Response Limits for Antiterrorism Design (PDC TR-06-08)," United States Army Corps of Engineers Protective Design Center.

United States Army Corps of Engineers (2013). *CEDAW*. United States Army Corps of Engineers Protective Design Center, 01 Mar 2012. Web. 04 Nov 2013. <https://pdc.usace.army.mil/software/cedaw>.

Wulfers, A., Myers, J.J., (2012) “Use of High Volume Fly-Ash Wood Fiber and Ployurea Layers for Blast Mitigation,” CIES Report for Department of Defense – Awareness and Localization of Explosives-Related Threats Center of Excellence, Missouri University of Science and Technology, Rolla, Missouri, June 2012, 173 pp.

VITA

Julie Anne Willey was born and raised in Saint Louis, Missouri. After discovering her love of rollercoasters and buildings while attending high school at Cor Jesu Academy, she moved to Rolla, Missouri in 2006 to begin her undergraduate degree at the University of Missouri – Rolla, now Missouri University of Science and Technology. While attending UMR/Missouri S&T she became involved in the campus Solar House Student Design Team, the Women's Club Volleyball Team, and the Chi Epsilon Honors Society. After five years of coursework and various job opportunities, she graduated with her Bachelor's Degree in both Civil and Architectural Engineering. After receiving her undergraduate degrees, she continued her educational experience at Missouri S&T working towards a Master's Degree in Civil Engineering in 2013. Upon completion of her work on this project, she began her career as part of the Structural Engineering Department at Cannon Design in Saint Louis, Missouri, and graduated with her Master's Degree in December 2013.